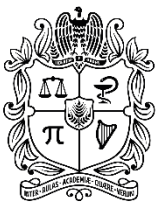

UNIVERSIDAD
NACIONAL
DE COLOMBIA

Understanding bio-oil droplets microexplosions in oxyfuel combustion

Javier Alonso Ordoñez Loza

Universidad Nacional de Colombia

Facultad de Minas, Departamento de Procesos y Energía

Medellín, Colombia

2020

Understanding bio-oil droplets microexplosions in oxyfuel combustion

Javier Alonso Ordoñez Loza

Thesis presented as a partial requirement to qualify for the title of:

Engineering PhD, Energy Systems

Doctorado en ingeniería, Sistemas Energéticos

Advisor:

Ph.D., Farid Chejne Janna

Co- Advisor:

Msc Andres Amell Arrieta

Line of research:

Energetic Systems

Research group:

Termodinámica Aplicada y Energías Alternativas TAYEA

Universidad Nacional de Colombia

Facultad de Minas, Departamento de Procesos y Energía

Medellín, Colombia

2020

A papá, en tu memoria encuentro paz.

Declaración de obra original

Yo declaro lo siguiente:

He leído el Acuerdo 035 de 2003 del Consejo Académico de la Universidad Nacional. «Reglamento sobre propiedad intelectual» y la Normatividad Nacional relacionada al respeto de los derechos de autor. Esta disertación representa mi trabajo original, excepto donde he reconocido las ideas, las palabras, o materiales de otros autores.

Cuando se han presentado ideas o palabras de otros autores en esta disertación, he realizado su respectivo reconocimiento aplicando correctamente los esquemas de citas y referencias bibliográficas en el estilo requerido.

He obtenido el permiso del autor o editor para incluir cualquier material con derechos de autor (por ejemplo, tablas, figuras, instrumentos de encuesta o grandes porciones de texto).

Por último, he sometido esta disertación a la herramienta de integridad académica, definida por la universidad.

Javier Alonso Ordoñez Loza
15/12/2020

Acknowledgment

First and foremost to my principal Professor Farid Chejne for all the patience and long conversations, for directing my ramblings to something scientifically correct, and for all his support outside of academia in illuminating the uncertain future with ideas and with all his support. . And to my co-advisor Professor Andres Amell Arrieta, who has been an example of leadership and work, thank you very much for your comments and your all your help in this work.

I also want to thank the members of my committee, Professor Mani Sarathy for opening the doors of his laboratory in which I carried out a large part of my experiments, as well as all his support and comments on the manuscripts of the works that have resulted from this thesis , to Professor Manuel Garcia Perez for his excellent comments and support during the writing of the first chapter of this thesis, his comments and great experience were invaluable support, and to Professor David Granados for taking the time to review this work and for his contributions and comments.

To Dr Carlos Valdez, Gloria Marrugo, Robert Macias and Dr Jorge Montoya, Dr Victor H Borda, and Dr Jader Alean, who were with me during many of the experiments and during the initial discussions that are part of the beauty of doing a doctorate. To Dr Carlos Gomez, who has always been there to support me. And to all the members of the TAYEA group, without any of them being left out of my thanks.

Thank you very much for all your help to Juan Guillermo Restrepo, with whom we had long and intense conversations and exhausting days of experiments, I also want to thank the CPC family at KAUST who gave me their sincere help and friendship during my internship, especially Dr Abdul Ganni for their interesting discussions.

The author wish to thank the Colciencias-Doctorados Nacionales 757-2016 fellowship and the project "Strategy of transformation of the Colombian energy sector in the horizon 2030" funded by call 788 of the Colciencias Scientific Ecosystem. Contract number FP44842-210-2018.

Finally thank my family, my father I know I would be proud that this chapter in my life has finished. my sisters, my brother, and my mother are and will always be incomparable support, this is for you.

Comprensión de las micro explosiones de gotas de bio-aceite en condiciones de oxicombustión

Resumen

El bio-aceite de bagazo de caña es un combustible de bajo poder calorífico producido por la pirólisis de bagazo de caña en atmósfera de nitrógeno, y puede considerarse como un futuro combustible alternativo. En esta tesis una caracterización detallada del bio-aceite fue desarrollada, y se evaluó el efecto del dióxido de carbono en la formación de carbonizado durante la descomposición térmica. También se analizó la cinética y etapas de descomposición fueron propuestas. Así mismo experimentos de evaporación de gotas de bio-aceite fueron realizados y permitieron identificar la naturaleza del fenómeno de las micro-explosiones y su relación con la formación de microburbujas, para complementar el trabajo un novedoso modelo para predecir las micro-explosiones fue desarrollado ofreciendo la posibilidad de entender el fenómeno de formación de micro-explosiones a partir de una colección de eventos fisicoquímicos que comienzan con la nucleación, coalescencia y explosione de microburbujas dentro de la gota.

Palabras clave: Bio-oil, Pyrolysis, CO_2, Char, char reactivity, droplet evaporation**.**

Abstract

Sugarcane bagasse bio-oil is a low calorific fuel produced by pyrolysis of cane bagasse in a nitrogen atmosphere and can be considered as a future alternative fuel. In this doctoral thesis, a detailed characterization of the bio-oil was developed, and the effect of carbon dioxide on char formation during thermal decomposition was evaluated. The kinetics was also analyzed, and decomposition stages were proposed. Likewise, bio-oil droplet evaporation experiments were carried out and allowed to identify the nature of the phenomenon of micro-explosions and its relationship with the formation of microbubbles, to complement the work, a novel model to predict micro-explosions were developed offering the possibility of understanding the phenomenon of micro-explosion formation from a collection of physicochemical events that begin with the nucleation, coalescence, and explosion of microbubbles within the drop.

Keywords : Bio-oil, Pyrolysis, CO_2, Char, char reactivity, droplet evaporation**.**

Table of contents

1 Introduction 1
1.1 Biomass to produce chemicals and fuels 2
1.2 Bio-oil combustion 4
1.3 Dissertation structure 12
1.4 References 17

2 Effect of Carbon Dioxide Environment on the Thermal Behavior of Sugarcane Pyrolysis Oil 1
2.1 Material and Methods 3
2.1.1 Experimental setup 3
2.1.2 Char samples preparation 4
2.1.3 Bio-oil Characterization 4
2.2 Results and Discussion 7
2.2.1 Bio-oil characterization 7
2.2.2 Bio-oil thermal degradation in N_2 and CO_2 atmospheres 12
2.2.3 The functional group of char products 15
2.3 Conclusions 22
2.4 Acknowledgments: 23
2.5 References 23

3 Investigation into the pyrolysis and combustion of bio-oil from sugarcane bagasse: Kinetics and evolved gases using TGA-FTIR 31
3.1 Material and Methods 34
3.1.1 Bio-oil production 34
3.1.2 TGA-FTIR 35
3.2 Results & Discussion 36
3.2.1 Pyrolysis of SCB bio-Oil 37
3.2.2 Combustion of Bio-Oil 38
3.2.3 Kinetic analysis of Bio-Oil combustion 42
3.2.4 FTIR results 45
3.3 Conclusions 52
3.4 Acknowledgments 53
3.5 References 54

4 An investigation into the break-up modes of bio-oil droplets from sugarcane bagasse in air and nitrogen atmosphere 63
4.1 Experimental 65
4.1.1 Droplet experiments 65
4.1.2 images post-processing 66
4.2 Results 66
4.2.1 Contour identification 67
4.2.2 suspended droplet dynamics in air atmosphere 67
4.2.3 suspended droplet dynamics in a Nitrogen atmosphere 72
4.3 Conclusions 75
4.4 References 76

5 On the modeling of the micro-explosions during the evaporation and pyrolysis of a bio-oil droplet. 83
5.1 Experimental 85
5.1.1 droplet experiments 85
5.1.2 images post-processing 86
5.2 Mathematical model 87
5.2.1 Gas generation 87
5.2.2 Bubble formation, growing, merging, and bursting 88
5.2.3 Energy equation 89
5.3 Numerical approach 90
5.4 Results 95
5.4.1 Effect of nucleation rate on droplet evaporation dynamics 96
5.4.2 Effect of bursting on droplet evaporation dynamics 100
5.5 Conclusions 103
5.6 References 103

List of figures

Chapter1

Figure 1-1 Scheme of the liquid combustion mechanism in a spray burner 5
Figure 1-2 micro-explosions of bio-oil droplets [28] 10
Figure 1-3 Explosión de una burbuja en una gota de celulosa fundida y eyección de líquidos [34] 11
Figure 1-4 D^2/D_0^2 evolution for bio-oil droplets suspended in platinum bare in 560°C air atmosphere, description of break-up events 14
Figure 1-5 D^2/D_0^2 evolution for bio-oil droplets suspended in platinum bare in 560°C air atmosphere 15
Figure 2-1. Experimental model for bio-oil production and char collection setup 4
Figure 2-2. GC-MS-FID chromatogram for SCB bio-oil 8
Figure 2-3. ESI (-)-FT-ICR-MS mass/z vs. H/C ratio for SCB bio-oil 10
Figure 2-4. Van-Krevelen diagram from ESI (-)-FT-ICR of hit compounds in SCB bio-oil 11
Figure 2-5. DBE vs. carbon number from ESI (-)-FT-ICR of hit compounds in SCB bio-oil 11
Figure 2-6. Oxygen family's classification of $C_xH_yO_zN_w$ Compounds and the number of Nitrogen atoms participation. 12
Figure 2-7. TG-DTG and heat flow of bio-oil in N_2 and CO_2 atmosphere 13
Figure 2-8 FT-IR spectra between 3000 and 2750 cm−1 of the char from the pyrolysis of bio-oil at 300-700°C 16
Figure 2-9 FT-IR spectra between 1850 and 900cm−1 of the char from the pyrolysis of bio-oil at 300-700°C 17

Figure 2-10. FT-IR spectra between 900 and 650 cm−1 of the char from the pyrolysis of bio-oil at 300-700°C. 18
Figure 2-11. FT-IR based index of the char from the pyrolysis of bio-oil at 300-700°C in N_2 and CO_2 a) Aromatic Index, b) Aliphatic index, c) Condensation index, and d) Branching index 21
Figure 3-1. Experimental set-up for SCB bio-oil production 34
Figure 3-2 TGA (continuous line) and DTG (dotted line) characteristics of SCB bio-oil pyrolysis 38
Figure 3-3 typical mechanism of LTO Oxidation [50] 39
Figure 3-4 TGA (continuous line) and DTG (dotted line) characteristics of SCB bio-oil combustion 40
Figure 3-5 DTG comparison of SCB bio-oil pyrolysis (dotted line) and combustion (continuous line) 42
Figure 3-6 activation energy vs reaction conversion (α) 43
Figure 3-7 activation energy vs temperature until reach α = 0.85 in each process 44
Figure 3-8. FTIR spectra of SCB bio-oil pyrolysis in N_2 at a heating rate of 5°C/min. 46
Figure 3-9 Selected wavenumbers evolution with temperature during pyrolysis of SCB bio-oil at heating rate of 5 °C/min 47
Figure 3-10. FTIR spectra of oxidation of SCB bio-oil in the air at a heating rate of 5°C/min 48
Figure 3-11 FTIR intensity evolution for 2360 cm-1, and 670 cm-1 wavenumbers 49
Figure 3-12 FTIR intensity evolution for 3733, 2119, and 1762 cm-1 during combustion 50
Figure 3-13 evolution of gases released during pyrolysis (a, b, c) and during combustion (e, f, g) the signals were assigned to the species methane (2850 cm-1), CO2 (2360 cm-1) and OH (3733 cm-1) 51
Figure 4-1 Experimental setup for the analysis of bio-oil micro explosions under pyrolysis and combustion conditions. T1 and T2 represent the thermocouples for controlling the resistors R1 and R2 65
Figure 4-2 droplet postprocessing for contour identification 67

Figure 4-3 D^2/D_0^2 evolution for bio-oil droplets suspended in platinum bare in 560°C air atmosphere 68
Figure 4-4 D^2/D_0^2 evolution for bio-oil droplets suspended in platinum bare in 560°C air atmosphere, description of evaporation releasing of vapors from bubble inside of a droplet of SCB Bio-oil 69
Figure 4-5 D^2/D_0^2 evolution for bio-oil droplets suspended in platinum bare in 560°C air atmosphere, description of break-up events 70
Figure 4-8 Events Intensity during bio-oil droplets suspended in platinum bare in 560°C air atmosphere, and distribution in time (upside) and Intensity distribution events (right side). 72
Figure 4-10 D^2/D_0^2 evolution for bio-oil droplets suspended in platinum bare in 560°C N_2 atmosphere 73
Figure 4-11 Events Intensity during bio-oil droplets suspended in platinum bare in 560°C air atmosphere, and distribution of intensity (right side). 74
Figure 4-12 char formation, evidenced at the end of the experiment carried out in a nitrogen atmosphere 74
Figure 5-1 montaje experimental para el análisis de las micro explosiones de bio-aceite en condiciones de pirolisis y combustión. T1 y T2 representan las termocuplas para el control de las resistencias R1 y R2 85
Figure 5-3 droplet postprocessing for contour identification 87
Figure 5-4 descripción geométrica de los nodos, y dimensiones generales usadas en el modelo, b) ubicación de una burbuja k dentro de la gota 91
Figure 5-5 detail of a bubble passing through a drop differential element 93
Figure 5-6 calculations flowchart for bubble dynamics 94
Figure 5-7 D^2/D_0^2 evolution for bio-oil droplets suspended in platinum bare in 560°C air atmosphere 95
Figure 5-8 numerical results according to the variation of the nucleation rate J 97
Figure 5-9 temperature field for J=B exp(-En/RT) and heating velocity 99
Figure 5-10 comparison between heating rate and bubble number in droplet 99

Figure 5-11 numerical results according to the variation of burstingtime with a nucleation rate J=B exp(-En/RT) 101
Figure 5-12 a) hist chart of bubbles born by nucleation at three different drainage time, b) hist chart of burst bubbles at three different drainage times. 102

List of tables

Table 2-1 Principal compounds identified in bio-oil GC -MS -FID 8
Table 3-1 Physical and chemical properties of SCB..... 36
Table 3-2 Thermal degradation characteristics of PKS under nitrogen and air atmosphere with different heating rates of 5, 10, and 20 °C min−1. 41
Table 5-1 general properties and values used for calculations 96

1 Introduction

The current environmental damage caused by the continuous and growing emissions of greenhouse gases into the atmosphere has encouraged research in basic science and applied to the combustion of existing fossil or renewable resources, seeking to improve the efficiency of energy production, reduce the environmental impact of its use and slow down existing environmental damage. This topic has become an attractive focus of research ranging from macro-scale production methodologies to the design of high-efficiency fuels.

In recent years, environmental phenomena have hampered environmental panorama because they are the product of existing pollution. Currently, the IPCC (IPCC - Intergovernmental Panel on Climate Change) has projected an increase of 1.5 °C in the average temperature of the earth's surface[1], [2]. With these projections, the objective set is to achieve that this increase in 2050 is less than 1.5°C (corresponding to 450 ppm of CO_2 in the atmosphere). Under this panorama, the development of technology and relevant studies related to the capture of CO_2 and new fuels becomes a topic of current interest and research.

In the current research landscape, to mitigate the existing environmental problem due to CO2 emissions into the atmosphere and polluting emissions from new types of fuels, there is a group of technologies called CO2 Capture and Storage (CCS - Carbon dioxide Capture and Storage) [3]. These are immediate solutions to counteract the current excess of emissions generated. According to IPCC[4], CCS will contribute between 15% and 55% of the cumulative global mitigation effort until 2100[5], thus presenting itself as a transitional technology to curb climate change. However, CO_2 capture is very

costly as carbon dioxide is found in very low concentrations (10 to 12%) in the exhaust gases of traditional combustion systems.

In addition to the environmental problem, fossil resources are depleted, energy consumption in developed countries has doubled in the period from 2000 to 2014[6] and worldwide it is expected that by 2025 energy demand will grow more than 50% [7], for this, they appear new types of fuels, some derived from high molecular weight hydrocarbon reserves that were discarded in the past or liquid fuels derived from organic matter transformation processes using biological or thermal technologies. These new sources of fuels present problems of direct application due to the obsolescence of the technology, since it was developed with inexhaustible resources in mind and under the panorama of change these technologies are not adequate to achieve efficient use of new resources.

On the other hand, in Colombia, obtaining fuels depends on the fossil resource, however, approximately 3 million hectares of permanent crops and annual cycles are planted, these crops are mainly coffee, rice, corn, bananas, plantains, and sugar cane. . From these cultivated hectares, about 72 million tons of organic waste can be obtained each year[8], this biomass has the potential to be transformed by biological or thermochemical routes into products of high added value, becoming a This is an issue of interest to the country because it would allow meeting the demand for fuel and improving the economy associated with the food production chain in isolated areas or areas with good availability of the residue.

1.1 **Biomass to produce chemicals and fuels**

lignocellulosic residual biomass (such as rice husk, wood residues, sugarcane bagasse among others) is present as microfibers in the cell walls of plants, it is mainly composed of 20 to 30 wt% hemicellulose and 35 to 50 wt% cellulose and 10 to 25% lignin, this mixture of macro polymers is linked by chemical interactions and

crosslinking of the microfibers. Cellulose can break down to C6 monosaccharides, hemicellulose can break down to C5 sugars, and lignin can break down to phenolic compounds such as guaiac, catechol among others.

The thermal decomposition of biomass (pyrolysis) is not a selective process but it allows obtaining liquid, solid and gaseous products that have been used for the production of fuels or chemicals using different routes to obtain them.

Biooil derived from biomass pyrolysis has become very important in recent years because its use in different fields allows closing the productive cycle of agroindustry. Thus, all the products of the agribusiness would be being used in the production of food, the generation of thermal or electrical energy, and the generation of chemical products in a wide spectrum that goes from pharmaceutical substances to fertilizers. In general, biooil derived from pyrolysis is a conglomerate of many chemical substances, mostly organic compounds, and some minerals that come from biomass[9]–[11]. This multi-component feature is responsible for some of the most unfavorable characteristics of bio-oil as a raw material for the manufacture of chemicals and fuels. Specifically, crude bio-oil has corrosive characteristics [12], it is highly heterogeneous (it presents mixtures of various physical phases) [9], it is thermally unstable, highly viscous, and with a tendency to re-polymerization on storage [13].

However, bio-oil is also one of the main alternatives as a raw material for the manufacture of chemical compounds of pharmaceutical and industrial interest. Some of its components such as levoglucosan are very attractive to the pharmaceutical industry, furfural and organic acids from acetic acid to reducing sugars such as cellovial are all some of the industrial precursors of great importance. Its use as a liquid fuel has

begun to be developed under the panorama of being a renewable fuel [11], [14]–[16]. However, there are engineering and science problems that have to be studied thoroughly. The first of them has to do with the thermal stability of the bio-oil because it has a high content of oxygenated compounds and therefore a strong tendency to polymerization inline or in the burner nozzles, which has led to the opening of a line of research related to the atomized combustion of biooil [17] and all the secondary processes necessary to improve the quality of biooil (upgrading).

1.2 **Bio-oil combustion**

In the field of bio-oil combustion, the necessary knowledge for the correct design of an adequate technology that allows taking advantage of the available energy is still under construction; Understanding the phenomena associated with the combustion of bio-oil and coupling them with a carbon capture technology such as oxy-fuel combustion will make the use of bio-oil as fuel with a low carbon footprint viable.

In liquid combustion, the determining phenomenon for correct use of energy and emission control occurs at the drop scale. There are works on this scale that have made it possible to understand the mechanism of formation, evaporation, and combustion. However, the multicomponent nature of biooil means that the theory established for other fuels cannot be extrapolated.

One of the main technologies for the combustion of bio-oil and combustible liquids, in general, is the atomization in co-flow of the fuel within a combustion chamber, this system became popular with the development of the combustion chambers of internal combustion engines. and today it is also used in most processes where the fuel is a liquid [14], [18], [19]. In the aerosol combustion of liquids, it is required to atomize the

fuel to generate a significant reduction in the size of the droplets [14], [20], [21], thus increasing the effective mass and heat transfer area to achieve complete oxidation of the fuel.

When liquid fuel is injected into a combustion chamber using an atomizer like the one presented in Figure 1-1, the liquid enters through an inner tube and the high-speed air stream generates a drag of the liquid forming a cone, which then begins a segmentation process until the size of the drops is small enough, at this point the transfer of heat from the medium into the fluid is such that it manages to break the energy barrier associated with the activation energy of the oxidation reaction and occurs the ignition process.

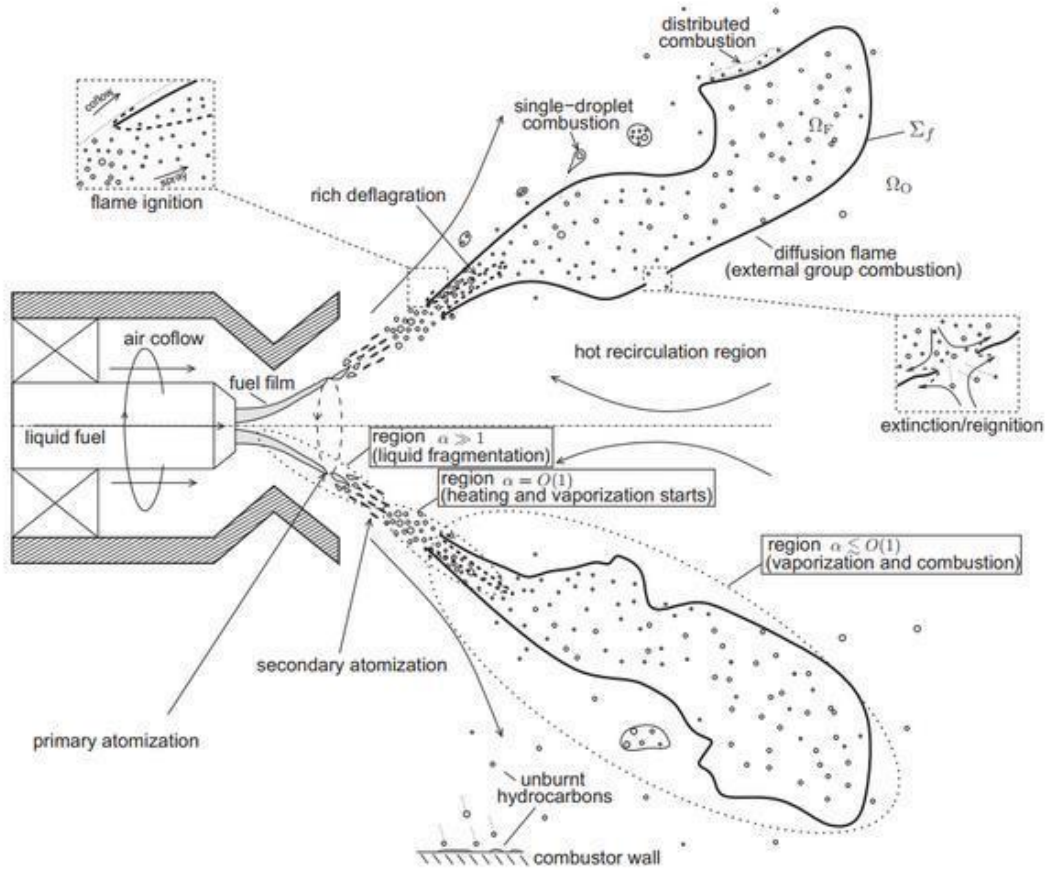

Figure 1-1 Scheme of the liquid combustion mechanism in a spray burner

The main stages of the atomization and subsequent combustion process can be summarized as an injection, fragmentation of the liquid into drops, heating, and evaporation of the surface layer of the drop, and finally ignition and combustion of the individual drops and their volatile fraction. In this combustion mechanism, the fragmentation of the fluid and the formation of droplets is the critical stage since it determines the physical characteristics of the combustion chamber and the formation of polluting gases can be associated with this stage. Some of the main problems identified in the combustion of liquids using aerosol burners are directly related to the size of the droplet, as this directly determines the rate of evaporation and ignition. To tackle this problem, nozzle designs have been proposed that seek to reduce the droplet size and form a cloud of droplets with a very uniform particle size distribution and thus achieve homogeneous combustion characteristics [22].

For the case of bio-oil combustion specifically. Its use as fuel has been limited due to the characteristics of the market (panorama of low crude oil prices), its application in other fields as a raw material for obtaining chemicals of interest in biorefineries, and due to its undesirable characteristics such as high viscosity, the high water content, the tendency to polymerization and the low calorific value, it presents [23]. However, the main efforts that have been made to use it as a fuel come from companies producing bio-oil such as Fenosa (1992), BTG (1999), Fortum (2002), and Dynamotive (2004) and VTT (2002) [11], [24].

The use of bio-oil in combustion engines, furnaces, and boilers has led to the study of its characteristics as fuel, and characteristics of the design of the nozzles or burners necessary to atomize it. The combustion of atomized bio-oil is one of the applications that most It has been sought to study because it is transversal to mass technologies of liquid combustion. Another field of interest in the research of bio-oil combustion is the

combustion of traditional fuel mixtures such as diesel or kerosene with bio-oil to improve their combustion performance [20]. It is relevant to mention that bio-oil combustion studies lead to the characterization of oxidation product species, to characterize the hydrodynamics of the reactive flow, the heat transfer product of the reaction, and the combustion dynamics at the drop scale.

Previous research on the combustion of pure fuel droplets has led to the development of models of vaporization and combustion of fuel droplets, allowing the understanding of the dynamics of the process. However, the potential that shows the possibility of using high molecular weight fossil fuels, such as shale oil, bio-oils, water/oil mixtures, coal / liquid fuels, and other substitutes for homomolecular fuels, requires taking into account the effects of multi-component interactions on combustion.

To understand the mechanism C. K Law [25] proposes three important factors to take into account:

- Relative concentrations and volatilities of the liquids in the mixture.
- The miscibility of the constituents of the liquid. This controls the phase shift characteristics. For example, the partial pressure of a miscible fuel mixture is strongly modified when it is emulsified in a small proportion with water.
- The intensity of movement within the liquid, this influences the speed with which liquid components can break the surface where gasification takes place.

The combustion characteristics of a multi-component droplet can be described in two ways as a function of the internal mixing rate: the first (called diffusion limit) in which there is no internal movement and the active transport mechanism is diffusion, and the second (distillation limit) postulates that mixing occurs too fast such that the states within the drop are always homogeneous.

The first case requires understanding that there is no circulation within the drop and that the diffusion of liquids is not equated with the rate of evaporation, so composition and stratification changes occur on the surface of the drop as well as negligible changes in composition in the inner core, the composition stratification that appears charged with itself, the occurrence of the phenomenon of micro-explosions, this occurs because on the surface there is a high concentration of a non-volatile compound with a high boiling point. When the drop is subjected to heating, the outer part has not yet volatilized, while the highly volatile substances inside have already done so and reached a superheat close to the boiling temperature, nucleating and raising the internal pressure until the drop explodes.

At the end of the nineties and beginning of the 2000s, research on the combustion of bio-oil droplets focused on evaluating the physical parameters such as droplet size, ignition temperature, and the mechanism of de-volatilization before the droplet ignited, for this, they used Three types of technologies or experimental routes, the first called Entrained Flow reactor, in this reactor the drop falls through a hot chamber above the ignition point and its path is followed using optical techniques to measure its characteristics. The second technology developed at that time is the drops suspended in fibers, this technique has experimental advantages since it allows to directly measure the history of the dropping temperature during the combustion process, however, as the drop is smaller, the Fibers present interference due to surface phenomena such as capillarity.

Finally, there are thermogravimetric techniques that offer the possibility of knowing the mass loss through a controlled heating rate. However, these combustion measurement techniques do not allow simulating real heating atmospheres such as those that occur inside a combustion chamber (high heating rates> 500 °C / s) and it

has been one of the main limitations. Its application allowed the development of studies on the oxidation kinetics of biooil and currently, they are used

As previously shown, one of the most important stages in the combustion of liquids is the formation of droplets and their subsequent ignition and combustion. Drop-scale studies have made it possible to identify some of the main mechanisms associated with bio-oil combustion and its relationship with the formation of pollutants.

The experimental work carried out by Shaddix [26] proposed to study the combustion of bio-oil / methanol mixtures at a drop scale, justifying that this stage is the fundamental one in the macroscopic process. Their study allowed identifying three important aspects:

- The multicomponent characteristic of bio-oil and the presence of water in it favors the formation of micro-explosions. That their formation mechanism is a nucleation process that occurs inside the drop due to sudden heating.
- Micro-explosions occur when the liquid reaches a superheating limit. Superheating occurs in substances that have a wide range of components. When the drop begins to heat up, heat transfer occurs at a higher rate than mass transfer (diffusion) processes and volatilization occurs within the drop, causing the internal pressure of the drop to increase until it explodes.
- The presence of particulate material within the bio-oil drop generates nucleation points that favor the formation of microbubbles and therefore the formation of micro-explosions.

Along the same lines, droplet-scale experimentation focuses on the understanding of combustion processes. the work of Teixeira [27], [28] who studies biooil microexplosions using high-speed cameras. In his experiment he drops a drop of oil on a ceramic plate with a controlled temperature, the drop lands on the plate and he

obtains the photographic record at a high-speed phenomenon. As can be seen in Figure 1-2

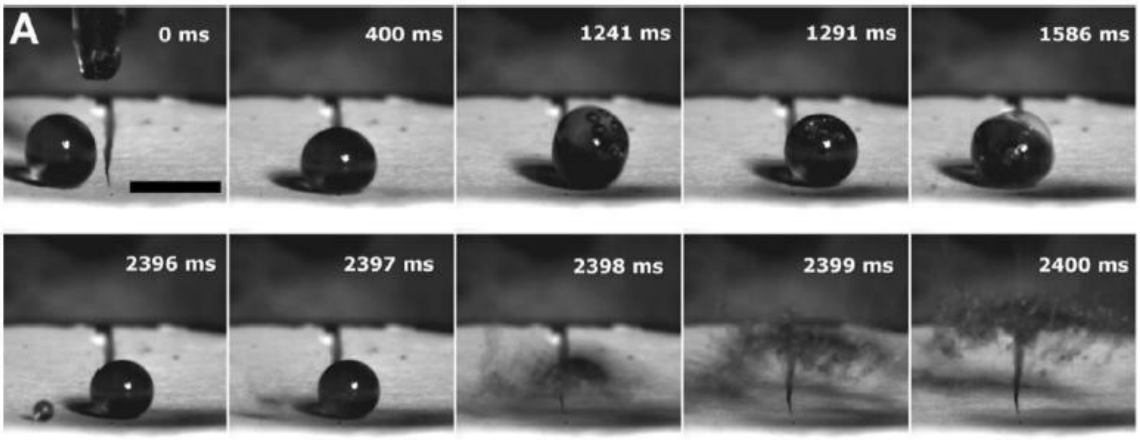

Figure 1-2 micro-explosions of bio-oil droplets [28]

In the Teixeira and Shaddix experiments, the volatilization stage of the bio-oil droplets is directly related to the speed of reduction in the diameter of the droplets. In the square diameter law model, the evaporation dynamics is characterized by the constant of evaporation [29], [30], and although there is a theory to determine the values of the constant based on the experimental evaporation rate, the model does not consider the possibility of microexplosions formation nor the formation of cenospheres.

2.2.2 Mathematical models for bio-oil combustion

Generalized models for the combustion of liquids, such as the classic model of spray or droplet combustion presented by Kee [31], coupled with kinetic models such as those developed by Ranzi [32] and Deviagui [33]. And together with the devolatilization and vaporization models of Branca [18] allow the macroscopic study of bio-oil combustion. However, the phenomenological knowledge on the combustion of bio-oil droplets is still very limited.

One of the drop-scale models that allow the integration of the chemical composition with the formation of aerosols ejected from a drop of liquid cellulose during a heating process is the model proposed by Teixeira [34]who, using a CFD technique for a system with variable volume manages to explain how the aerosol is ejected from the molten cellulose drop; The phenomenon represented occurs when the microbubble inside the drop approaches the surface, it breaks the surface and generates the ejection of liquids and vapors as can be seen in Figure 1-3.

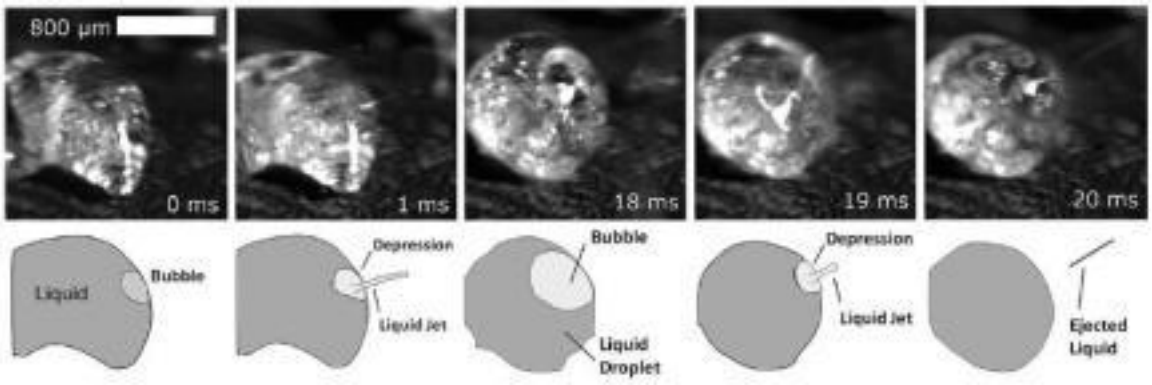

Figure 1-3 Explosión de una burbuja en una gota de celulosa fundida y eyección de líquidos [34]

The solution strategy of the CFD model with mobile borders that are necessary to characterize the ejection of the liquid requires the implementation of transport and capillarity models in a volume of Eulerian fluid (VOF) as a methodology to achieve correct modeling and solution of the equations of Navier-Stocks for compressible fluids. Then, experimentally, he correlates the changes in viscosity of the main substances found in a bio-oil, cellulose, hemicellulose, and levoglucosan concerning temperature and performs the simulations with the new values of viscosity and surface tension. This model seeks to get closer to the effect that chemical compounds have on the phenomenon of microexplosion.

1.3 **Dissertation structure**

In the chapter entitled "**Effect of Carbon Dioxide Environment on the Thermal Behavior of Sugarcane Pyrolysis Oil**, the results of the characterization that was carried out on bio-oil produced by pyrolysis of sugarcane bagasse are presented. This bagasse was characterized using a set of techniques including ESI (-) - FT-ICR-MS which allowed us to analyze the complexity of the bio-oil obtained.

Specifically, The ESI (-) - FT-ICR-MS analysis allows us to observe that chemical compounds with six oxygen atoms in their structure, representing 35.46% of all the molecules identified in the bio-oil, and 10% of all oxygenated compounds have more than ten oxygen atoms in their structure. There is evidence to show that oligomers with high molecular weight and a large number of oxygens in their structure are involved in dehydration reactions, thereby forming structures of greater molecular weight.

The results of the carbonization of bio-oil in a nitrogen atmosphere and in CO2 are also presented to simulate the effect of the oxy-fuel atmosphere, although a considerable increase in the production of char was not found during the thermal decomposition in carbon dioxide. , it was possible to identify that the degree of saturation and condensation of the char obtained is greater than when it is obtained in nitrogen, in practical terms this can be understood that the chemical reactivity of the biochar obtained in a carbon dioxide atmosphere is more thermally stable, which results in that char formed as unburned within a combustion chamber will not achieve a thermal transformation.

On the path of understanding how the thermal decomposition and combustion of bio-oil process is, in chapter 3 entitled "**Investigation into the pyrolysis and combustion of bio-oil from sugarcane bagasse: Kinetics and evolved gases using TGA-FTIR"** the analysis of the gases released during thermal decomposition at low heating rates, this to ensure kinetic regime.

The gases produced by thermal decomposition were analyzed online in an infrared spectrophotometer with Fourier transform FTIR, which allowed to identify the formation of permanent gases such as carbon dioxide, carbon monoxide, methane and water. Likewise, the evolution of the different stages of thermal decomposition of bio-oil during combustion is presented and the kinetic energy of the global process was estimated using the kinetic model of Miura and Maki, with this it was possible to have a compression of like the innumerable Parallel decomposition and oxidation reactions occur, especially it is interesting to see how the oxygen adsorption stage after the degradation of the fuel in an air atmosphere occurs.

From the kinetic analysis it was concluded that the thermal decomposition of the compounds present in the bio-oil leads to the formation of high molecular weight organic structures (char). These organic structures interact with the oxygen present in the air and this is absorbed at the surface as a previous step to oxidation at high temperatures. The Miura and Maki method is suitable for this analysis, since it allowed determining that the activation energy during the devolatilization stage for a heating rate of 5 ° C / min varies between 50 and 100 kJ / mol. The decomposition stage of the fuel has a maximum activation energy value to be reached of 176 kJ / mol, and in the case of high temperatures oxidation the maximum energy that must be reached to trigger the oxidation is 320kJ / mol.

Having described the global kinetic behavior of bio-oil, drop-scale measurements of the thermal decomposition in nitrogen atmospheres and air of bio-oil droplets were carried out in chapter 4 entitled "**An investigation into the break-up modes of bio-oil droplets from sugarcane bagasse in air and nitrogen atmosphere** "presents an experimental setup to measure the evolution of the drop diameter during heating, to identify the modes, a contour recognition software was developed and the results of the experiments carried out in air and in nitrogen were presented, the events of rupture of the drop due to the formation of internal bubbles were shown and the

intensity of the events was measured using image analysis. As shown in figure 1.4

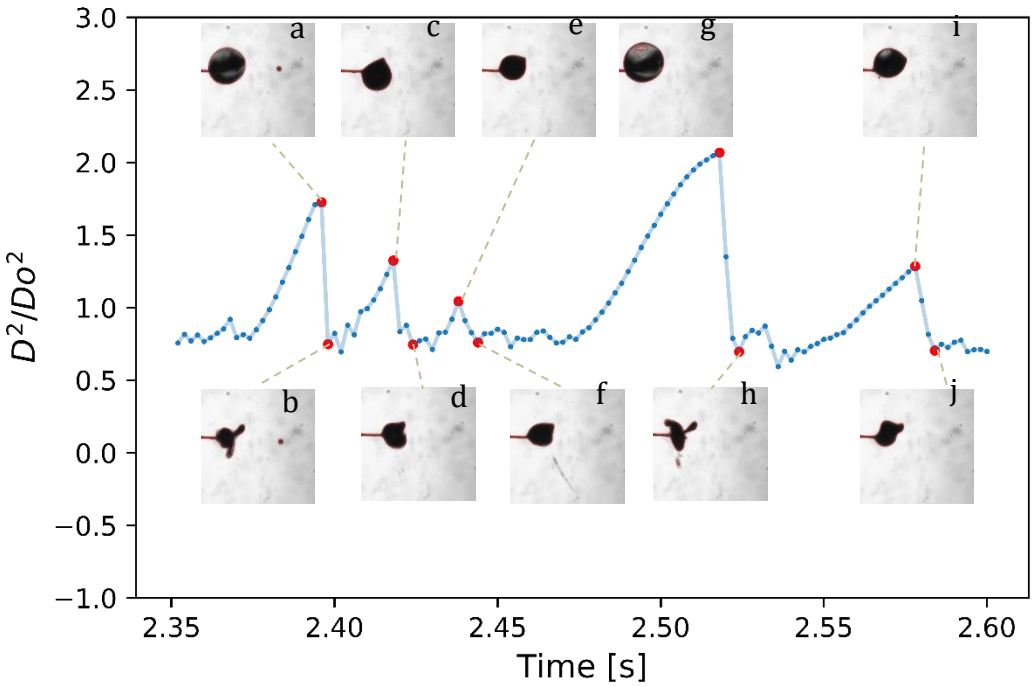

Figure 1-4 D^2/D_0^2 evolution for bio-oil droplets suspended in platinum bare in 560°C air atmosphere, description of break-up events

As a result of this chapter, three important findings can be concluded

- High magnitude events during pyrolysis and combustion have a low frequency of occurrence and are visible in the first seconds of the experiment where the viscosity of the liquid is still low, the magnitude of the events is also related to the speed of volatile formation and is strongly influenced by heat transfer. which is affected by the outer layer of the drop formed by the vapors and their differences in thermal properties
- The formation of disruptive events always starts from the formation of bubbles inside the drop, the formation of bubbles is the key factor in the event of breaking of the drop if the time that the bubble remains inside the drop is very high pressure will increase sufficiently to break the barrier that covers the surface.

- In the last stage of pyrolysis, the formation of Char could be measured, this char obtained after the pyrolysis process and the degradation and volatilization of many compounds products of pyrolysis is the result of the formation of porous carbonaceous structures formed by the swelling of a high molecular weight polymer that comes from.

And finally, the chapter entitled "**On the modeling of the micro-explosions during the evaporation and pyrolysis of a bio-oil droplet**" is presented, where a proposal for a new mathematical model based on the appearance of bubbles within the drops of fuel while it is being heated.

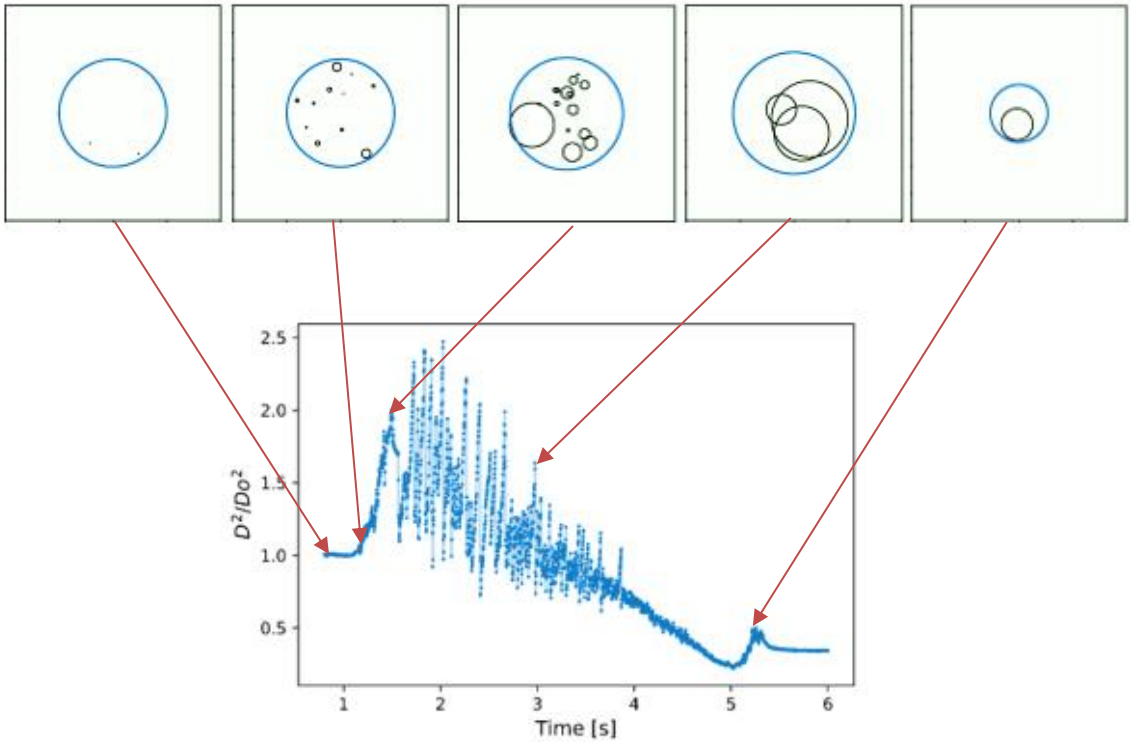

Figure 1-5 D^2/D_0^2 evolution for bio-oil droplets suspended in platinum bare in 560°C air atmosphere

The theoretical representation of the growth of bubbles in a ideal spherical drop is shown in Figure 1-5 in which the theoretical behavior is correlated with the experimental one. The model developed takes into account the coalescence and the time that the bubbles take on the surface as a tool to predict their behavior.

This model is a new position different from the traditional one in which disruptive events are quantified and these have tried to be expressed as functions of the physical properties of the fuel, in this model the formation of microexplosions is explained starting from the formation of bubbles in the inside the drop, while the bubbles travel through the liquid of the drop and it evaporates superficially. This new model allows it to be extrapolated to different fuel mixtures and becomes a contribution to the field of micro-explosion studies.

1.4 References

[1] "3rd International Conference on Energy and Environmental Protection, ICEEP 2014," *Adv. Mater. Res.*, vol. 953–954, 2014.

[2] R. Global, G. Gas, and E. Pathways, "What are the effects of global warming ?," in *Reaching Net Zero*, 2020, pp. 75–98.

[3] M. B. Toftegaard, J. Brix, P. A. Jensen, P. Glarborg, and A. D. Jensen, "Oxy-fuel combustion of solid fuels," *Prog. Energy Combust. Sci.*, vol. 36, no. 5, pp. 581–625, 2010, doi: 10.1016/j.pecs.2010.02.001.

[4] V. Daioglou, J. C. Doelman, B. Wicke, A. Faaij, and D. P. Van Vuuren, "Integrated assessment of biomass supply and demand in climate change mitigation scenarios," *Glob. Environ. Chang.*, vol. 54, no. April 2018, pp. 88–101, 2019, doi: 10.1016/j.gloenvcha.2018.11.012.

[5] T. Wilberforce, A. G. Olabi, E. Taha, K. Elsaid, and M. Ali, "Science of the Total Environment Progress in carbon capture technologies," *Sci. Total Environ.*, no. xxxx, p. 143203, 2021, doi: 10.1016/j.scitotenv.2020.143203.

[6] J. Meng, X. Hu, P. Chen, D. M. Coffman, and M. Han, "The unequal contribution to global energy consumption along the supply chain," *J. Environ. Manage.*, vol. 268, no. February, p. 110701, 2020, doi: 10.1016/j.jenvman.2020.110701.

[7] A. J. Ragauskas *et al.*, "The Path Forward for Biofuels," *Science (80-.).*, vol. 484, no. 311, 2006, doi: 10.1126/science.1114736.

[8] UPME, *Atlas del Potencial Energético de la Biomasa Residual en Colombia*. 2015.

[9] A. Oasmaa, I. Fonts, M. R. Pelaez-Samaniego, M. E. Garcia-Perez, and M. Garcia-Perez, "Pyrolysis Oil Multiphase Behavior and Phase Stability: A Review," *Energy and Fuels*, vol. 30, no. 8, pp. 6179–6200, 2016, doi:

10.1021/acs.energyfuels.6b01287.

[10] J. I. Montoya *et al.*, "Bio-oil production from Colombian bagasse by fast pyrolysis in a fluidized bed : An experimental study," *J. Anal. Appl. Pyrolysis*, vol. 112, pp. 379–387, 2015, doi: 10.1016/j.jaap.2014.11.007.

[11] S. Y. No, "Application of bio-oils from lignocellulosic biomass to transportation, heat and power generation - A review," *Renew. Sustain. Energy Rev.*, vol. 40, pp. 1108–1125, 2014, doi: 10.1016/j.rser.2014.07.127.

[12] A. K. Hossain and P. A. Davies, "Pyrolysis liquids and gases as alternative fuels in internal combustion engines - A review," *Renew. Sustain. Energy Rev.*, vol. 21, pp. 165–189, 2013, doi: 10.1016/j.rser.2012.12.031.

[13] F. Yu *et al.*, "Physical and chemical properties of bio-oils from microwave pyrolysis of corn stover," *Appl. Biochem. Biotechnol.*, vol. 137–140, no. 1–12, pp. 957–970, 2007, doi: 10.1007/s12010-007-9111-x.

[14] J. L. Zheng and Y. P. Kong, "Spray combustion properties of fast pyrolysis bio-oil produced from rice husk," *Energy Convers. Manag.*, vol. 51, no. 1, pp. 182–188, 2010, doi: 10.1016/j.enconman.2009.09.010.

[15] R. H. C. R. Shaddix, D, "Combustion Properties of Biomass Flash Pyrolysis Oils : Final Project Report," 1999.

[16] J. Shankar, T. Idaho, W. Idaho, R. Hess, I. National, and A. View, "A Review on Biomass Densification for Energy Applications," *Idaho Natl. Lab.*, no. May 2014, pp. 1–73, 2011.

[17] J. Lehto, A. Oasmaa, Y. Solantausta, M. Kytö, and D. Chiaramonti, "Fuel oil quality and combustion of fast pyrolysis bio-oils," *VTT Publ.*, no. 87, p. 79, 2013, doi: 10.1016/j.apenergy.2013.11.040.

[18] C. Branca and C. Di Blasi, "Multistep mechanism for the devolatilization of

biomass fast pyrolysis oils," *Ind. Eng. Chem. Res.*, vol. 45, no. 17, pp. 5891–5899, 2006, doi: 10.1021/ie060161x.

[19] M. Garcia-Perez *et al.*, "Evaporation and combustion characteristics of biomass vacuum pyrolysis oils," *IFRF Combust. J.*, vol. 200601, no. 200601, pp. 1–27, 2006.

[20] S. I. Yang, T. C. Hsu, and M. S. Wu, "Spray combustion characteristics of kerosene/bio-oil part II: Numerical study," *Energy*, vol. 115, pp. 458–467, 2016, doi: 10.1016/j.energy.2016.09.047.

[21] P. Tóth, Y. Ögren, A. Sepman, T. Vikström, P. Gren, and H. Wiinikka, "Spray combustion of biomass fast pyrolysis oil : Experiments and modeling," *Fuel*, vol. 237, no. May 2018, pp. 580–591, 2019, doi: 10.1016/j.fuel.2018.10.031.

[22] J. A. Bossard and R. E. Peck, "Droplet Size Distribution Effects in Spray Combustion," *Proc. Combust. Inst.*, vol. 26, no. Mmd, p. 1671, 1996.

[23] J. Lehto, A. Oasmaa, Y. Solantausta, M. Kytö, and D. Chiaramonti, "Review of fuel oil quality and combustion of fast pyrolysis bio-oils from lignocellulosic biomass," *Appl. Energy*, vol. 116, pp. 178–190, 2014, doi: 10.1016/j.apenergy.2013.11.040.

[24] G. Anitescu and T. J. Bruno, "Liquid biofuels: Fluid properties to optimize feedstock selection, processing, refining/blending, storage/transportation, and combustion," *Energy and Fuels*, vol. 26, no. 1, pp. 324–348, 2012, doi: 10.1021/ef201392s.

[25] C. K. Law, "Mechanisms of droplet combustion C.," Illinois, 1982.

[26] C. R. Shaddix and P. J. Tennison, "Effects of Char Content and Simple Additives on Biomass Pyrolysis Oil Droplet Combustion," pp. 1907–1914, 1998.

[27] A. R. Teixeira *et al.*, "Aerosol generation by reactive boiling ejection of molten cellulose," *Energy Environ. Sci.*, vol. 4, no. 10, pp. 4306–4321, 2011, doi:

10.1039/c1ee01876k.

[28] A. R. Teixeira *et al.*, "Microexplosions in the upgrading of biomass-derived pyrolysis oils and the effects of simple fuel processing," *ACS Sustain. Chem. Eng.*, vol. 1, no. 3, pp. 341–348, 2013, doi: 10.1021/sc300148b.

[29] C. H. Wang, X. Q. Liu, and C. K. Law, "Combustion and microexplosion of freely falling multicomponent droplets," *Combust. Flame*, vol. 56, no. 2, pp. 175–197, 1984, doi: 10.1016/0010-2180(84)90036-1.

[30] C. Call, D. L. Zhu, C. K. Law, and S. C. Deevi, "Combustion and microexplosion of han-based liquid gun propellants at elevated pressures," *J. Propuls. Power*, vol. 13, no. 3, pp. 448–450, 1997, doi: 10.2514/2.5185.

[31] R. J. Kee, *REACTING FLOW CHEMICALLY Theory and Practice*. WILEY INTERSCIENCE.

[32] E. Ranzi, M. Corbetta, F. Manenti, and S. Pierucci, "Kinetic modeling of the thermal degradation and combustion of biomass," *Chem. Eng. Sci.*, vol. 110, pp. 2–12, 2014, doi: 10.1016/j.ces.2013.08.014.

[33] P. E. A. Debiagi *et al.*, "Detailed kinetic mechanism of gas-phase reactions of volatiles released from biomass pyrolysis," *Biomass and Bioenergy*, vol. 93, pp. 60–71, 2016, doi: 10.1016/j.biombioe.2016.06.015.

[34] A. R. Teixeira *et al.*, "Aerosol generation by reactive boiling ejection of molten cellulose," *Energy Environ. Sci.*, vol. 4, no. 10, p. 4306, 2011, doi: 10.1039/c1ee01876k.

2 Effect of Carbon Dioxide Environment on the Thermal Behavior of Sugarcane Pyrolysis Oil

The gradual reduction of cheap high-quality petroleum sources with the consequent increase in petroleum extraction and refining cost are important drivers for the increased interest in alternative sources of fuel production. Biomass represents 12.8% of the world's energetic matrix and it is mainly used for electricity (0.4%), transport (0.9%), industry heat (1.4%), and district heat (9.2%) [1]. Liquid bio-oil from biomass pyrolysis provides a great opportunity for countries like Colombia where waste biomass from palm oil residue, sugar cane bagasse, banana trunks and fiber, and the coffee residue is more than 50 million tons per year [2]. Of this, less than 30% is used to produce fuels today.

Bio-oil from biomass pyrolysis is a complex mixture of organics (sugars, esters, furans, acids, ketones, alcohols, phenols, guaiacols, etc.)[3,4]. The presence of acidic compounds and heavy oligomers is responsible for bio-oil high viscosity and acidity. This mixture of reactive oxygenated groups is prone to condensation reactions to form high molecular weight carbon precursors. The reduction in the content of light molecules and the formation of water and high molecular weight oligomers induce phase separation during storage [5].

Bio-oil composition and physicochemical properties are directly linked with biomass feedstock make-up, pyrolysis conditions (temperature, pressure, residence time), and condensation parameters[5–8]. The yield of pyrolysis oil can be described using global models to predict product distribution from cellulose, hemicellulose, and lignin. The

mechanism for cellulose decomposition proposed by Chaiwat et al. [9] showed the structure cellulose is modified by the competition of dehydration and glycosidic cleavage reactions to form partially cross-linked precursors, which are transformed in decomposition products as levoglucosan and furfural, gases as carbon dioxide, and solids by carbonization way. The decomposition of cross-linked precursors begins with the transformation of OH cellulose groups into the water, then the de-polymerization and release of light compounds take place, and finally, the carbonization of high molecular weight aromatic compounds is carried out. Low heating rates favor the dehydration reactions forming new compounds with higher molecular weight.

During the spray combustion of bio-oil, 60% of the weight is released by evaporation and cracking mechanism. Then the fixed carbon is formed by re-polymerization reactions [10,11] while the oxygenated compounds bonded to aromatic structures and high temperature allow the dehydration reactions to the formation of polyaromatic compounds [12], and the follow coke structures formation which one is modified strongly by the heating rate [11,13].

Oxy-fuel combustion is one of the most promising technologies for carbon capture and storage. This technology uses a mixture of recycled carbon dioxide and oxygen for fuel combustion and it has been widely studied and applied to carbon-based power plants. [14,15] The implementation of carbon dioxide allows flame temperature control and reduces NO_x formation. Ahmed et al. [16] and Wang et al., [14], examined numerically and experimental the oxy-fuel combustion in a burner of heavy oil. Their results showed a reduction in NO_x formation with the production of flue gas with CO_2 concentrations higher than 95% of volumetric concentration, making the sequestration process technically viable.

On the other hand, The presence of CO_2 during the pyrolysis of lignocellulosic material has an impact on the yield and chemical characteristics of char and liquids produced [17–20], for example, Seneca et al. [17,20] showed that carbon dioxide accelerates the thermal decomposition of the hemicellulose. Also, carbon dioxide modifies the chemical characteristics of the char and the liquids obtained after pyrolysis increasing the number of compounds with more than three aromatic rings in their structure [21].

Considering that there is limited knowledge of the use of pyrolysis oils in oxy-fuel combustion, their thermal behavior in the presence of carbon dioxide warrants further investigation.

2.1 Material and Methods

2.1.1 Experimental setup

The bio-oil studied in this manuscript was produced from sugar cane bagasse (SCB) from sugarcane mill Risaralda, Colombia. A detailed physicochemical characterization of this material was published elsewhere [15]. The bio-oil was produced in a spoon (see Figure 1) using a horizontal electric furnace of 30 cm in length. A quartz tube of 3 cm in diameter was placed inside the furnace, A flow of 50 cm^3/min of N_2 provided an inner atmosphere, and like a carrier gas, the temperature of the furnace was set in 550°C. This temperature was chosen from previous work on SCB pyrolysis [22]. When the temperature was stable, a stainless-steel spoon with 1.5 g of SCB was introduced into the hot zone reaching heating rates between 100 and 200 °C/s and an estimated residence time of 50 s for the gases and vapors released, and products from the reactions were immediately condensed in a U-type stainless-steel trap, submerged in an ice bath. A similar experimental set-up was reported elsewhere [23,24].

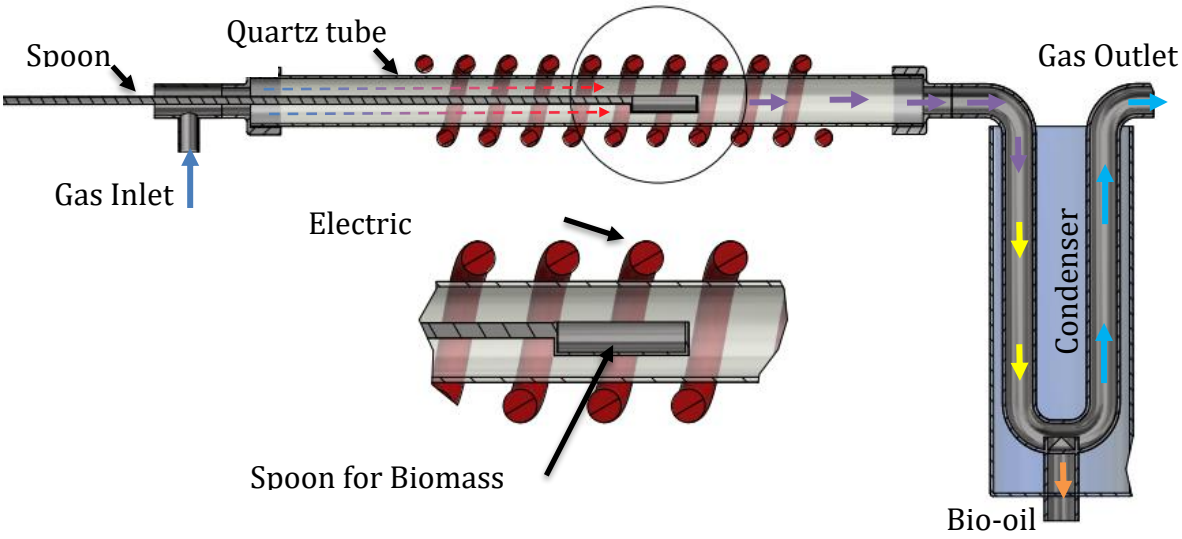

Figure 2-1. Experimental model for bio-oil production and char collection setup

2.1.2 Char samples preparation

The char samples were collected after pyrolysis, with controlled conditions in the model previously described. The furnace heating rate was set at 10°C/min., from room temperature to 900°C, the flow of N_2 and CO_2 was set in 50 ml/min. and maintained during the entire run. A sample of 2 ml of bio-oil was placed in the stainless-steel spoon at room temperature inside the furnace. Char material was sampled when the sample reached the desired temperature (400 and 700 °C), then the spoon was quickly removed from the hot zone and cooled in the same atmosphere using an ice bath.

2.1.3 Bio-oil Characterization

Due to the complexity of the mixture of organic compounds in bio-oil and the wide range of molecular mass distribution, a quantitative macro analysis (Elemental analysis, Karl-Fischer titration) coupled with qualitative techniques (GC-MS-FID, ESI-FT-ICR MS) was used to determine the composition and molecular parameters of the bio-oil studied.

***GC-MS-FID Characterization*:** A qualitative gas chromatography/mass spectrometry (GC-MS) analysis was performed in a THERMO Trace GC Ultra with MS DSQ II, the system was fitted with a flame ionization detector (FID) to integrate the main identified light compounds in bio-oil. Liquid samples were filtered and diluted with methanol (1:10). The capillary column was a DB-Petro (50 m × 0.25 mm ID × 0.50 µm film thickness) with helium as a carrier gas with a flow of 2.3 ml/min. First, the oven was set with a temperature was of 40°C (4 min), followed by a heating rate of 1°C/min up to 55°C; the second heating rate was 2°C/min to 185°C, then 10°C/min to 250°C; finally, when the temperature reached 250°C, it was maintained for 60 minutes. The temperature of the injector, the ion source, and the transfer line was maintained at 300, 230, and 280 ºC respectively. A sample volume of 1 µl was injected applying 1:7 split mode. After a solvent delay of eight minutes, a full mass spectrum was obtained. The MS was operated within a positive electron ionization mode and an m/z range from 30 to 500 was scanned. The voltage applied to the multiplier detector was 1275 V to obtain the total ion chromatograms (TICs) using a full-scan acquisition method whit a scan velocity of 1600 µ/second. The identification of peaks was based on computer matching of the mass spectra with that in the NIST library.

ESI-FT-ICR: The bio-oil sample was analyzed using a SolariX XR Fourier Transform Ion Cyclotron Resonance Mass Spectrometer (Bruker Daltonik GmbH, Bremen, Germany), equipped with a 9.4 T superconducting magnet and an analyzer Paracell. 50 µL bio-oil is dissolved in 5 mL of dichloromethane to form the sample solution, which is further diluted in methanol (5ppm). The instrument was operated under ESI (-) ionization source, with the infusing flow rate of 10 µL/min. The instrument was externally calibrated with sodium formate within the mass range of 154-1150 Da and 8 M data points, and the data were acquired with the same mass range and data size, 300 scans were accumulated for each acquisition. For ESI settings, the temperature of the vaporizer was set at 240 °C, drying gas temperature at 200 °C, the pressure of the nebulizer at 1 bar. The resulted mass spectrum was internally calibrated with known

homologous series and the overall mass accuracy was less than 0.5 ppm. The calibrated data were further analyzed by PetroOrg software. The peaks, which can be assigned a unique chemical formula within the chemical formula range of C1-100 H1-200 O0-10 N0-6 with a mass error lower than 0.5 ppm, were further discussed. The aromaticity of the bio-oil was deduced from double bond equivalents (DBE) value using the following equation: $DBE = c - h/2 + n/2 + 1$, where c, h, and n are the numbers of carbon, hydrogen, and nitrogen atoms, respectively, in the molecular formula.

TGA-DSC Pyrolysis study: A TGA-DSC pyrolysis test was performed in a Linseis STA PT1600-furnace L75/230 with a range of operation that varied from room temperature to 900°C. A heating rate of 10°C/min was set, and the flow mass control was maintained in 50 ml/min during all the testing. N_2 and CO_2 gases were used as the surrounding gas. In each test, 10 mg of sample was placed into the furnace and flushed with N_2 or CO_2 for 20 min to displace the remnant oxygen in the furnace. Each thermogram was repeated three times and the average found was implemented to assess the results.

FTIR: The characterization of the chemical structure of the char samples was carried out the using a Fourier-transform infrared (FTIR) spectrometer, Shimadzu brand, model IRTracer-100, with DLATGS detector and laser He/Ne, typically KBr pellets were prepared with a 2% sample, and for each sample, 30 spectra between 4000 to 400 cm-1 with 2 cm-1 as resolution were accumulated and averaged. The results were reported in absorbance as the average of tree samples at the same temperature.

2.2 Results and Discussion

2.2.1 Bio-oil characterization

Bio-oil from SCB showed an organic phase content (free of water) of carbon (46.6 wt. %), hydrogen (2.3 wt. %), nitrogen (0.14 wt. %), oxygen (14.6 wt. %), and a very low percentage of sulfur (0.09 wt. %). These values were within the range of bio-oil from biomass pyrolysis [7,25–27]. Also, an important characteristic of the bio-oil is the amount of oxygen because its stability is related to the oxygenated groups. On the other hand, a 32.5 ± 2 % content of water in the bio-oil, measured by Karl-Fischer, could be explained as a result of the low heat velocity at pyrolysis as well as large particles and large residence time of the vapors.

The species composition of the bio-oil was analyzed in gas chromatography coupled to mass spectrometry (GC-MS-FID) to determine the main organic compounds. Figure 2 shows a typical chromatogram. Table 1 lists those, which were the most likely to be identified by the MS search file (HP-ChemStation).

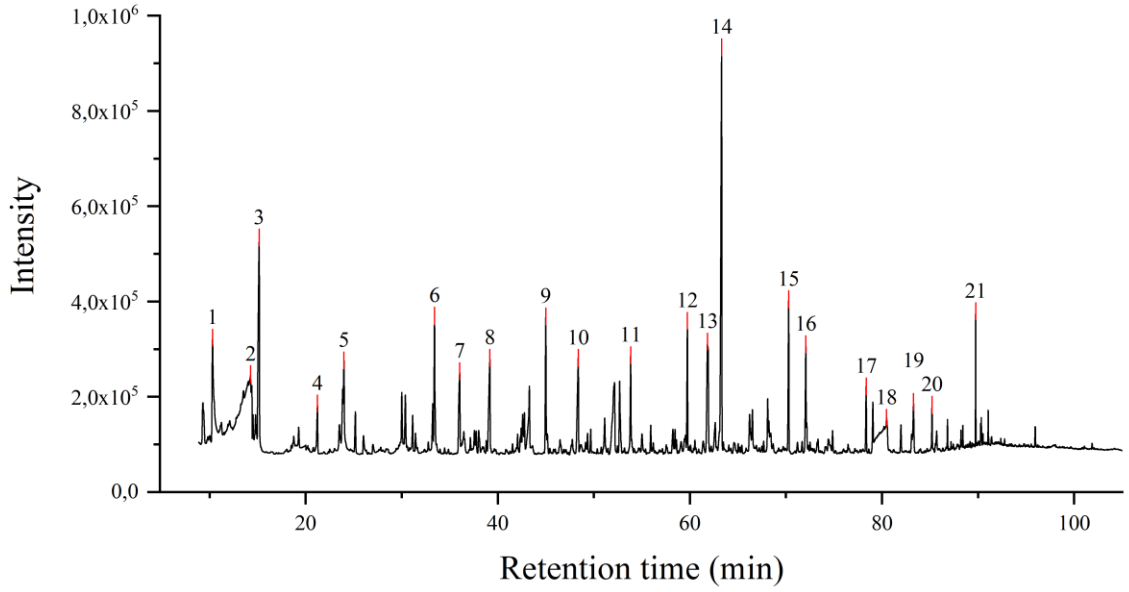

Figure 2-2. GC-MS-FID chromatogram for SCB bio-oil

A semi-quantitative analysis shows that the area of the peaks in Table 2-1 represents approximately 65% of the total area of the peaks quantified during the GC-MS-FID test. Acetic acid, 2,3-dihydrobenzofuran, 1-hydroxy-2-propanone, 2-ethoxyphenol, furfuryl alcohol, hydroxy acetaldehyde, and, 1,6-anhydro-β-D-glucopyranose are the most important ones found in this fraction as other authors have reported [20]. On the other hand, the presence of oxygenated compounds is a characteristic of the bio-oil from biomass, and they were identified from this analysis.

Table 2-1 Principal compounds identified in bio-oil GC -MS -FID

Index	Retention time (min)	Area (%)	Probable substance
1	10.3	3.3	hydroxyacetaldehyde (glycolaldehyde)
2	14.3	10.3	acetic acid
3	15.2	5.7	1-hydroxy-2-propanone (acetol)
4	21.2	0.7	glycerin

5	24.0	2.7	1-hydroxy-2-butanone
6	33.4	3.5	furfuryl alcohol
7	36.0	2.9	2(5H)-furanone
8	39.2	2.7	2-hydroxy-2-cyclopenten-1-one
9	45.0	2.5	phenol
10	48.4	2.3	2-hydroxy-3-methyl-2-cyclopenten-1-one
11	53.8	1.8	2-methoxyphenol
12	59.7	2.5	4-ethylphenol
13	61.8	3.5	2-ethoxyphenol
14	63.3	9.3	2,3-dihydrobenzofuran (Coumaran)
15	70.3	2.4	2-methoxy-4-vinylphenol
16	72.1	2.1	2,6-dimethoxy-phenol
17	78.3	0.9	1,2,4-trimethoxybenzene
18	80.5	3.2	1,6-anhydro-β-D-glucopyranose (Levoglucosan)
19	83.3	1.3	hexahydro-4,4,7a-trimethyl-2(3H)-benzofuranone
20	85.2	0.5	4-chromanediol 2-(3,4-dimethoxyphenyl)-6-methyl-3
21	89.8	0.9	2,6-dimethoxy-4-(2-propenyl)-phenol

The bio-oil has a broad distribution of compounds from low molecular to high molecular weight such as pyrolignic or poly-sugars compounds, which are not possible to identify in GC-FID-MS. For this reason, ESI(-)-FT-ICR analysis was used to determine molecular compounds over a broad spectrum. Figure 2-3 shows the ESI(-)-FT-ICR mass spectra for the SCB bio-oil. The ESI(-)-FT-ICR analysis depicts the distribution of polar species with high molecular weight (mainly oxygen-containing compounds derived from the cellulose, sugars, and lignin pyrolysis that gas chromatography cannot identify[28,29]). Values of m/z are between 150 and 800 Da represent the 80% of the cumulative mass as report elsewhere [13,30], reaching a molecular weight average close to 539 Da, and, the $C_zH_wO_xN_y$ compounds represent 75 % of the total compounds identified.

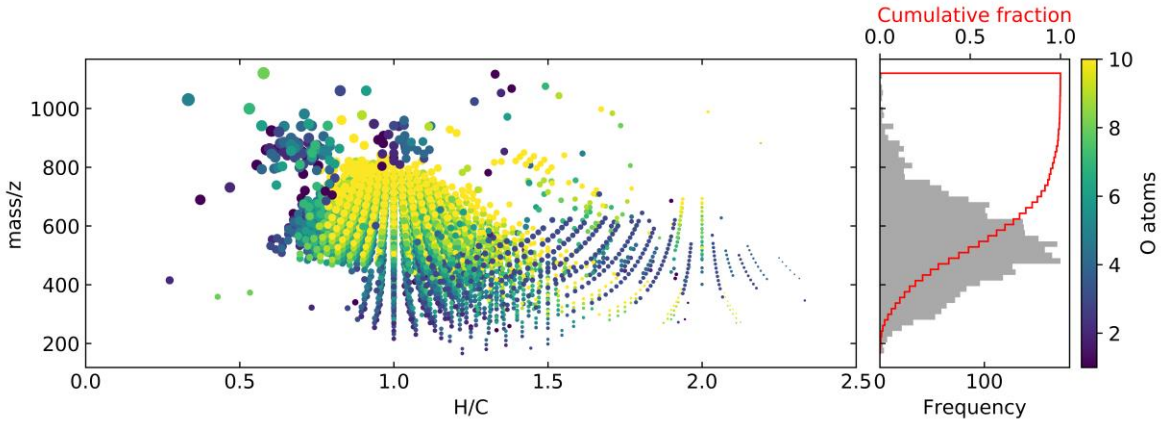

Figure 2-3. ESI (-)-FT-ICR-MS mass/z vs. H/C ratio for SCB bio-oil

Figure 2-4 shows the Van-Krevelen diagram, which reveals the distribution of compounds using the atomic ratio between hydrogen/carbon and oxygen/carbon. The upper histogram of figure 4 shows that the O/C relationship has a bimodal distribution, the first peak appears around a relationship of O/C = 0.1 and the second round a relation of 0.2, and in the histogram, on the right side of figure 4, it can be seen that the data are centered around a relation H/C = 1 which means that the number of hydrogen atoms is equal to the number of carbon atoms in the species. This is a characteristic of compounds with aromatic rings, thus, the compounds of this region have been assigned to decomposition products of lignin and have a large number of oxygen atoms in their structure. Furthermore, as can be seen in Figure 4, the size of the markers used represents the DBE (Double bonding equivalents) that represents the degree of unsaturation or rings present in the molecular formula. DBE increases in the region below an H/C ratio of less than 1 and O/C less than 0.2. This characteristic is feasible because bio-oil was produced from the thermal decomposition of lignin, cellulose, and hemicellulose. The oxygenated groups present in the heavier fraction come from the polymerization of sugars and molecules with thermal stability such as lignin.

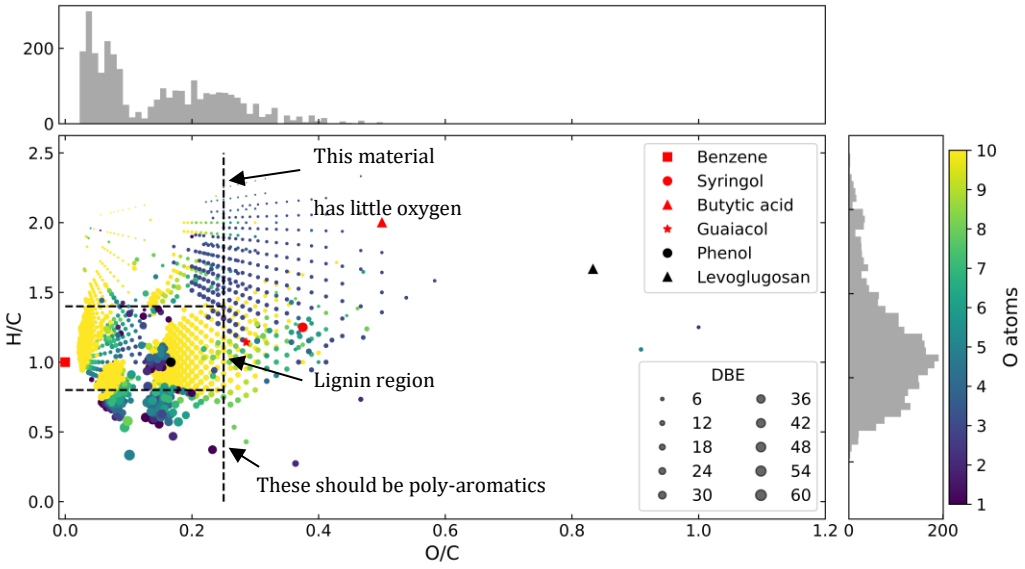

Figure 2-4. Van-Krevelen diagram from ESI (-)-FT-ICR of hit compounds in SCB bio-oil

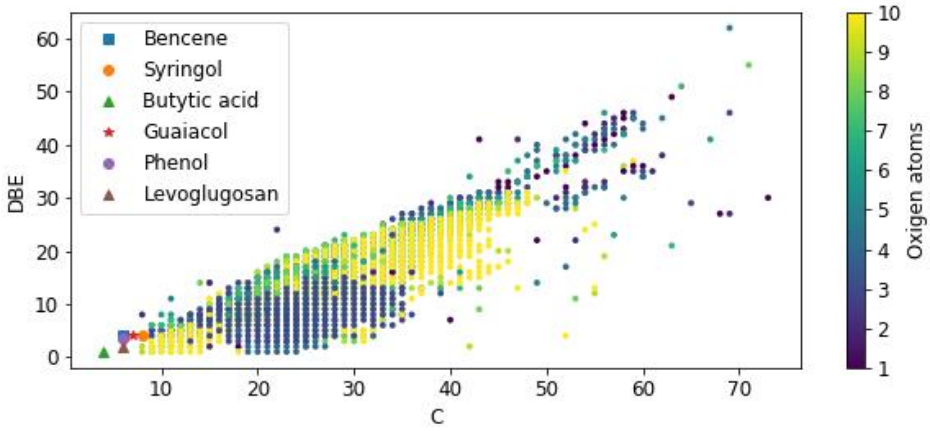

Figure 2-5. DBE vs. carbon number from ESI (-)-FT-ICR of hit compounds in SCB bio-oil

The chemical structure of the bio-oil shows the distribution of carbon numbers between ten to 70 carbon atoms in the identified compounds. Figure 2-5 shows the DBE scatter vs. carbon atoms in the molecular formula, and the color scale represents the amount of oxygen in each species. The DBE show values in the region from five to

50, indicating that the main structure is a polyaromatic ring with a high number of oxygen atoms, the oxygen classification is shown in Figure 2-6. A significant fraction of the species showed more than six oxygen atoms with four nitrogen atoms and the number of carbon atoms between ten and 40.

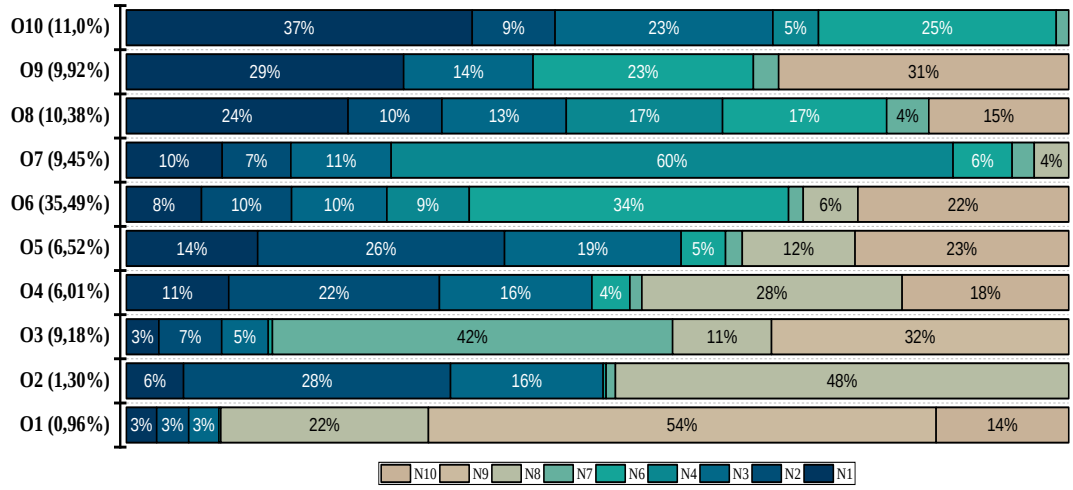

Figure 2-6. Oxygen family's classification of $C_xH_yO_zN_w$ Compounds and the number of Nitrogen atoms participation.

In general, the chemical structure of bio-oil has a high amount of oxygen atoms in its structure mainly in a mixture of different functional groups, The average molecular weight is close to 250 Da and the results of the ESI (-)-FT-ICR-MS possible to determine that the poly-aromatic rings are formed from biomass pyrolysis by thermal degradation of stable molecular polymeric chains such as lignin. Also, the cenosphere and unburned residue are produced by this heavy fraction of bio-oil during combustion or oxy-combustion[31–33].

2.2.2 Bio-oil thermal degradation in N_2 and CO_2 atmospheres

TG, DTG, and DSC for SCB bio-oil in N_2 and CO_2 atmospheres are shown in Figure 2-7,

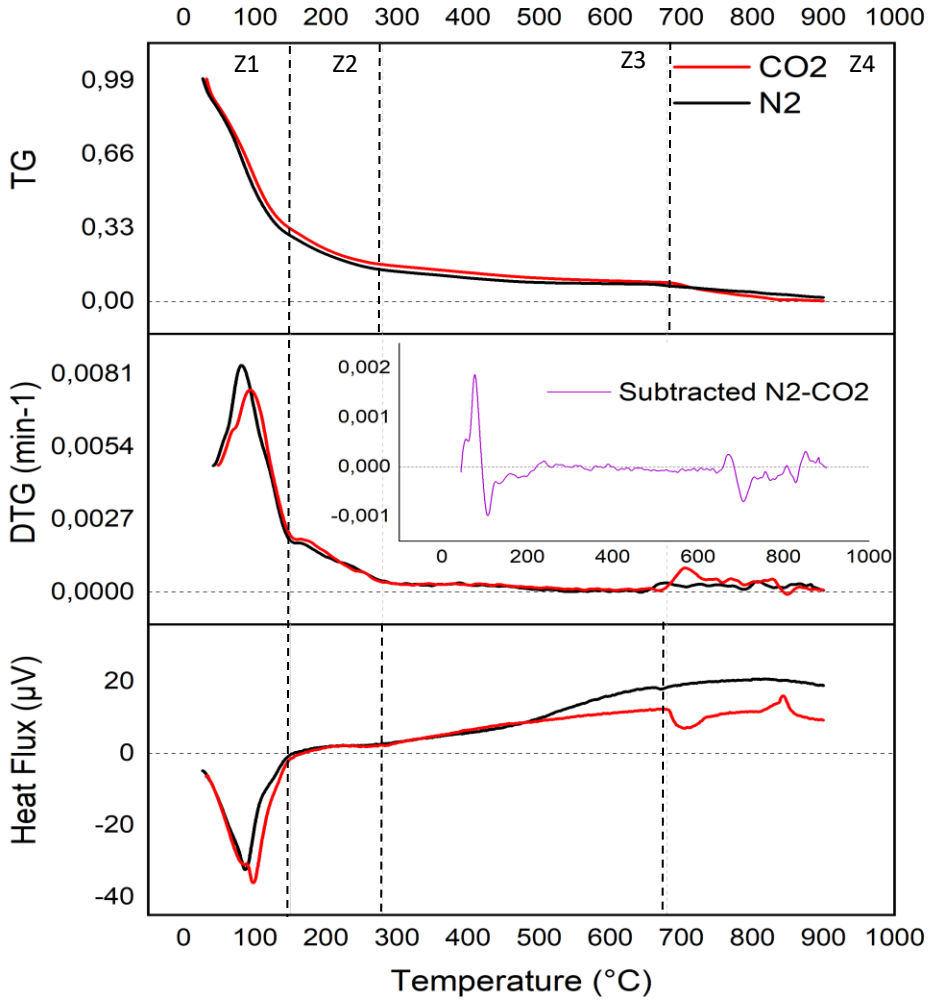

Figure 2-7. TG-DTG and heat flow of bio-oil in N_2 and CO_2 atmosphere

The thermal behavior of the bio-oil shows four zones as shown in figure 7: The first zone, from room temperature to 150 °C, characterized by the vaporization of polar light compounds such as alcohols, aldehydes, ketones, and water, with a weight loss of 49.78 wt. % at 100°C. The next evaporation stage occurs from 150°C to 280°C, this zone also includes the evaporation of some monosugars and the cracking of poly-sugars a weight loss around 80% in this zone according to Branca and Di Blasi [34]. The third zone is characteristic of carbonization reactions which take place up to 280°C to 680°C,

corresponding to the formation of solid char. Finally, in Zone 4, there is an increase in DTG due to the weight loss by gasification reactions.

In figure 7, zone 1 it can be seen that the volatility release rate is higher in nitrogen than in CO_2, this can be interpreted as difficulties in the transport of light species in atmospheres rich in CO_2, this under the assumption that CO_2 does not it solubilizes in the remaining bio-oil. Also, as shown below there are differences in the reorganization of functional groups, specifically in the formation of aromatic compounds during the carbonization stage. Previous works [9,35] showed than the carbonization reactions as crosslinking occurs at temperatures up to 400°C, and the char is a product promoted by the interaction of the pyro-lignin with the high molecular weight molecules [13]. When it releases water, the crosslinking reaction takes place to produce a net of organic compounds, and the aromaticity of this char increase[9], Therefore, carbon dioxide increases the degree of aromatization in carbonized more than nitrogen at the same temperature [24].

In bio-oil evaporation and pyrolysis, zone 2 is associated with the degradation of mono sugars and the first stages of formation of polyaromatics of high molecular weight [36,37]. These compounds are the product of the glycosidic cleavage and dehydration reactions of the cellulose and hemicellulose[9]. Seneca et al[20]. had study the pyrolysis of hemicellulose in a carbon dioxide atmosphere, and its pyrolysis rate was notoriously affected by the carbon dioxide presence. Hence, there was evidence that carbon dioxide affected the pyrolysis of oxygenated structures as sugars (xylose, arabinose). In our measurements the pyrolysis rate in zone 2, don't show a significant effect of carbon dioxide compared with the nitrogen atmosphere, a small difference in the rate of weight loss can be appreciated. However, as the otter's authors had reported the amount of mono-sugars product of hemicellulose decomposition is in the

range of 4 to 10 [mg/g bio-oil][38], Thus, the effect of carbon dioxide in this zone is not enough to be detected.

Concerning the zone 3, there is no significant change in the speed of the process due to the presence of carbon dioxide. However, in zone 4 the results show a significant loss of mass, with an increase in the rate of thermal degradation and a clear decrease in the heat released. This suggests the occurrence of an endothermic reaction above 680 °C, this behavior is typical of the gasification reaction with carbon dioxide as described elsewhere [39,40]

Finally, during the thermal decomposition of bio-oil at temperatures higher than 400 °C in N_2 and CO_2, a secondary char is formed[40]; the char obtained possibly present changes in its chemical structure, these changes, in that case, the changes found will be the product of the interaction of the compounds formed during pyrolysis with the carbon dioxide present in the atmosphere as will be shown below in this work. These changes in the structure of the char have been studied previously in coal pyrolysis, and the processes are characterized by two kinds of phenomena crosslinking and thermal annealing [41], and both are strongly affected by the presence of CO_2 [30,39].

2.2.3 The functional group of char products

The char samples obtained in both atmospheres were analyzed using FT-IR to identify the chemical functional groups. All the FT-IR spectra are firstly baseline corrected and the average and Standard deviation (STD) of three samples were calculated. Three sections of the spectrum are of interest. The first one is placed between 3000 and 2750 cm^{-1} corresponding to the stretching vibrations of $-CH_3$, $-CH_2$, and -CH. The second region (1850-900 cm^{-1}) that allows evaluating groups such as C-O and O-H single bonds (1350–900 cm^{-1}) and C = O bond (1850–1650 cm^{-1}), and finally the third region

(900 to 650 cm^{-1}) showing characteristic signals of aromatic substitutions. The results of the average spectrum and its standard deviation for each temperature in N_2 and CO_2 atmosphere are shown in figure 8,9 and 10 respectively

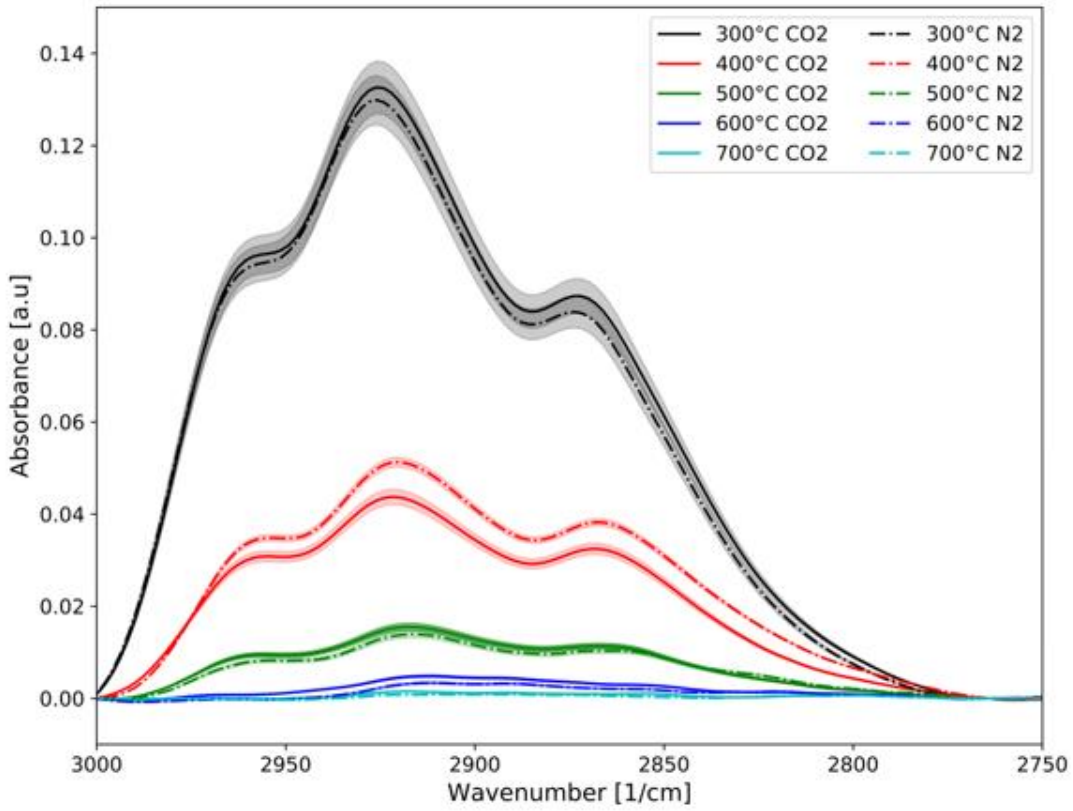

Figure 2-8 FT-IR spectra between 3000 and 2750 cm−1 of the char from the pyrolysis of bio-oil at 300-700°C

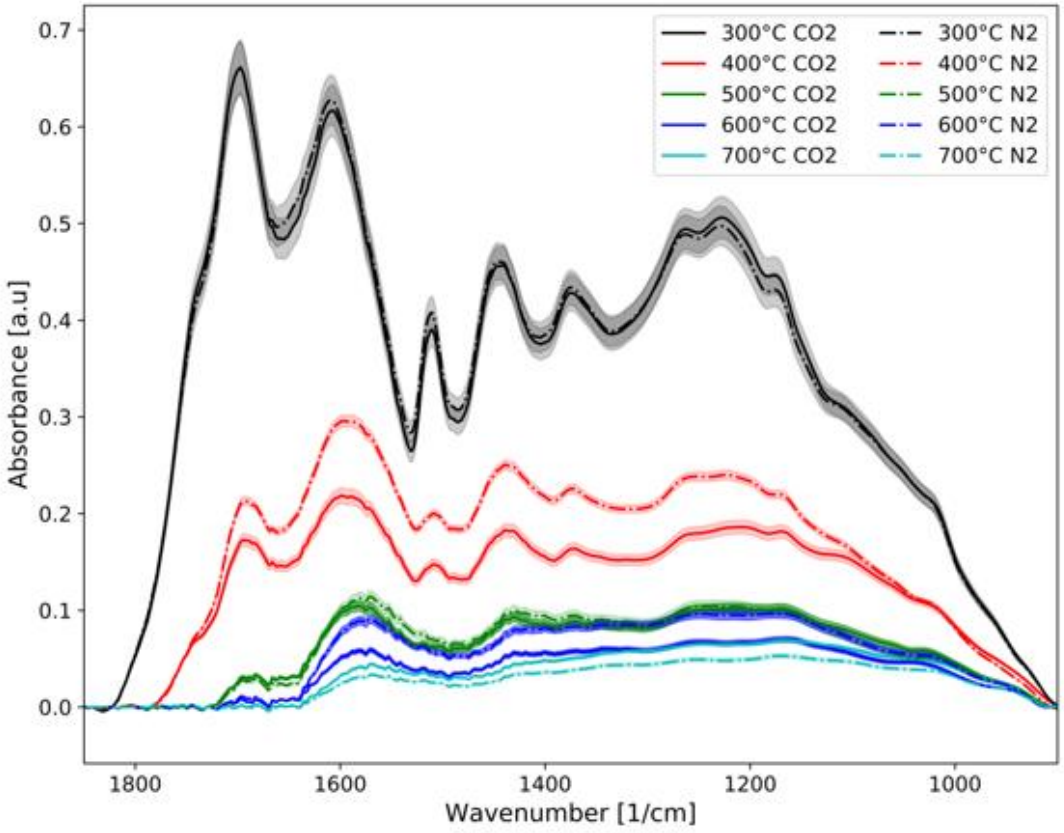

Figure 2-9 FT-IR spectra between 1850 and 900cm−1 of the char from the pyrolysis of bio-oil at 300-700°C

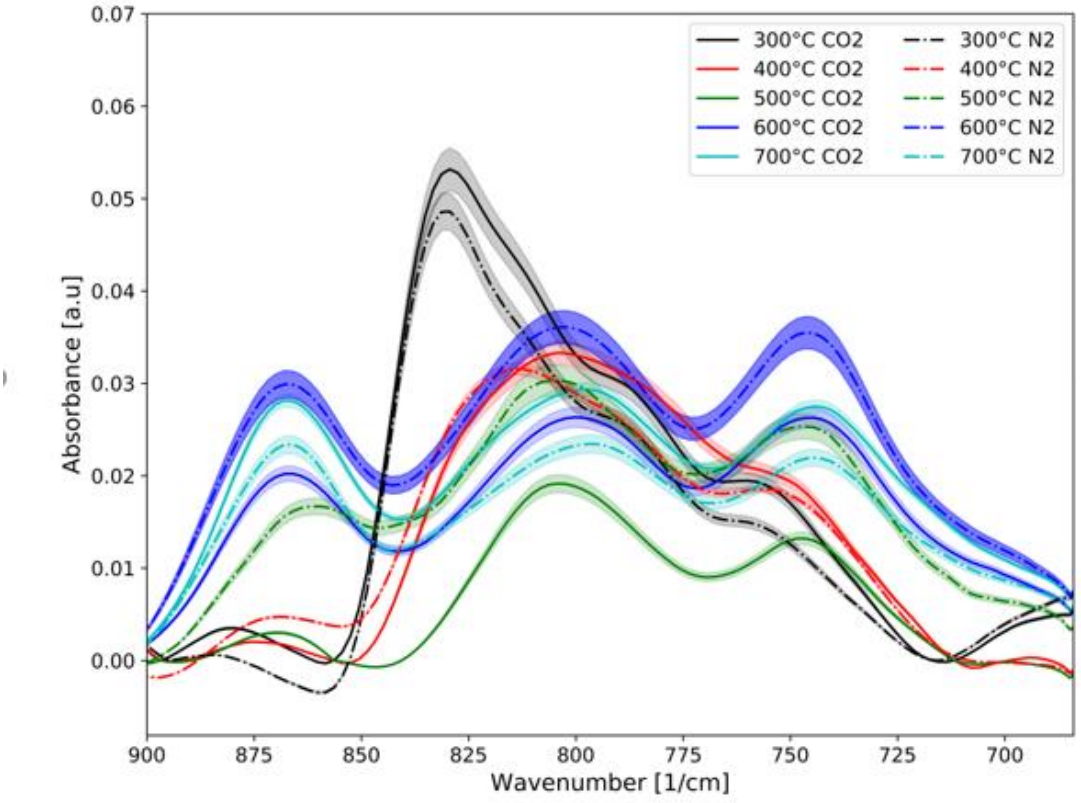

Figure 2-10. FT-IR spectra between 900 and 650 cm−1 of the char from the pyrolysis of bio-oil at 300-700°C.

Figure 2-8 shows that the intensity of the stretching vibrations of -CH3, -CH2, and -CH is reduced as the temperature is increasing. The latter could be because the CH3, -CH2, and -CH functional groups from aliphatic chains are reduced during char formation. The signal of the samples obtained at 600 °C and 700 °C is very weak because the solid structure is condensed into aromatic rings with very low stretching vibrations for these functional groups. The presence of carbon dioxide does not show a significant difference in the evolution of these functional groups.

Figure 2-9 shows the FT-IR spectra in the region of 1850 to 900 cm^{-1}. In this region, it is possible to identify the group's CO, OH of a single bond and C = O in a double bond, as well as the band located around 1603 cm^{-1} characteristic of the C = C bonds of aromatic rings, the intensity of the signal in this region, decreases as the temperature increases such as it occurs in the vibrations of aliphatic groups. The oxygen-containing groups promote the formation of char and therefore its intensity is reduced to become very weak as reported by previous work[12,13,42–45]. Additionally, the presence of carbon dioxide as a pyrolysis atmosphere shows a decrease in the intensity of the char signal obtained at 400 ° C. the characteristic signal of 1650 cm-, shows a decay with the increase in temperature, but the reduction in absorbance between 300 and 400 ° C is greater in CO_2 atmosphere than in nitrogen, This seems to be due to greater interaction of carbon dioxide with oxygen-containing groups.

Finally, Figure 2-10. FT-IR spectra between 900 and 650 cm−1 of the char from the pyrolysis of bio-oil at 300-700°C.shows the FT-IR spectra in the region of less than 900 cm^{-1}, typically for coals and char are characterized by bands of aromatic structures with isolated aromatic hydrogen (870 cm^{-1}), two adjacent aromatic hydrogens per ring (815 cm^{-1}) and four adjacent aromatic hydrogens (750 cm^{-1}) respectively [46]. These substitutions do not seem to have the same decreasing behavior that was shown in the stretching signals and the oxygenated groups. As expected, in the char obtained at 500,600 and 700°C the degree of aliphatic substitutions on aromatic rings increases as the temperature increases and the carbon dioxide shows a positive effect in the generation of structures with a high degree of saturation of aromatic structures. However, there are differences between the spectra of the char obtained at 300 and 400 C from the others. the char spectra obtained at 300 and 400°C in nitrogen and carbon dioxide shows a reduction of the peak with high intensity around 825 [1/cm]. This signal is typical of the aliphatic substitution of monoaromatics in position para, while the three predominant signals of the char obtained at 500, 600, and 700 are typical of the aliphatic substitution of mono and polyaromatics in position Meta

To realize a semi quantification of the char evolution in both atmospheres, four indexes were used to analyze the char obtained: The aromaticity index I_A, a ratio between the signal of aromatic compounds C=C (1603 cm^{-1}) y C-H ([869-747] cm^{-1}) and the total area assigned to the aromatic and paraffinic signals (Eqn 1) [47]. The aliphatic index I_{Aliph}, which one allow to assess the ratio of aliphatic signals by stretching with the aromatic and paraffinic signals(Eqn 2), The Branching index BI(Eqn 3), and the condensation index I_C (Eqn 1)[48] were used to evaluate the dispersion of functional aliphatic groups in the macrostructure, and the relationship between the isolated organic structures by comparison with the concentrated aromatic structures as multi rings aromatics respectively.

$$I_A = \frac{A_{1603} + A_{869-747}}{A_{1700} + A_{1603} + A_{1465} + A_{1377} + A_{1031} + A_{869-747} + A_{(2954+2925+2850)}} \quad (1)$$

$$I_{Aliph} = \frac{A_{1465} + A_{1377}}{A_{1700} + A_{1603} + A_{1465} + A_{1377} + A_{1031} + A_{869-747} + A_{(2954+2925+2850)}} \quad (2)$$

$$BI = \frac{A_{1377}}{A_{1465} + A_{1377}} \quad (3)$$

$$I_C = \frac{A_{869-747}}{A_{1603}} \quad (4)$$

A_i is the relative area of the peak at the i wavenumber or range. The result of the indexes is displayed in Figure 2-11. In the chars obtained, the aromatic index (Figure 2-11a) increases with the increment of the temperature, this behavior has sense because the condensation reactions involved in the crosslinking process occurred during the carbonization and is promoted by the temperature. In this sense, the aromatic rings increasing in the char implies the disappearance of aliphatic groups as we can see in Figure 2-11b.

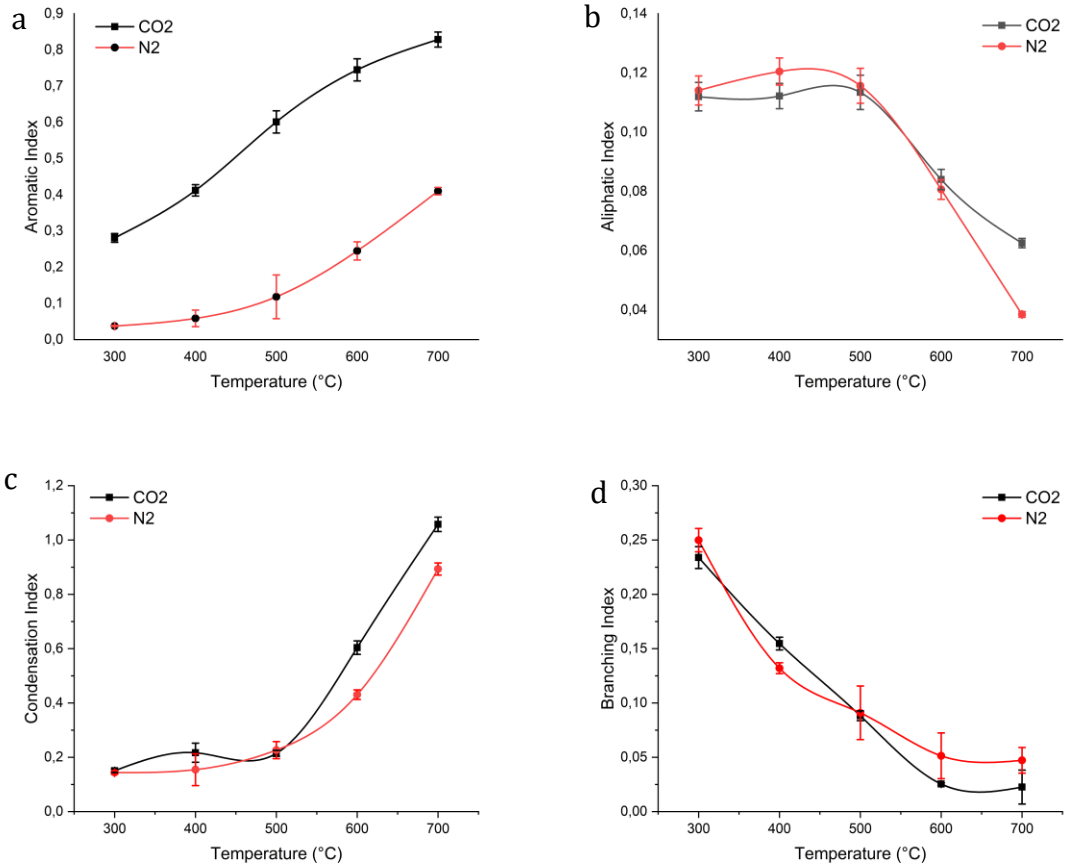

Figure 2-11. FT-IR based index of the char from the pyrolysis of bio-oil at 300-700°C in N_2 and CO_2 a) Aromatic Index, b) Aliphatic index, c) Condensation index, and d) Branching index

The branching and condensation index account for the degree of distribution of aliphatic and aromatic functional groups respectively. In Figure 2-11c. the condensation index increases with the temperature and is an indicator of multiple rings bounding evolution, typically this behavior has been described in coal structure evolution during pyrolysis and gasification. On the other hand, the branching index Figure 2-11d, which is an indicator of the length of the chains outside the organic matrix (aliphatic groups substituting aromatic rings or sets of aromatic rings) shows a decrease with increasing temperature, this means that the length of the chains has

been diminished possibly by those chains helped the formation of aromatic rings. The results obtained in these experiments are consistent with the work of Xiong [11], however, we found that the presence of CO_2 accelerates the aromatization of carbonized. Moreover, the results also show that at any temperature the presence of aromatic groups is greater than the carbonized obtained in nitrogen.

2.3 **Conclusions**

In this paper, we analyze the chemical composition and distribution of the oxygenated functional groups in the bio-oil obtained by rapid pyrolysis using. Gas chromatography coupled to mass spectrometry was used to describe the volatile components present. Also, an analysis of heavy compounds by ESI (-) - FT-ICR-MS was performed to provide an overview of the distribution of oxygen in heavy molecules, as well as the types of bonds in the functional groups obtained.

The ESI (-) - FT-ICR-MS analysis allows us to observe that chemical compounds with six oxygen atoms in their structure, representing 35.46% of all the molecules identified in the bio-oil, and 10% of all oxygenated compounds have more than ten oxygen atoms in their structure. There is evidence to show that oligomers with high molecular weight and a large number of oxygens in their structure are involved in dehydration reactions, thereby forming structures of greater molecular weight.

The char formation during the pyrolysis of bio-oil in nitrogen and carbon dioxide and their chemical characteristics were investigated in this study. Our results show that the char obtained in carbon dioxide has a higher degree of aromaticity, than the samples obtained in nitrogen, and these functional groups are concentrated in

aromatic groups with external substitutions with a short size, this was verified by the values obtained with the branching index.

2.4 Acknowledgments:

The authors wish to thank the Colciencias-Doctorados Nacionales 757-2016 fellowship and the project "Strategy of a transformation of the Colombian energy sector on the horizon 2030" funded by call 788 of the Colciencias Scientific Ecosystem. Contract number FP44842-210-2018. This work was partially performed at King Abdullah University of Science and Technology (KAUST) Clean Combustion Research Center (CCRC) with funding from the KAUST Center Applied Research Fund (CARF). This research used resources of the Core Labs of King Abdullah University of Science and Technology (KAUST).

2.5 References

[1] D. Hales, Renewables 2018 global status report, 2018.

[2] UPME, Atlas del Potencial Energético de la Biomasa Residual en Colombia, 2015. https://biblioteca.minminas.gov.co/pdf/ATLAS POTENCIAL ENERGETICO BIOMASA RESIDUAL COL. UPME.pdf.

[3] C. Branca, C. Di Blasi, R. Elefante, Devolatilization and Heterogeneous Combustion of Wood Fast Pyrolysis Oils, Ind. Eng. Chem. Res. 44 (2005) 799–810. https://doi.org/10.1021/ie049419e.

[4] A.V. Bridgwater, Review of fast pyrolysis of biomass and product upgrading, Biomass and Bioenergy. 38 (2012) 68–94. https://doi.org/10.1016/j.biombioe.2011.01.048.

[5] J.P. Diebold, A review of the chemical and physical mechanisms of the storage stability of fast pyrolysis bio-oils, 2000. https://doi.org/10.2172/753818.

[6] J.I. Montoya Arbeláez, F. Chejne Janna, M. Garcia-Pérez, Fast pyrolysis of biomass: A review of relevant aspects. Part I: Parametric study, Dyna. 82 (2015) 239–248. https://doi.org/10.15446/dyna.v82n192.44701.

[7] J. Montoya, B. Pecha, D. Roman, F. Chejne, M. Garcia-perez, Effect of temperature and heating rate on product distribution from the pyrolysis of sugarcane bagasse in a hot plate reactor, J. Anal. Appl. Pyrolysis. 123 (2017) 347–363. https://doi.org/10.1016/j.jaap.2016.11.008.

[8] N. Gao, C. Quan, Z. Ma, C. Wu, Thermal Characteristics of Biomass Pyrolysis Oil and Potential Hydrogen Production by Catalytic Steam Reforming, Energy and Fuels. 32 (2018). https://doi.org/10.1021/acs.energyfuels.8b00365.

[9] W. Chaiwat, I. Hasegawa, T. Tani, K. Sunagawa, K. Mae, Analysis of cross-linking behavior during pyrolysis of cellulose for elucidating reaction pathway, Energy and Fuels. 23 (2009) 5765–5772. https://doi.org/10.1021/ef900674b.

[10] Y. Wang, D. Mourant, X. Hu, S. Zhang, C. Lievens, C. Li, Formation of coke during the pyrolysis of bio-oil, Fuel. 108 (2013) 439–444. https://doi.org/10.1016/j.fuel.2012.11.052.

[11] Z. Xiong, Y. Wang, S.S.A. Syed-Hassan, X. Hu, H. Han, S. Su, K. Xu, L. Jiang, J. Guo, E.E.S. Berthold, S. Hu, J. Xiang, Effects of heating rate on the evolution of bio-oil during its pyrolysis, Energy Convers. Manag. 163 (2018) 420–427. https://doi.org/10.1016/j.enconman.2018.02.078.

[12] Z. Xiong, S.S.A. Syed-hassan, J. Xu, Y. Wang, S. Hu, S. Su, Evolution of coke structures during the pyrolysis of bio-oil at various temperatures and heating rates, J. Anal. Appl. Pyrolysis. 134 (2018) 336–342. https://doi.org/10.1016/j.jaap.2018.06.023.

[13] Z. Xiong, S.S.A. Syed-hassan, X. Hu, J. Guo, J. Qiu, X. Zhao, Pyrolysis of the aromatic-poor and aromatic-rich fractions of bio-oil : Characterization of coke structure and elucidation of coke formation mechanism, Appl. Energy. 239 (2019) 981–990. https://doi.org/10.1016/j.apenergy.2019.01.253.

[14] Z. Wang, M. Liu, X. Cheng, Y. He, Y. Hu, C. Ma, Experimental study on oxy-fuel combustion of heavy oil, Int. J. Hydrogen Energy. 42 (2017) 20306–20315. https://doi.org/10.1016/j.ijhydene.2017.06.105.

[15] G. Marrugo, C.F. Valdés, F. Chejne, Characterization of Colombian Agroindustrial Biomass Residues as Energy Resources, Energy & Fuels. 30 (2016) 8386–8398. https://doi.org/10.1021/acs.energyfuels.6b01596.

[16] P. Ahmed, M.A. Habib, R. Ben-Mansour, A.F. Ghoniem, Computational Fluid Dynamics (CFD) Investigation of the Oxy-combustion Characteristics of Diesel Oil, Kerosene, and Heavy Oil Liquid Fuels in a Model Furnace, Energy and Fuels. 30 (2016) 2458–2473. https://doi.org/10.1021/acs.energyfuels.5b02794.

[17] O. Senneca, F. Cerciello, S. Heuer, P. Ammendola, Slow pyrolysis of walnut shells in nitrogen and carbon dioxide, Fuel. 225 (2018) 419–425. https://doi.org/10.1016/j.fuel.2018.03.094.

[18] A.H. Tchapda, V. Krishnamoorthy, Y.D. Yeboah, S. V. Pisupati, Analysis of tars formed during co-pyrolysis of coal and biomass at high temperature in carbon dioxide atmosphere, J. Anal. Appl. Pyrolysis. 128 (2017) 379–396. https://doi.org/10.1016/j.jaap.2017.09.011.

[19] T.S. Farrow, C. Sun, C.E. Snape, Impact of CO_2 on biomass pyrolysis, nitrogen partitioning, and char combustion in a drop tube furnace, J. Anal. Appl. Pyrolysis. 113 (2015) 323–331. https://doi.org/10.1016/j.jaap.2015.02.013.

[20] O. Senneca, F. Cerciello, C. Russo, A. Wütscher, M. Muhler, B. Apicella, Thermal treatment of lignin, cellulose and hemicellulose in nitrogen and carbon dioxide, Fuel. 271 (2020) 117656. https://doi.org/10.1016/j.fuel.2020.117656.

[21] J. Lee, X. Yang, H. Song, Y. Sik, E.E. Kwon, Effects of carbon dioxide on pyrolysis of peat, Energy. (2016). https://doi.org/10.1016/j.energy.2016.11.143.

[22] J.I. Montoya, C. Valdés, F. Chejne, C.A. Gómez, A. Blanco, G. Marrugo, J. Osorio, E. Castillo, J. Aristóbulo, J. Acero, Bio-oil production from Colombian bagasse by fast pyrolysis in a fluidized bed: An experimental study, J. Anal. Appl. Pyrolysis. 112 (2015) 379–387. https://doi.org/10.1016/j.jaap.2014.11.007.

[23] E. Alsbou, B. Helleur, Accelerated aging of bio-oil from fast pyrolysis of hardwood, Energy and Fuels. 28 (2014) 3224–3235. https://doi.org/10.1021/ef500399n.

[24] C. Branca, P. Giudicianni, C. Di Blasi, GC / MS Characterization of Liquids Generated from Low-Temperature Pyrolysis of Wood, Ind. Eng. Chem. Res. 42 (2003) 3190–3202. https://doi.org/10.1021/ie030066d.

[25] J. Lehto, A. Oasmaa, Y. Solantausta, M. Kytö, D. Chiaramonti, Review of fuel oil quality and combustion of fast pyrolysis bio-oils from lignocellulosic biomass, Appl. Energy. 116 (2014) 178–190. https://doi.org/10.1016/j.apenergy.2013.11.040.

[26] A. Oasmaa, I. Fonts, M.R. Pelaez-Samaniego, M.E. Garcia-Perez, M. Garcia-Perez, Pyrolysis Oil Multiphase Behavior and Phase Stability: A Review, Energy and Fuels. 30 (2016) 6179–6200. https://doi.org/10.1021/acs.energyfuels.6b01287.

[27] Q. Sohaib, A. Muhammad, M. Younas, Fast pyrolysis of sugarcane bagasse: Effect of pyrolysis conditions on final product distribution and properties, Energy Sources,

Part A Recover. Util. Environ. Eff. 39 (2017) 184–190. https://doi.org/10.1080/15567036.2016.1212292.

[28] B. Scholze, C. Hanser, D. Meier, Characterization of the water-insoluble fraction from fast pyrolysis liquids (pyrolytic lignin) Part II . GPC , carbonyl goups , and 13 C-NMR, J. Anal. Appl. Pyrolysis. 59 (2001) 387–400.

[29] B. Scholze, D. Meier, Characterization of the water-insoluble fraction from pyrolysis oil (pyrolytic lignin). Part I . PY – GC / MS , FTIR , and functional groups, 60 (2001) 41–54.

[30] C.F. Valdés, F. Chejne, Effect of reaction atmosphere on the products of slow pyrolysis of coals, J. Anal. Appl. Pyrolysis. 126 (2017) 105–117. https://doi.org/10.1016/j.jaap.2017.06.019.

[31] M. Garcia-Perez, P. Lappas, P. Hughes, L. Dell, A. Chaala, D. Kretschmer, C. Roy, Evaporation and combustion characteristics of biomass vacuum pyrolysis oils, IFRF Combust. J. 200601 (2006) 1–27.

[32] J. D'alessio, M. Lazzaro, P. Massoli, V. Moccia, Thermo-optical investigation of burning biomass pyrolysis oil droplets, Symp. Combust. 27 (1998) 1915–1922. https://doi.org/10.1016/S0082-0784(98)80035-0.

[33] M.J. Wornat, B.G. Porter, N.Y.C. Yang, Single Droplet Combustion of Biomass Pyrolysis Oils, Energy & Fuels. 8 (1994) 1131–1142. https://doi.org/10.1021/Ef00047a018.

[34] C. Branca, C. Di Blasi, Multistep mechanism for the devolatilization of biomass fast pyrolysis oils, Ind. Eng. Chem. Res. 45 (2006) 5891–5899. https://doi.org/10.1021/ie060161x.

[35] M.S. Oh, W.A. Peters, J.B. Howard, An experimental and modeling study of softening coal pyrolysis, AIChE J. 35 (1989) 775–792. https://doi.org/10.1002/aic.690350509.

[36] F. Stankovikj, M. Garcia-perez, TG-FTIR Method for the Characterization of Bio-oils in Chemical Families, Energy & Fuels. 30 (2017) 1689–1701. https://doi.org/10.1021/acs.energyfuels.6b03132.

[37] M. Garcia-Perez, A. Chaala, H. Pakdel, D. Kretschmer, C. Roy, Characterization of bio-oils in chemical families, Biomass and Bioenergy. 31 (2007) 222–242. https://doi.org/10.1016/j.biombioe.2006.02.006.

[38] Y. Yu, Y.W. Chua, H. Wu, Characterization of Pyrolytic Sugars in Bio-Oil Produced from Biomass Fast Pyrolysis, Energy and Fuels. 30 (2016) 4145−4149. https://doi.org/10.1021/acs.energyfuels.6b00464.

[39] O. Senneca, B. Apicella, C. Russo, F. Cerciello, P. Salatino, S. Heuer, A. Wu, M. Schiemann, M. Muhler, Pyrolysis and Thermal Annealing of Coal and Biomass in CO_2-Rich Atmospheres, Energy & Fuels. 32 (2018) 10701–10708. https://doi.org/10.1021/acs.energyfuels.8b02417.

[40] J. Billaud, S. Valin, M. Peyrot, S. Salvador, Influence of H2O , CO_2 and O2 addition on biomass gasification in entrained flow reactor conditions : Experiments and modelling, Fuel. 166 (2016) 166–178. https://doi.org/10.1016/j.fuel.2015.10.046.

[41] O. Senneca, F. Cerciello, L. Cortese, S. Heuer, M. Schiemann, V. Scherer, Effects of CO2 enriched atmosphere on chars from walnut shells pyrolysis in a drop tube reactor, Fuel. 229 (2018) 235–240. https://doi.org/10.1016/j.fuel.2018.04.152.

[42] W.R. Hesp, P.L. Waters, Thermal Cracking of Tars and Volatile Matter from Coal Carbonization, Ind. Eng. Chem. Prod. Res. Dev. 9 (1970) 194–202. https://doi.org/10.1021/i360034a016.

[43] M.S. Talmadge, R.M. Baldwin, M.J. Biddy, R.L. McCormick, G.T. Beckham, G.A. Ferguson, S. Czernik, K.A. Magrini-Bair, T.D. Foust, P.D. Metelski, C. Hetrick, M.R. Nimlos, A perspective on oxygenated species in the refinery integration of pyrolysis oil, Green Chem. 16 (2014) 407–453. https://doi.org/10.1039/c3gc41951g.

[44] Z. Xiong, Y. Wang, S.S.A. Syed-hassan, X. Hu, H. Han, S. Su, Effects of heating rate on the evolution of bio-oil during its pyrolysis, Energy Convers. Manag. 163 (2018) 420–427. https://doi.org/10.1016/j.enconman.2018.02.078.

[45] F. Stankovikj, A.G. McDonald, G.L. Helms, M. Garcia-Perez, Quantification of Bio-Oil Functional Groups and Evidences of the Presence of Pyrolytic Humins, Energy and Fuels. 30 (2016) 6505–6524. https://doi.org/10.1021/acs.energyfuels.6b01242.

[46] A.J.B. José V. Ibarra,Rafael Moliner, FTIR during investigation on char formation the early stages of coal pyrolysis, Fuel. 73 (1994) 918–924. https://doi.org/10.1016/0016-2361(94)90287-9.

[47] J. Lamontagne, P. Dumas, V. Mouillet, J. Kister, Comparison by Fourier transform infrared (FTIR) spectroscopy of different ageing techniques : application to road bitumens, Fuel. 80 (2001) 483–488. https://doi.org/10.1016/S0016-2361(00)00121-6.

[48] R. García, C. Barriocanal, Influence of binder type on greenhouse gases and PAHs from the pyrolysis of biomass briquettes, Fuel Process. Technol. 171 (2018) 330–338. https://doi.org/10.1016/j.fuproc.2017.11.029.

3 Investigation into the pyrolysis and combustion of bio-oil from sugarcane bagasse: Kinetics and evolved gases using TGA-FTIR

Energy consumption in developing countries has doubled in the period between 2000 to 2014 [1] and by 2025 the worldwide energy demand is expected to grow by more than 50% [2]. Lignocellulosic biomass is now considered as a renewable resource for the production of biofuels and a number of specialty chemicals. Biomass valorization to energy offers an ideal substitute to reduce and replace petroleum-based fuels as a renewable energy source. Lignin, which is one of the primary components of biomass is highly aromatic in nature and a number of studies [3,4] have reported its potential in producing phenolic high value bio-oils. Pyrolysis of biomass is a convenient method of transforming it into bio-oils that can be used as cheap fuels wholly by themselves or blended with fossil fuels to improve various combustion properties like octane number, cetane number, sooting propensity etc. For example, bio-ethanol is largely blended with gasoline (by up to 15 %) as an octane booster. Oxygenate rich bio-oils[5] have also been blended as diesel fuel additives to reduce the formation of soot and particulate matter emissions in diesel engines. Various biomass resources like rice husk [6], kraft lignin [7], alkali lignin [8], wood waste[9], palm kernel[10], cotton seed [11], palm biomass [12] and others [13] have been used for the production of bio-oil through pyrolysis.

Sugarcane Bagasse (SCB), which is the fraction of biomass left after the juice is extracted from the sugarcane, is a cheap and promising and renewable resource for the

production of bio-oil. It is a fibrous residue that is made up of cellulose (50 %), hemicellulose (25 %) and lignin (25%) [14]. SCB is one of the main agricultural residues in Colombia and it is estimated that 25 M tons / year of SCB is produced and nearly 85% of it is used for steam generation in the sugar industry [15]. SCB has a high content of volatile material (80% w/w) which has a high potential to convert into oxygen-rich fuels [16]. During pyrolysis, cellulose and hemicellulose present in SCB undergo chemical transformation into oxygenated sugar-derived products such as furfural, monosaccharides and linear oxygenated compounds as alcohols, aldehydes and ketones that have shown very good characteristics as fuels [17], as well as into phenolic compounds that represent 10% of the bio-oil from lignin [18].

Pyrolysis technologies enable the production of biofuels from biomass, garbage or organic waste [19–21]. SCB pyrolysis represents an alternative to cogeneration, and allows an integration option for bio-refineries for the manufacture of fuels and high value compounds. Most bio-oils obtained from pyrolysis are characterized as poor fuels due to a number of issues like low calorific value, high moisture and oxygen contents, poor miscibility with petroleum fuels, propensity to cause corrosion, chemical instability, acidity issues etc. Characterization of bio-oils is an important step in understanding their physical and chemical properties so appropriate upgrading techniques like fast pyrolysis, catalytic cracking, catalytic hydrogenation, emulsification etc. can be implemented to improve their physical and thermo-chemical properties. Advanced characterization techniques like NMR spectroscopy[7,22–24], gas chromatography-mass spectroscopy (GC-MS) [6], Fourier transform-ion cyclotron resonance (FT-ICR) mass spectrometry[25] etc. can shed light on the fuel molecular structure but cannot provide insight on the thermal stability or pollutant gases formed during combustion. Such information is useful for the design of combustors where the combustion efficiency of the bio-fuels can be maximized while minimizing the emissions and particulate matters. Techniques like thermo-gravimetric analysis coupled to Fourier transform infrared spectroscopy (TGA-FTIR) have been widely employed to investigate the combustion characteristics and pollutant emission profiles of a number of samples like heavy fuel oil [26], rice husk [6], alkali lignin [8], wood

waste [9] etc. TGA-FTIR has a number of advantages like, high accuracy and sensitivity, small sample requirements in the order of a few milligrams, real time measurements etc. It can help study mass loss characteristics, thermal degradation pathways, kinetic parameters and on-line analysis of gases and functional groups evolved from the sample[27].

The TGA-FTIR analysis allows not only to roughly evaluate the evolution of the mass during the heating of the biofuel and to determine its kinetic parameters. If not, it is also possible to identify the evolution of the functional groups released and permanent gases such as CO2, N2, CO, CH4 during heating in real-time. There are few studies focused on the comparison of the pyrolysis and combustion of bio-oil from biomass using TGA, as is the case of bio-oil produced from rice husk [28], Bio-oil from swine manure [29], as well as its aqueous fraction of the biooil of pyrolysis of wheat stalk [30], in these works the authors agree that the oxidation of the biooil occurs in three stages, the evaporation of volatiles, the stage of formation of high molecular weight volatiles and the oxidation of char, several models have been adjusted to calculate the kinetic parameters of combustion and pyrolysis of the bio-oil. However, the complexity of the bio-oil composition does not allow its results to be extrapolated and a better description of the oxidation is needed.

The objective of this work is to investigate the pyrolysis and combustion of SCB bio-oil using TGA-FTIR. The thermal degradation and oxidation of the bio-oil was analyzed using thermo-gravimetric (TG) and differential thermo-gravimetric (DTG) curves. Kinetic analysis of the bio-oil pyrolysis and combustion was carried out to estimate the Arrhenius kinetic parameters using the distributed activation energy model by Miura and Maki [31,32]. From the evolution of the activation energy as a function of the

conversion, the reaction stages, and the role that oxygen plays during combustion are clarified. The composition of the evolved gases in real-time was analyzed using FTIR spectroscopy.

3.1 Material and Methods

3.1.1 Bio-oil production

Fresh SCB bio-oil was produced by pyrolysis at a temperature of 550 °C. It was produced in a spoon reactor using a horizontal electric furnace. A 30 cm long quartz tube with a diameter of 3 cm was used and flushed with 50 ml/min of N_2, to provide an inert atmosphere. The carrier gas and the furnace was set at 550 °C and a stainless-steel spoon containing 1.5 g of SCB was introduced into the hot zone, reaching heating rates between 100 and 200 °C/s. The products from the pyrolytic reactions were immediately condensed in a U-type stainless-steel trap, submerged in an ice bath (see Figure 1).

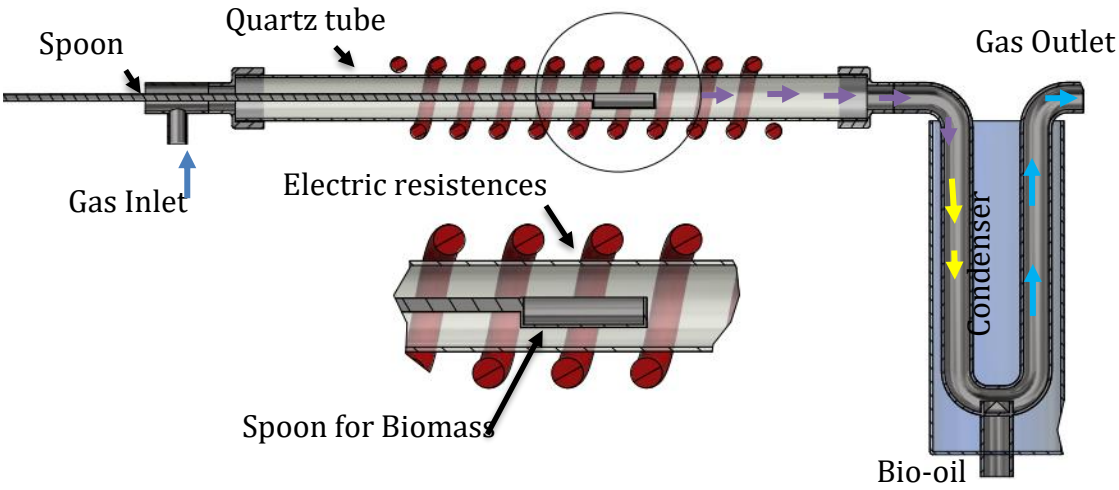

Figure 3-1. Experimental set-up for SCB bio-oil production

3.1.2 TGA-FTIR

TG analysis was performed on Mettler Toledo TGA/DSC 1 (thermal gravimetric analysis / differential scanning calorimetry) instrument equipped with a GC 200 gas controller and an auto-sampler. For each test approximately 10 mg of bio-oil was used, and it was purged for 15 min at room temperature with a flow of 50ml / min of N_2 (99.9999% purity) or ZERO air to displace CO_2 and water vapor introduced into the TG furnace during sample insertion. The samples were heated up to 900 °C at three heating rates of 5, 10 and 20 °C/min.

The gases evolved from the bio-oil during heating were transported to an IR Cell through a heated line (Thermo Scientific TGAFTIR Interface Nicolet iZ10) which was constantly maintained at 190 °C and equipped with a Swagelok 15 µm filter to remove any solid particles. The IR cell was kept at 200 °C to avoid condensation of vapors produced during thermal decomposition of the bio-oil. FTIR spectra of the gases were collected during the TGA heating ramp, every 25 s with a resolution of 4 cm-1 in the region of 400 to 4000 cm-1, using a Thermo Scientific Nicolet iS10 connected to Nicolet iZ10 interface, equipped with a deuterated triglycine sulfate (DTGS) detector and KBr beam splitter.

2.3 Kinetic modelling

The distributed activation energy model of Miura and Maki [31,32] was used in the present work to model the SCB bio-oil pyrolysis and combustion. This model has been widely used by a number of researchers [26,33,34] since it allows us to find both the kinetic parameters (activation energy, E_a and pre-exponential factor, A) and the ability to re-plot the TG profiles for comparison with experimental data. The Arrhenius based Miura and Maki model approximates the reaction rate using a first order equation represented by equation 1.

$$\frac{d\alpha}{dT} = \frac{k_0}{\beta} \exp\left(-\frac{E_a}{RT}\right) f(\alpha) \qquad (1)$$

Where α is conversion defined by the equation 2., and β is the heating rate.

$$\alpha = \frac{m - m_f}{m_i - m_f} \quad (2)$$

The terms m_i, m_f are the initial and final weights. E_a, and $k_0$correspond to selected conversion values and these can be obtained from the slope and intercept of each Arrhenius plot using equation 3 for each of the three heating rates employed, 5, 10 and 20°C/min.

$$\ln\left(\frac{d\alpha}{dT}\beta\right) = \ln\left[k_0 * f(\alpha)\right] + \left(-\frac{E_a}{RT}\right) \quad (3)$$

3.2 Results & Discussion

The physical, chemical and thermo-chemical properties of the SCB bio-oil produced in the present work are reported in Table 1. The physical characteristics of the bio-oil are related to the lignocellulose composition of the biomass and the pyrolytic process conditions such as temperature, heating rate, and retention time of the vapors in the reactor[35,36]. SCB bio-oil has high water content of 32.5 wt %, which hinders ignition and increases the ignition delay time (IDT) due to the reduction in the rate of vaporization of the droplet in a burner [37]. The acidity of SCB bio-oil is of interest, due to the presence of oxygenated chemical compounds produced during pyrolysis and the organic acids in the bio-oil react with the storage materials and catalyze the formation of high molecular weight compounds during heating. The total acid number (TAN) of SCB bio-oil measured was 95 mg KOH/g of bio-oil which is close to the typically expected value of 100. The residual solids content of the pyrolysis bio-oil, measured by filtration after dilution with methanol, is less than the prescribed tolerance value of 2.5 wt %. The lower heating value (LHV) is close to 15 MJ/ kg, which makes the bio-oil a good quality fuel, according to the ASTM burner fuel standard D 7544 for fast pyrolysis bio-oils. These values indicate that the SCB bio-oil has good properties needed for a bio-fuel on the market and to promote its acceptance as a fuel [38].

Table 3-1 Physical and chemical properties of SCB

Property	Units	Value	Method

Density (at 288K)	kg/m^3	1170	ASTM D4052-11
Kinematic viscosity (at 288K)	cSt	8.14 ±0,2	ASTM D445-12
Water (Karl fisher titration)	wt %	32.5 ± 2	ASTM E203
Total Phenolic content	mg GAE/g bio-oil	3145 ± 35	Folin-Ciocalteu colorimetry
Total acid number (TAN)	mg KOH/g	95	ASTM D664
Pyrolysis solids content, max	wt %	1.5	ASTM D7579
LHV	MJ/kg (wet basis)	13.5	
Ultimate analysis			
carbon	wt %	47.6	EPA 440
hydrogen	wt %	3.3	EPA 440
oxygen	wt %	15.6	EPA 440
nitrogen	wt %	0.14	EPA 440
sulfur	wt %	0.09	ASTM D4294-10

The elemental (CHNSO) values of SCB bio-oil are also within the range of values observed from various pyrolysis bio-oils [36,39–41].

3.2.1 Pyrolysis of SCB bio-Oil

The TG and DTG results of the pyrolysis (in N_2 atmosphere) of SCB bio-oil using the three heating rates (5, 10 and 20 °C/min) are shown in Figure 3-2. The bio-oil undergoes thermal decomposition due to the absence of oxygen and a notable mass loss is observed between 70 and 200 °C. This region is characteristic of the elimination of water which forms a major portion of the bio-oil, and removal of acids, alcohols and other aromatic oxygenates such as mono-phenols and furans [42]. DTG peaks are observed in this region at temperatures of 77, 107 and 119 °C, at the heating rates of 5, 10 and 20 °C, respectively. The peaks move towards higher temperatures when the heating rate is increased due to thermal hysteresis, which increases at higher heating rates. At temperatures between 200 to 350°C, the decomposition of mono-sugars such as levoglucosan and poly-sugars such as cellobiosan takes place as reported

elsewhere[42,43]. The remaining bio-oil that underwent dehydration and crosslinking reactions [44–46] now forms carbonaceous structures that correspond to about 11.5% of the initial mass and are a result of the decomposition of pyro-lignin which is the heaviest fraction of the bio-oil[47]. The rate of mass loss continues to fall steadily beyond 350 °C as the volatile content is depleted and the residue left at the end is mostly carbonaceous char that does not decompose further.

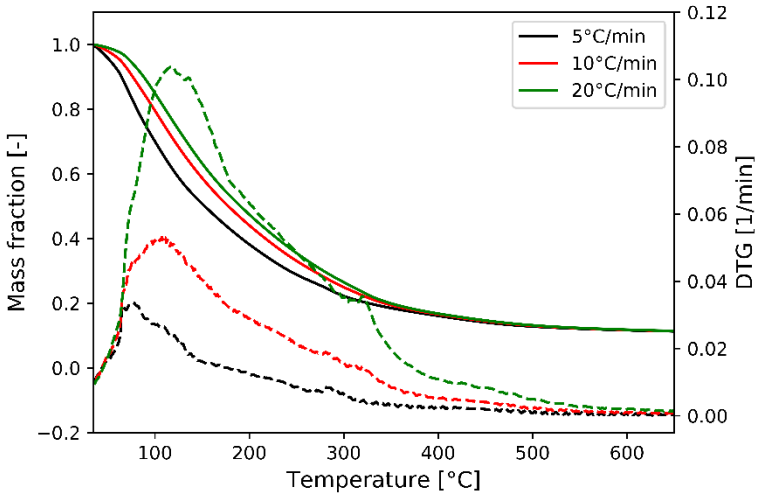

Figure 3-2 TGA (continuous line) and DTG (dotted line) characteristics of SCB bio-oil pyrolysis

3.2.2 Combustion of Bio-Oil

SCB bio-oil is a complex mixture of organic compounds and a large number of parallel oxidation reactions occur due to the presence of oxygen in the bio-oil and in the oxidizer air with increase in temperature. Figure 3-4 shows the TG and DTG histories of the bio-oil obtained during its combustion (in air) at the three heating rates. Analyzing the curves obtained, three zones are clearly identifiable: low temperature oxidation (LTO), fuel decomposition (FD), and high temperature oxidation (HTO). During the LTO phase, the fuel undergoes processes like boiling and devolatilization, where low molecular weight compounds are eliminated. Aromatic oxygenated compounds have also been

shown to oxidize at temperatures associated with the homogenous LTO phase (see Figure 3-3) [48–50].

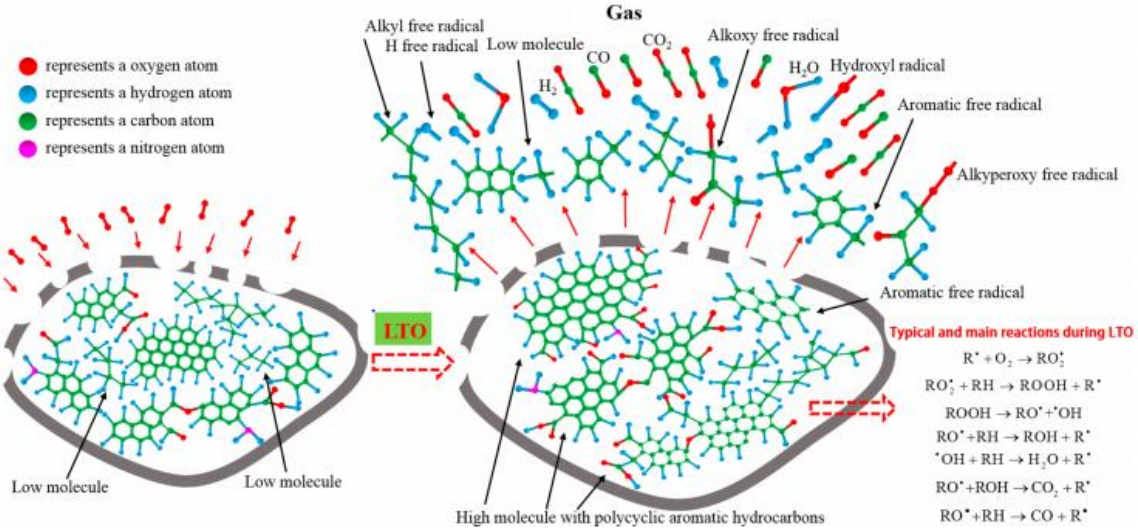

Figure 3-3 typical mechanism of LTO Oxidation [50]

The combustion characteristics of the fuel at the LTO stage resembles closely with that observed during the initial stages of pyrolysis. Maximum weight loss is observed at temperatures of 91, 103 and 129 °C, at heating rates of 5, 10 and 20 °C, respectively.

The fuel decomposition stage (FD) is characterized by a reduction in the rate of mass loss. This deceleration occurs mainly due to the decomposition of the fuel (thermal cracking) that requires the absorption of oxygen for the formation of intermediaries. In this stage there are a large number of high molecular weight components in the plastic layer [51] formed by the carbonization and crosslinking reactions, similar to the behavior reported in the pyrolysis of biomass [35,52]. During this stage the temperatures are sufficiently high as in order for the mineral content present in the bio-oil such as potassium to promote catalytic decomposition reactions [53,54]. This thermal decomposition stage occurs in the range of 289-407 °C at 5 °C/min, 307- 429 °C at 10 °C/min, and 339-449 °C at 20 °C/min. The low rate of thermal decomposition observed here is largely due to the stability of lignin, The pyrolytic lignin present in the bio-oil is a highly cross-linked polymeric form of lignin, composed

of phenolic groups which have lost a high number of substitutions due to the pyrolysis process to which they were subjected, its structure requires high energy for its bonds to be able to break, and generally the main component remaining at these temperatures [47].

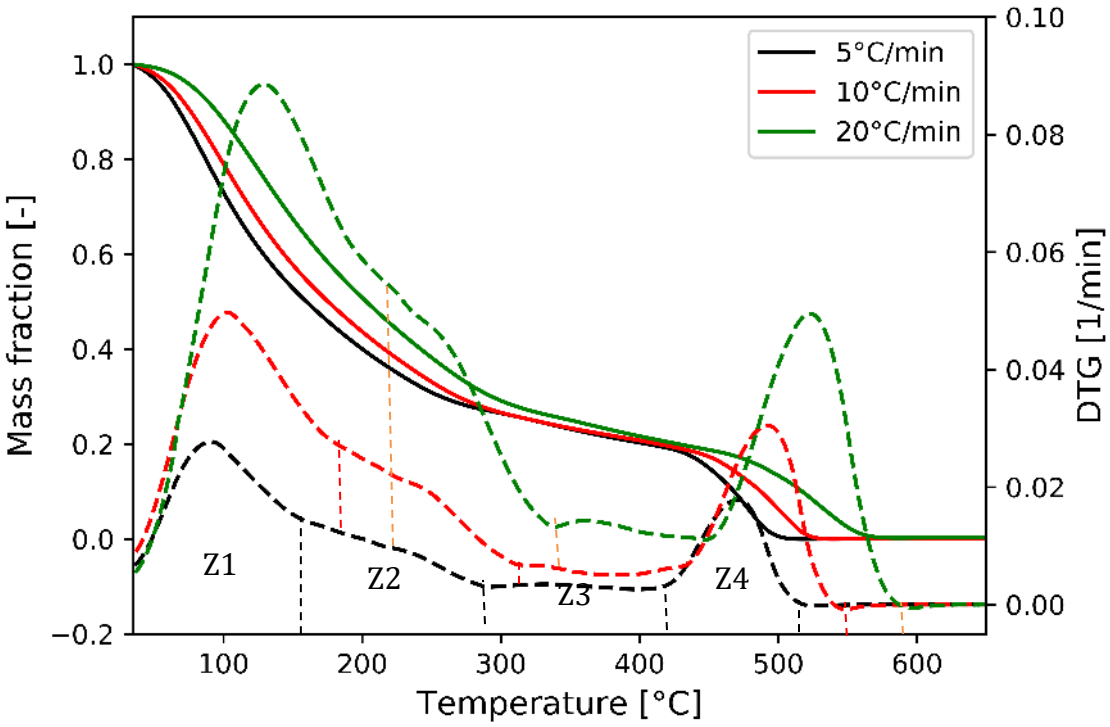

Figure 3-4 TGA (continuous line) and DTG (dotted line) characteristics of SCB bio-oil combustion

After the fuel decomposition stage, the solids formed pass to a stage in which high temperature oxidation reactions (HTO) occur as the activation energy necessary for the oxidation reactions in this stage is reached the R1 reactions R4 is very important because they are responsible for the formation of methane, carbon monoxide and dioxide. The gasification reactions are endothermic, however their products are highly combustible in the gas phase and this maintains the thermal balance[55]. The HTO stage is observed in the temperature ranges between 415-518 °C for a heating rate of

5°C/ min, 433-545°C at 10°C/ min and 449-593°C at 20°C / min. The solids formed in the fuel decomposition stage (FD) now go through a thermal cracking process on their surface that allows the migration of oxygen by diffusion through its pores, resulting in an almost complete oxidation close to 99.6% of the total mass of bio-oil.

R1) $C+O_2 \rightarrow CO_2$ ($\Delta H_{rxn}°$ (kJ/mol) −394)

R2) $C+H_2O \rightarrow CO+H_2$ ($\Delta H_{rxn}°$ (kJ/mol) +131)

R3) $C+CO_2 \rightarrow 2CO$ ($\Delta H_{rxn}°$ (kJ/mol) +172)

R4) $C+2H_2 \rightarrow CH_4$ ($\Delta H_{rxn}°$ (kJ/mol) −75)

Finally, Table 2 summarizes the possible zones found, the temperature at which the peaks identified by DTG appear and the Weight loss rate at the peak, something remarkable in these results is that as the heating rate of the peaks moves towards higher temperatures, this as suggested by other authors [56] may be related to the thermal delay that occurs at high heating rates [57] and therefore the time the sample is exposed to a heating stage

Table 3-2 Thermal degradation characteristics of PKS under nitrogen and air atmosphere with different heating rates of 5, 10, and 20 °C min−1.

β °C/min	Temperature range in zone °C				Peak temperature °C				Weight loss rate at the peak 1/min			
	Zone I	Zone II	Zone III	Zone IV	Tp1	Tp2	Tp3	Tp4	WLRp1	WLRp2	WLRp3	WLRp4
N2-5	61-182	/	260-319	/	78	/	287	/	0,033	/	0,008	/
N2-10	61-185	/	266-325	/	106	/	318	/	0,053	/	0,014	/
N2-20	61-187	/	300-352	/	118	/	319	/	0,103	/	0,035	/
Air-5	55-171	171-296	296-417	417-521	91	235	317	469	0,027	0,009	0,003	0,017
Air-10	55-224	224-302	302-425	425-548	102	250	336	494	0,050	0,020	0,007	0,030
Air-20	55-190	190-322	322-448	448-598	130	261	363	523	0,088	0,044	0,014	0,049

Figure 3-5 shows the DTG curves of the bio-oil pyrolysis and combustion at the three heating rates. The shape of the pyrolysis and combustion curves during the LTO stage is similar until it reaches a temperature at which a hysteresis is generated, which is characteristic of the oxygen absorption [58].

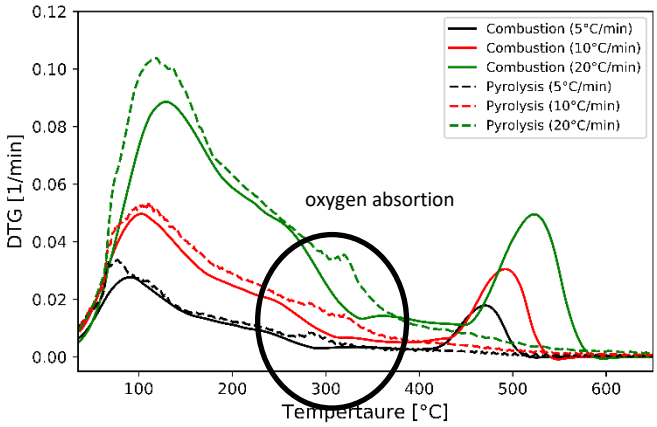

Figure 3-5 DTG comparison of SCB bio-oil pyrolysis (dotted line) and combustion (continuous line)

It would be expected that the DTG analysis between 100 and 300 °C for the case of pyrolysis and combustion at 20 °C /min would be very similar, however, it is evident that there are significant differences mainly due to two phenomena, the first is that The first stage of volatile release is difficult to replicate due to the experimental difficulties due to the evaporation of light components before carrying out the TGA analysis. And the second is the influence of the atmosphere, the oxygen present in the atmosphere is could be adsorbed to low temperatures on the liquid surface and this phenomenon reduces the rate of evaporation weight loss, this difference between the behavior of pyrolysis and combustion becomes less evident at a lower rate of heating because the exposure time at a given temperature increases, so the phenomenon is not appreciable

3.2.3 Kinetic analysis of Bio-Oil combustion

Kinetic modeling of the pyrolysis and combustion of the SCB bio-oil can help us understand the degradation/oxidation characteristics and aid in the design of combustors that can enhance efficiency and minimize emissions. Combustion of SCB bio-oil is a multi-component oxidation process[49,59], and it is known that the activation energy changes with the degree of conversion. The Miura and Maki model can be used to obtain a distribution of activation energies as a function of the reaction conversion (α) as shown in Figure 3-6. In the plot, the colored area next to the curve is the confidence interval of the fitting lines for each α selected.

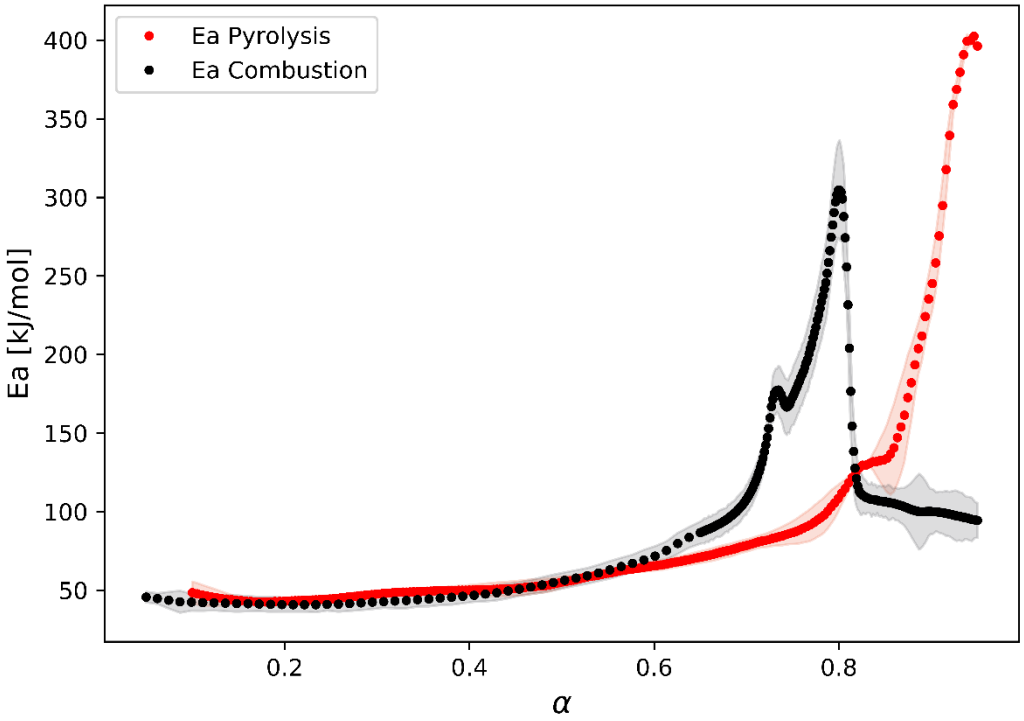

Figure 3-6 activation energy vs reaction conversion (α)

In Figure 3-6 it can be observed in the case of combustion and pyrolysis that the activation energy increases gradually from α = 0.1 to 0.8 ,. This increase may be the result of the decomposition of high molecular weight compounds, which are the product of the dehydration reactions of the lignin oligomers present in the bio-oil. This formed carbon is thermally stable and requires more energy to achieve oxidation. However, in the case of combustion, after reaching a maximum value at α = 0.8, the calculated activation energy falls. This can be explained because when the maximum rate of reaction and heat release is reached, this released heat spontaneously promotes the oxidation of the structures that have not yet oxidized, generating a reduction in the activation energy calculated with this model.

During pyrolysis, for alpha <0.5, E_a close to 65 kJ/mol was obtained. This value is close to other E_a values, reported by other authors in the devolatilization stage of low molecular weight compounds [49]. At higher conversions, E_a reaches values close to

150 kJ/mol corresponding to the values associated with the pyrolysis reaction of lignin oligomers [60] found in the bio-oil. At this stage cross-linking chain reactions occur as a result of decay reactions or exposed functional groups in the carbonaceous solids formed[61].

During combustion of SCB bio-oil, it can be seen that the activation energy distribution shows two clearly defined peaks, the first at α = 0.73 which is just before the decomposition reactions of the fuel are triggered. The second peak seen at α=0.8 corresponds to the HTO stage. The maximum E_a value in the FD stage was 179.4 kJ/mol and that during the HTO stage was 303.47 kJ/mol.

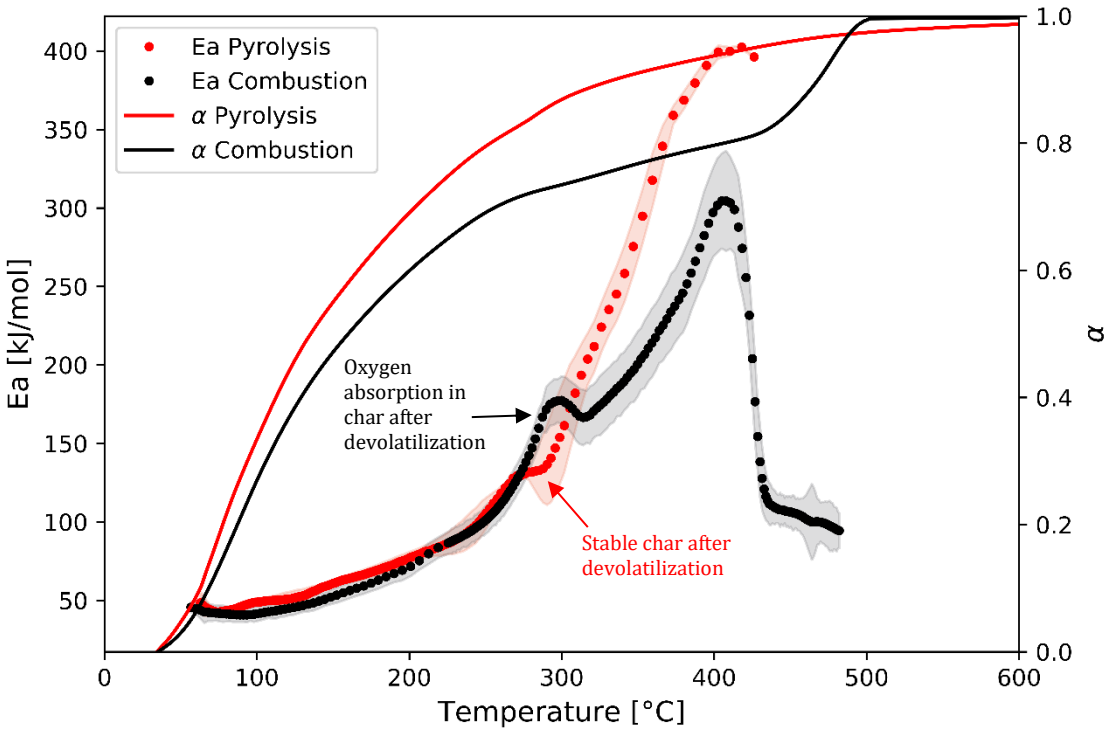

Figure 3-7 activation energy vs temperature until reach α = 0.85 in each process

Figure 3-7 shows the plot of E_a versus temperature for both pyrolysis and combustion at a heating rate of 5°C/min. It can be seen that in the case of pyrolysis the temperature required to reach α = 0.85 is only 326 °C, whereas the same conversion is achieved at a

higher temperature of 450 °C during combustion. This is due to the oxidation of the char formed at the end of the FD stage and char oxidation requires higher temperatures than devolatilization.

In Figure 3-7 it can be seen that at temperatures lesser than 250 °C the activation energy values are similar for both pyrolysis and combustion. This is mainly because similar processes like devolatilization occur during both processes. At temperatures between 250 and 320 °C, significant differences in the activation energies are observed between pyrolysis and combustion, which is due to the absorption of oxygen prior to the FD stage as explained before. The E_a increases due to the absorption of oxygen by the carbonaceous solids formed. Significant differences in the E_a are also observed between pyrolysis and combustion at temperatures greater than 320 °C. The apparent difference between the E_a values in the three combustion stages (LTO, FD and HTO) of SCB bio-oil shows the usefulness of the Miura and Maki model in capturing the reaction kinetics.

3.2.4 FTIR results

The coupling of the FTIR cell with the TG furnace allows us to measure the composition of the gases released during the pyrolysis and combustion of the bio-oil using characteristic IR absorbance bands. The measured IR absorbance corresponds to the amount of energy absorbed by the vibrational modes of various bonds and functional groups present in the gases. This allows us to identify and quantify the composition of gases such as carbon dioxide, carbon monoxide, and water amongst others[62]. Furthermore, it is also possible to give a qualitative description of the presence of aromatic C-C, aliphatic C-H, and C-O bonds in the gases.

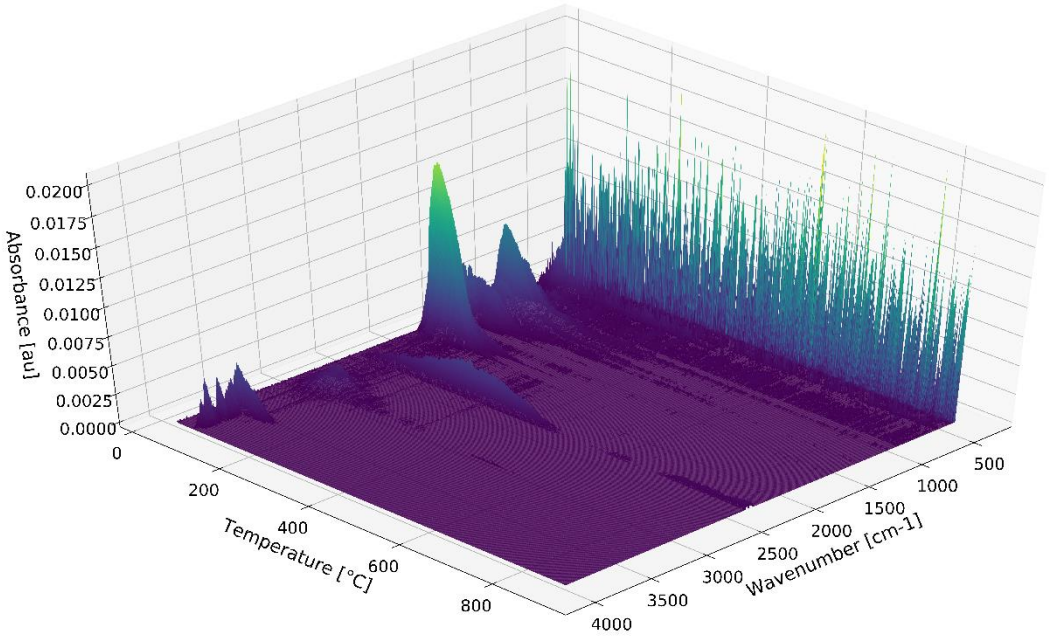

Figure 3-8. FTIR spectra of SCB bio-oil pyrolysis in N_2 at a heating rate of 5°C/min

3.3.1 *Evolved gases during pyrolysis*

Figure 3-8 shows the FTIR spectra of the gases evolved during the pyrolysis of the bio-oil at a heating rate of 5 °C/min. The main signals that produce a strong IR intensity are the stretching of the O-H group (3300 to 4000 cm^{-1}) [10,42,63], unsaturated and saturated C-H stretch in aromatic and aliphatic compounds (2600 to 3100 cm^{-1}) respectively, carbon dioxide (2360 cm^{-1}), oxygenated functional groups such as aldehydes, ketones and carboxylic acids C = O (1630 to 1780 cm^{-1}), aromatic C = C bond (1500 to 1600 cm^{-1}) and the bending vibrations in the fingerprint region (below 1500cm^{-1}) [10,62,63].

As observed during the pyrolysis of bio-oil at a temperature of 200 °C (see Figure 3-2), nearly 60% of the mass was lost due to devolatilization and this includes water, oxygenates and volatile organic compounds [42,49]. Five signals are of interest and their evolution along with the temperature is shown in Figure 3-9. The signals at 1745 and 1840 cm^{-1} correspond to C=O vibrational stretching of aldehydes, ketones and carboxylic acids (likely associated with acetic acid, and acetol), 1080 cm^{-1} correspond

to C–O bond stretch related to the presence of oxygenated compounds (associated with presence of anhydrides), 3870 cm^{-1} for H_2O, and 2360 cm^{-1} for CO_2.

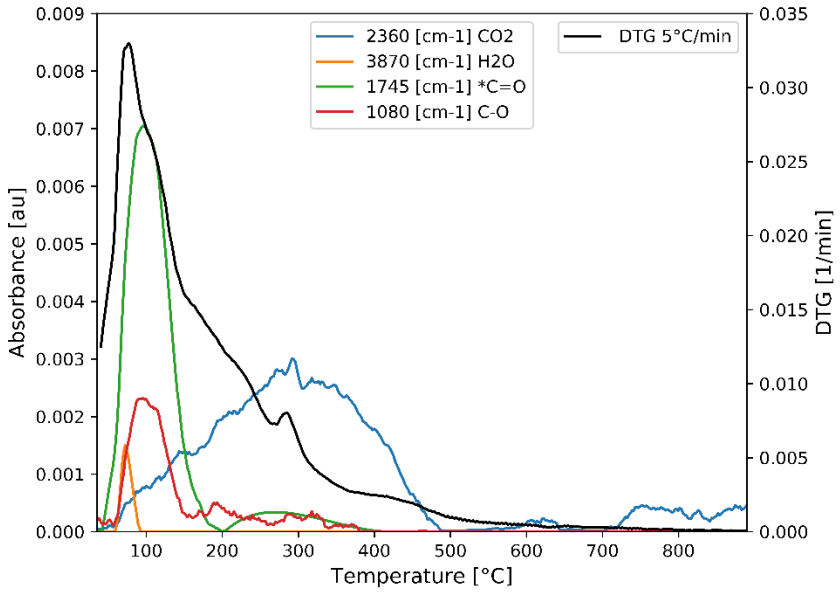

Figure 3-9 Selected wavenumbers evolution with temperature during pyrolysis of SCB bio-oil at heating rate of 5 °C/min

The signal associated with water shows a maximum at a temperature close to 90 °C and corresponds to the evaporation of water present in the bio-oil. The functional groups related to oxygenated compounds (C = O and CO) show a peak in the range from 100 to 200 °C and the signal at 1745 cm^{-1} is the most intense since aldehyde, ketone and carboxylic acid groups are abundant in the bio-oil. On the other hand, CO_2 shows a considerable presence beginning at 70 °C with a maximum concentration at temperatures close to 300 °C. The evolution of CO_2 completely ceases close to 500 °C, which indicates that it is a product of the decomposition of organic components in the bio-oil.

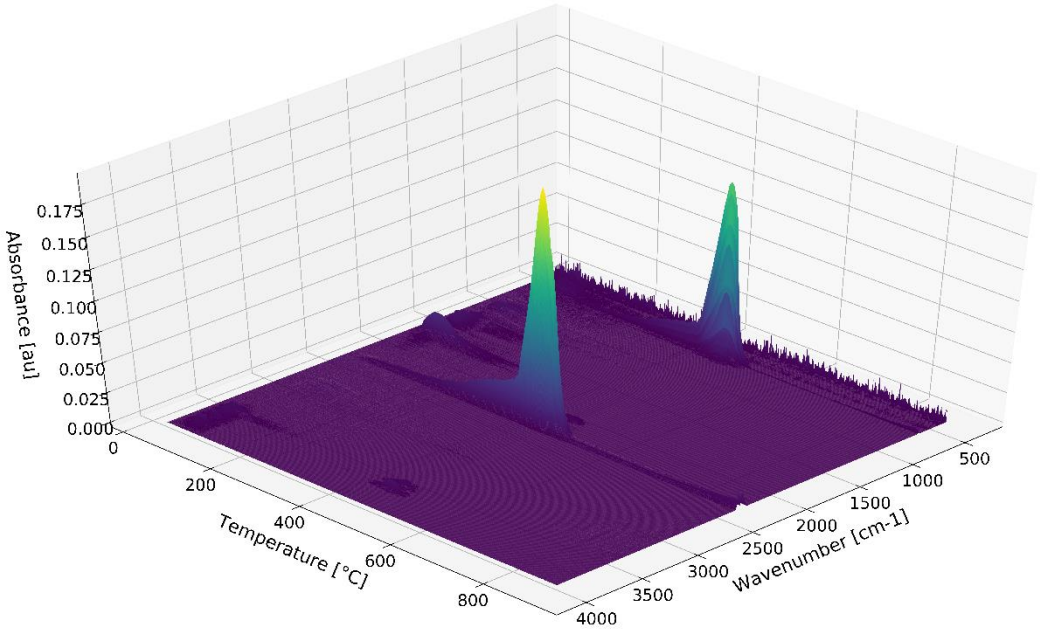

Figure 3-10. FTIR spectra of oxidation of SCB bio-oil in the air at a heating rate of 5°C/min

3.3.2 Evolved gases during combustion

Figure 3-10 shows the FTIR spectra of the gases evolved during the combustion of the bio-oil at a heating rate of 5 °C/min. In the region between 1850 to 500 cm^{-1} and temperatures below 200 °C, a pattern very similar to that obtained during bio-oil pyrolysis is observed, however, the intensity of the signal associated with CO_2 is ten times higher. This is due to the gas phase oxidation of the evolved gases from the bio-oil during the LTO stage. The peak corresponding to CO_2 which appears at 2360 cm^{-1} and the confirmation peak at 670 cm^{-1} in the fingerprint region is shown in Figure 3-11.

As can be seen in Figure 3-11, the carbon dioxide peak fits very well into the high-temperature oxidation region. This explains that the increase in mass loss measured in TG is because in this temperature range the greatest amount of combustion gases such as CO2, CO, and H2O are released.

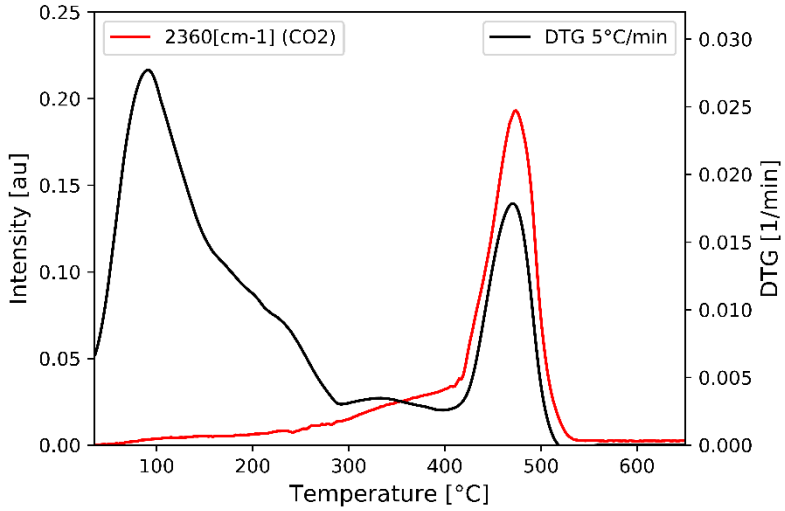

Figure 3-11 FTIR intensity evolution for 2360 cm-1, and 670 cm-1 wavenumbers

Figure 3-12 shows the evolution of H_2O (3733 cm^{-1}), CO (2119 cm^{-1}), and NO (1762 cm^{-1}) during the combustion of bio-oil at a heating rate of 5 °C/min. A prominent water peak appears at 73 °C owing to the evaporation of water in the bio-oil and then falls rapidly disappearing at 140 °C. The water peak re-appears in the range of (300 to 400°C) that corresponds to the fuel decomposition stage (FD) where the absorption of oxygen at the surface occurs along with carbonization reactions [64,65]. Between 400 to 500 °C, H_2O evolution increases, and peak intensity can be observed because of oxidation at high temperatures. In this range, the formation of CO is also observed due to the partial oxidation of the macromolecules formed during the FD stage[66].

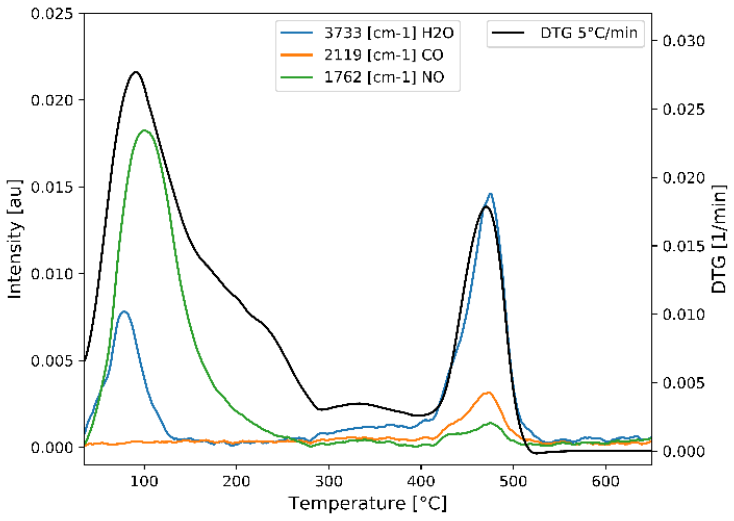

Figure 3-12 FTIR intensity evolution for 3733, 2119, and 1762 cm-1 during combustion

The nitrogen content of the bio-oil (0.14 wt %) is responsible for the fuel NO_x emissions during combustion. The contribution due to thermal NO_x may or may not be relevant due to the absence of high temperatures (>1500 °C) needed for its formation. A characteristic signal of the N-O interaction is associated with the signal of (1762 cm^{-1}) [12,67] and the NO signal attains a peak at 105 °C, soon after the maximum devolatilization peaks at 91°C. This can be attributed to the homogenous oxidation of N-containing low molecular weight compounds that are released during the LTO stage. During the HTO stage, the N-O signal corresponds to the nitrogen oxides formed due to the combustion of the carbonaceous macromolecules that contain nitrogen atoms in their core structure.

Comparing the gases released during combustion and pyrolysis, it is important to analyze the behavior of three gases, especially Methane, the functional group -OH, which can come mainly from water, and carbon dioxide. Figure 3-13 shows the curves of the three gases selected using different heating rates, how it can be seen both in pyrolysis and in combustion when increasing the heating rate increases the intensity of the signal peak and there is also a small displacement of the peak, this occurs because the gases released at a higher heating rate occupy the same volume of the measurement cell in a shorter time, so the relative concentration of the gases increases and this

increases the absorbance, and the displacement of the peak is the effect of the thermal delay suffered by the sample at a higher heating rate

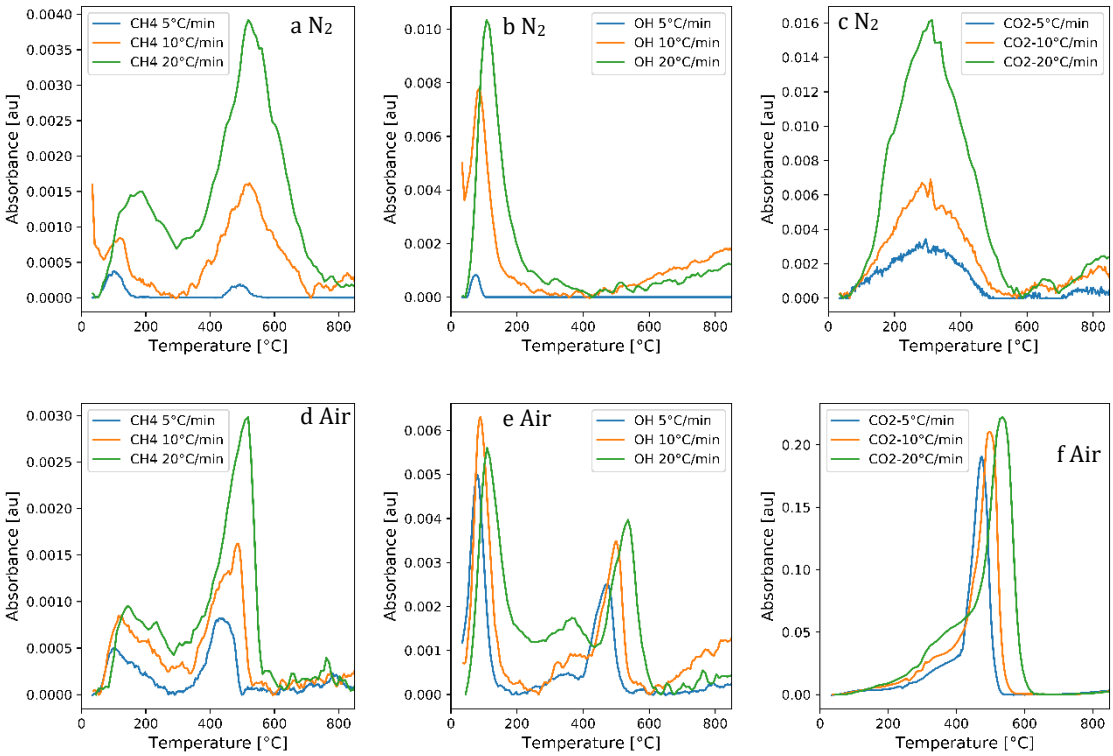

Figure 3-13 evolution of gases released during pyrolysis (a, b, c) and during combustion (e, f, g) the signals were assigned to the species methane (2850 cm-1), CO2 (2360 cm-1) and OH (3733 cm-1)

The methane released in both processes, pyrolysis and combustion has been previously reported [68,69] as the result of the decomposition of the methoxy group (-OCH3) or the methyl (-CH3) or methyl group (-CH3-). The methoxy group is usually associated with the decomposition of lignin or its derivative compounds during pyrolysis and methyl or methyl is associated with side chains in glycosidic compounds that come from the hemicellulose and lignin of the biomass with which the bio-oil was produced. Figure 3-13a and Figure 3-13d shows the evolution of methane during pyrolysis and combustion, respectively, the first peak may come from the decomposition of the methoxy groups from the pyrolytic lignin present in the bio-oil, and at high temperatures, it is produced by the effect of the decomposition of the side chains of the

high molecular weight char formed. Under combustion conditions, the intensity of the low signal is due to the formation of other gases such as water and carbon monoxide that dilute the gas, as reported in the case of the biomass Zhongqing Ma et al. [56].

Water, on the other hand, can appear by evaporation of water present in the bio-oil, by the formation of water during carbonization by dehydration reactions, and in air atmospheres as a result of the oxidation of the char. As can be seen in Figure 3-13b, there is a defined peak at low temperatures as a result of the evaporation of the water present in the bio-oil, and above 400 °C a signal of considerable intensity begins to appear as a result of the condensation reactions that are responsible for the formation of char. On the other hand, in the case of Figure 3-13e, there is a very defined peak between 400 and 600 °C that is the product of combustion.

And carbon dioxide in pyrolysis atmospheres (Figure 3-13c) can appear as a result of decarboxylation or decarbonylation as a route for thermal decomposition, for the case of biomass pyrolysis there are studies of TGA FTIR of hemicellulose [69,70] and cellulose [71,72], where two peaks of interest appear, the first associated with hemicellulose is by decarboxylation reactions of oxygenated groups (-COOH, C = O) linked to glucuronic acid units of xylan and the CO_2 peak reported high temperatures are associated with thermal decomposition of cellulose, However, extrapolating these studies to the composition of the bio-oil, the formation of carbon dioxide may be the result of the decarboxylation reactions of sugars present in the bio-oil. However, in the case of combustion, carbon dioxide (Figure 3-13f) is mainly the product of the oxidation of high molecular weight compounds that remain after the first stages of evaporation of light compounds.

3.3 **Conclusions**

The present investigation presents a TG-FTIR study on the pyrolysis and oxidation of bio-oil from sugarcane bagasse, using three heating rates, 5, 10 and 20 °C/min and the compositional analysis of the evolved gases. From the TG/DTG oxidation curves, three

macroscopic stages occurring during the thermal degradation of SCB bio-oil were identified. The low temperature oxidation (LTO) stage was characterized by the release water and oxygenates as identified from the FTIR spectra, for 20 °C / min it occurs at temperatures below350°C. Fuel decomposition (FD) stage identified by DTG analysis and kinetic analysis, identified between 350-450°C , and high temperature oxidation (HTO), which corresponds to a clear signal in FTIR of oxidation products such as CO2, H2O and CO and occurs at temperatures above 450 for a heating rate of 20 °C / min.

In the case of pyrolysis, after the devolatilization stage the formation of carbonized occurs, the fixed carbon obtained was 11.5% of the initial mass and are a result of the decomposition of pyro-lignin which is the heaviest fraction of the bio -oil, in the formation of carbonized it is possible to observe an FTIR signal assigned to CO2 and some oxygenated compounds released as a result of the re-polymerization reactions. In the case of combustion, although the signals of the aromatic groups released during devolatilization are very similar, the intensity of the CO2 peak is ten times higher, this because it is a product of oxidation at high temperatures.

From the kinetic analysis it was concluded that the thermal decomposition of the compounds present in the bio-oil leads to the formation of high molecular weight organic structures (char). These organic structures interact with the oxygen present in the air and this is absorbed at the surface as a previous step to oxidation at high temperatures. The Miura and Maki method is suitable for this analysis, since it allowed determining that the activation energy during the devolatilization stage for a heating rate of 5 °C/min varies between 50 and 100 kJ/mol. The decomposition stage of the fuel has a maximum activation energy value to be reached of 176 kJ/mol, and in the case of high temperatures oxidation the maximum energy that must be reached to trigger the oxidation is 320kJ/mol.

3.4 **Acknowledgments**

The authors wish to thank the Colciencias-Doctorados Nacionales 757-2016 fellowship and the project "Strategy of transformation of the Colombian energy sector in the horizon 2030" funded by call 788 of the Colciencias Scientific Ecosystem. Contract number FP44842-210-2018. This work was performed at King Abdullah University of Science and Technology (KAUST) Clean Combustion Research Center (CCRC) with funding from the KAUST Center Applied Research Fund (CARF). This research used resources of the KAUST Catalysis Center (KCC).

3.5 References

[1] J. Meng, X. Hu, P. Chen, D.M. Coffman, M. Han, The unequal contribution to global energy consumption along the supply chain, J. Environ. Manage. 268 (2020) 110701. https://doi.org/10.1016/j.jenvman.2020.110701.

[2] A.J. Ragauskas, A.J. Ragauskas, C.K. Williams, B.H. Davison, G. Britovsek, J. Cairney, C.A. Eckert, W.J.F. Jr, J.P. Hallett, D.J. Leak, C.L. Liotta, J.R. Mielenz, R. Murphy, R. Templer, T. Tschaplinski, The Path Forward for Biofuels, Science (80-.). 484 (2006). https://doi.org/10.1126/science.1114736.

[3] J. Kim, Production , separation and applications of phenolic-rich bio-oil – A review, Bioresour. Technol. 178 (2015) 90–98. https://doi.org/10.1016/j.biortech.2014.08.121.

[4] D. Shen, G. Liu, J. Zhao, J. Xue, S. Guan, R. Xiao, Thermo-chemical conversion of lignin to aromatic compounds : Effect of lignin source and reaction temperature, J. Anal. Appl. Pyrolysis. 112 (2015) 56–65. https://doi.org/10.1016/j.jaap.2015.02.022.

[5] R. Vallinayagam, S. Vedharaj, W.M. Yang, P.S. Lee, K.J.E. Chua, S.K. Chou, Combustion performance and emission characteristics study of pine oil in a diesel engine, Energy. 57 (2013) 344–351. https://doi.org/10.1016/j.energy.2013.05.061.

[6] D. Chen, J. Zhou, Q. Zhang, Effects of Torrefaction on the Pyrolysis Behavior and Bio-Oil Properties of Rice Husk by Using TG-FTIR and Py-GC / MS, Energy & Fuels. 28 (2014) 5857–5863. https://doi.org/10.1021/ef501189p.

[7] H. Ben, A.J. Ragauskas, NMR Characterization of Pyrolysis Oils from Kraft Lignin, Energy & Fuels. 25 (2011) 2322–2332. https://doi.org/10.1021/ef2001162.

[8] Z. Ma, Q. Sun, J. Ye, Q. Yao, C. Zhao, Study on the thermal degradation behaviors and kinetics of alkali lignin for production of phenolic-rich bio-oil using TGA – FTIR and Py – GC / MS, J. Anal. Appl. Pyrolysis. 117 (2016) 116–124. https://doi.org/10.1016/j.jaap.2015.12.007.

[9] S. Singh, C. Wu, P.T. Williams, Pyrolysis of waste materials using TGA-MS and TGA-FTIR as complementary characterisation techniques, J. Anal. Appl. Pyrolysis. 94 (2012) 99–107. https://doi.org/10.1016/j.jaap.2011.11.011.

[10] Z. Ma, D. Chen, J. Gu, B. Bao, Q. Zhang, Determination of pyrolysis characteristics and kinetics of palm kernel shell using TGA – FTIR and model-free integral methods, Energy Convers. Manag. 89 (2015) 251–259. https://doi.org/10.1016/j.enconman.2014.09.074.

[11] E. Apaydin-varol, E. Pütün, Synthetic fuel production from cottonseed : Fast pyrolysis and a TGA / FT-IR / MS study, J. Anal. Appl. Pyrolysis. 105 (2014) 83–90. https://doi.org/10.1016/j.jaap.2013.10.006.

[12] G.K. Parshetti, A. Quek, R. Betha, R. Balasubramanian, TGA – FTIR investigation of co-combustion characteristics of blends of hydrothermally carbonized oil palm biomass (EFB) and coal, Fuel Process. Technol. 118 (2014) 228–234. https://doi.org/10.1016/j.fuproc.2013.09.010.

[13] G.D. Strahan, C.A. Mullen, A.A. Boateng, Characterizing Biomass Fast Pyrolysis Oils by 13 C NMR and Chemometric Analysis, Energy & Fuels. 25 (2011) 5452–5461. https://doi.org/https://doi.org/10.1021/ef2013166.

[14] B. Parameswaran, Sugarcane Bagasse, in: P.A. Singh nee' Nigam P. (Ed.), Biotechnol. Agro-Industrial Residues Util., Springer, Dordrecht, 2009: pp. 239–

240. https://doi.org/10.1007/978-1-4020-9942-7.

[15] ASOCAÑA, Aspectos Generales del sector agroindustrial de la caña 2018-2019, 2019. https://www.asocana.org/modules/documentos/.

[16] J.I. Montoya, C. Valdés, F. Chejne, C.A. Gómez, A. Blanco, G. Marrugo, J. Osorio, E. Castillo, J. Aristóbulo, J. Acero, Bio-oil production from Colombian bagasse by fast pyrolysis in a fluidized bed : An experimental study, J. Anal. Appl. Pyrolysis. 112 (2015) 379–387. https://doi.org/10.1016/j.jaap.2014.11.007.

[17] S. Tarazanov, K. Grigoreva, A. Shipitcyna, O. Repina, Assessment of the chemical stability of furfural derivatives and the mixtures as fuel components, Fuel. 271 (2020) 117594. https://doi.org/10.1016/j.fuel.2020.117594.

[18] P.R. Patwardhan, R.C. Brown, B.H. Shanks, Understanding the Fast Pyrolysis of Lignin, ChemSusChem. 4 (2011) 1629–1636. https://doi.org/10.1002/cssc.201100133.

[19] J. Lehto, A. Oasmaa, Y. Solantausta, M. Kytö, D. Chiaramonti, Fuel oil quality and combustion of fast pyrolysis bio-oils, VTT Publ. (2013) 79. https://doi.org/10.1016/j.apenergy.2013.11.040.

[20] S. Arya, A. Sharma, M. Rawat, A. Agrawal, Tyre pyrolysis oil as an alternative fuel : A review, Mater. Today Proc. (2020) 4–7. https://doi.org/10.1016/j.matpr.2020.04.797.

[21] R. Kumar, V. Strezov, H. Weldekidan, J. He, S. Singh, T. Kan, B. Dastjerdi, Lignocellulose biomass pyrolysis for bio-oil production : A review of biomass pre-treatment methods for production of drop-in fuels, Renew. Sustain. Energy Rev. 123 (2020) 109763. https://doi.org/10.1016/j.rser.2020.109763.

[22] A. Gani, A. Jameel, N. Naser, G. Issayev, J. Touitou, M. Kumer, A. Emwas, A. Farooq, S. Dooley, S.M. Sarathy, A minimalist functional group (MFG) approach for surrogate fuel formulation, Combust. Flame. 192 (2018) 250–271. https://doi.org/10.1016/j.combustflame.2018.01.036.

[23] A. Gani, A. Jameel, N. Naser, A. Emwas, S.M. Sarathy, Surrogate formulation for

diesel and jet fuels using the minimalist functional group (MFG) approach, Proc. Combust. Inst. 37 (2019) 4663–4671. https://doi.org/10.1016/j.proci.2018.09.035.

[24] A.G. Abdul Jameel, S.M. Sarathy, Lube Products: Molecular Characterization of Base Oils, Encycl. Anal. Chem. (2018) 1–14. https://doi.org/10.1002/9780470027318.a1824.pub2.

[25] A.M. Elbaz, A. Gani, N. Hourani, A.H. Emwas, S.M. Sarathy, W.L. Roberts, TG/DTG, FT-ICR Mass Spectrometry, and NMR Spectroscopy Study of Heavy Fuel Oil, Energy and Fuels. 29 (2015) 7825–7835. https://doi.org/10.1021/acs.energyfuels.5b01739.

[26] A. Gani, A. Jameel, Y. Han, O. Brignoli, S. Telalovi, Heavy fuel oil pyrolysis and combustion : Kinetics and evolved gases investigated by TGA-FTIR, 127 (2017) 183–195. https://doi.org/10.1016/j.jaap.2017.08.008.

[27] R. Palani, A. AbdulGani, N. Balasubramanian, Treatment of Tannery Effluent Using a Rotating Disc Electrochemical Reactor, Water Environ. Res. 89 (2016) 77–85. https://doi.org/10.2175/106143016x14609975746046.

[28] R. Zhang, Z. Zhong, Y. Huang, Combustion characteristics and kinetics of bio-oil, Front. Chem. Eng. China. 3 (2009) 119–124. https://doi.org/10.1007/s11705-009-0068-x.

[29] S. Xiu, H.K. Rojanala, A. Shahbazi, E.H. Fini, L. Wang, Pyrolysis and combustion characteristics of Bio-oil from swine manure, J. Therm. Anal. Calorim. 107 (2012) 823–829. https://doi.org/10.1007/s10973-011-1604-8.

[30] S. Liu, M. Chen, Q. Hu, J. Wang, L. Kong, The kinetics model and pyrolysis behavior of the aqueous fraction of bio-oil, Bioresour. Technol. 129 (2013) 381–386. https://doi.org/10.1016/j.biortech.2012.11.006.

[31] K. Miura, A new and simple method to estimate f(E) and ko(E) in the distributed activation energy model from three sets of experimental data, Energy & Fuels. 9 (1995) 302–307. https://doi.org/10.1021/ef00050a014.

[32] K. Miura, T. Maki, A Simple Method for Estimating f(E) and k0(E)inthe Distributed Activation Energy Model, Energy & Fuels. 0 (1998) 864–869. https://doi.org/10.1021/ef970212q.

[33] X. Zhang, W. de Jong, F. Preto, Estimating kinetic parameters in TGA using B-spline smoothing and the Friedman method, Biomass and Bioenergy. 33 (2009) 1435–1441. https://doi.org/10.1016/j.biombioe.2009.06.009.

[34] J. Iván, M. Arbeláez, Kinetic Study and Phenomenological Modeling of a Biomass Particle during Fast Pyrolysis Process, Universidad Nacional de Colombia, 2016. http://bdigital.unal.edu.co/56371/1/1152202970.2016.pdf.

[35] J.I. Montoya Arbeláez, F. Chejne Janna, M. Garcia-Pérez, Fast pyrolysis of biomass: A review of relevant aspects. Part I: Parametric study, Dyna. 82 (2015) 239–248. https://doi.org/10.15446/dyna.v82n192.44701.

[36] J. Montoya, B. Pecha, D. Roman, F. Chejne, M. Garcia-perez, Effect of temperature and heating rate on product distribution from the pyrolysis of sugarcane bagasse in a hot plate reactor, J. Anal. Appl. Pyrolysis. 123 (2017) 347–363. https://doi.org/10.1016/j.jaap.2016.11.008.

[37] R.H. C. R. Shaddix, D, Combustion Properties of Biomass Flash Pyrolysis Oils : Final Project Report, 1999. https://doi.org/10.2172/5983.

[38] ASTM, ASTM D7544-12 Standard Specification for Pyrolysis Liquid Biofuel, 2017. https://doi.org/10.1520/D7544-12R17.Copyright.

[39] A. Oasmaa, I. Fonts, M.R. Pelaez-Samaniego, M.E. Garcia-Perez, M. Garcia-Perez, Pyrolysis Oil Multiphase Behavior and Phase Stability: A Review, Energy and Fuels. 30 (2016) 6179–6200. https://doi.org/10.1021/acs.energyfuels.6b01287.

[40] J. Lehto, A. Oasmaa, Y. Solantausta, M. Kytö, D. Chiaramonti, Review of fuel oil quality and combustion of fast pyrolysis bio-oils from lignocellulosic biomass, Appl. Energy. 116 (2014) 178–190. https://doi.org/10.1016/j.apenergy.2013.11.040.

[41] Q. Sohaib, A. Muhammad, M. Younas, Fast pyrolysis of sugarcane bagasse: Effect of pyrolysis conditions on final product distribution and properties, Energy Sources, Part A Recover. Util. Environ. Eff. 39 (2017) 184–190. https://doi.org/10.1080/15567036.2016.1212292.

[42] F. Stankovikj, M. Garcia-perez, TG-FTIR Method for the Characterization of Bio-oils in Chemical Families, Energy & Fuels. 30 (2017) 1689–1701. https://doi.org/10.1021/acs.energyfuels.6b03132.

[43] M. Garcia-Perez, A. Chaala, H. Pakdel, D. Kretschmer, C. Roy, Characterization of bio-oils in chemical families, Biomass and Bioenergy. 31 (2007) 222–242. https://doi.org/10.1016/j.biombioe.2006.02.006.

[44] Z. Xiong, S.S.A. Syed-hassan, X. Hu, J. Guo, J. Qiu, X. Zhao, Pyrolysis of the aromatic-poor and aromatic-rich fractions of bio-oil : Characterization of coke structure and elucidation of coke formation mechanism, Appl. Energy. 239 (2019) 981–990. https://doi.org/10.1016/j.apenergy.2019.01.253.

[45] Z. Xiong, Y. Wang, S.S.A. Syed-hassan, X. Hu, H. Han, S. Su, Effects of heating rate on the evolution of bio-oil during its pyrolysis, Energy Convers. Manag. 163 (2018) 420–427. https://doi.org/10.1016/j.enconman.2018.02.078.

[46] Z. Xiong, S.S.A. Syed-hassan, X. Hu, J. Guo, Y. Chen, Q. Liu, Effects of the component interaction on the formation of aromatic structures during the pyrolysis of bio-oil at various temperatures and heating rates, Fuel. 233 (2018) 461–468. https://doi.org/10.1016/j.fuel.2018.06.064.

[47] B. Scholze, D. Meier, Characterization of the water-insoluble fraction from pyrolysis oil (pyrolytic lignin). Part I . PY – GC / MS , FTIR , and functional groups, 60 (2001) 41–54.

[48] C. Branca, P. Giudicianni, C. Di Blasi, GC / MS Characterization of Liquids Generated from Low-Temperature Pyrolysis of Wood, Ind. Eng. Chem. Res. 42 (2003) 3190–3202. https://doi.org/10.1021/ie030066d.

[49] C. Branca, C. Di Blasi, Multistep mechanism for the devolatilization of biomass fast

pyrolysis oils, Ind. Eng. Chem. Res. 45 (2006) 5891–5899. https://doi.org/10.1021/ie060161x.

[50] S. Zhao, W. Pu, M.A. Varfolomeev, C. Yuan, A.A. Rodionov, Integrative Investigation of Low-Temperature Oxidation Characteristics and Mechanisms of Heavy Crude Oil, Ind. Eng. Chem. Res. 58 (2019) 14595–14602. https://doi.org/10.1021/acs.iecr.9b03346.

[51] Y. Chen, S. Lee, A. Tahmasebi, J. Bai, M. Mahoney, J. Yu, Review article A review of the state-of-the-art research on carbon structure evolution during the coking process : From plastic layer chemistry to 3D carbon structure establishment, Fuel. 271 (2020) 117657. https://doi.org/10.1016/j.fuel.2020.117657.

[52] A.R. Teixeira, K.G. Mooney, J.S. Kruger, C.L. Williams, W.J. Suszynski, L.D. Schmidt, D.P. Schmidt, P.J. Dauenhauer, Aerosol generation by reactive boiling ejection of molten cellulose, Energy Environ. Sci. 4 (2011) 4306. https://doi.org/10.1039/c1ee01876k.

[53] Q. Li, X. Wang, Y. Xin, Z. Zhang, Y. Zhang, C. Hao, M. Meng, L. Zheng, L. Zheng, A unified intermediate and mechanism for soot combustion on potassium-supported oxides, (2014) 1–6. https://doi.org/10.1038/srep04725.

[54] M. Safar, B. Lin, W. Chen, D. Langauer, J. Chang, H. Raclavska, A. Pétrissans, P. Rousset, M. Pétrissans, Catalytic effects of potassium on biomass pyrolysis , combustion and torrefaction, Appl. Energy. 235 (2019) 346–355. https://doi.org/10.1016/j.apenergy.2018.10.065.

[55] T.H. Fletcher, Gasification fundamentals, Elsevier Ltd, 2017. https://doi.org/10.1016/B978-0-08-100167-7.00006-8.

[56] Z. Ma, J. Wang, Y. Yang, Y. Zhang, C. Zhao, Y. Yu, S. Wang, Comparison of the thermal degradation behaviors and kinetics of palm oil waste under nitrogen and air atmosphere in TGA-FTIR with a complementary use of model-free and model-fitting approaches, J. Anal. Appl. Pyrolysis. 134 (2018) 12–24. https://doi.org/10.1016/j.jaap.2018.04.002.

[57] M.A. Gómez, M.A. Álvarez, P. Eguía, R. Comesa, Thermal lag analysis on a simulated TGA-DSC device, Thermochim. Acta. 547 (2012) 13–21. https://doi.org/10.1016/j.tca.2012.08.008.

[58] J. Deng, L. Ren, L. Ma, C. Lei, G. Wei, W. Wang, Effect of oxygen concentration on low-temperature exothermic oxidation of pulverized coal, Hermochimica Acta. 667 (2018) 102–110. https://doi.org/10.1016/j.tca.2018.07.012.

[59] M. Garcia-Perez, P. Lappas, P. Hughes, L. Dell, A. Chaala, D. Kretschmer, C. Roy, Evaporation and combustion characteristics of biomass vacuum pyrolysis oils, IFRF Combust. J. 200601 (2006) 1–27.

[60] P.J. De Wild, W.J.J. Huijgen, H.J. Heeres, Pyrolysis of wheat straw-derived organosolv lignin, J. Anal. Appl. Pyrolysis. 93 (2012) 95–103. https://doi.org/10.1016/j.jaap.2011.10.002.

[61] W. Chaiwat, I. Hasegawa, T. Tani, K. Sunagawa, K. Mae, Analysis of cross-linking behavior during pyrolysis of cellulose for elucidating reaction pathway, Energy and Fuels. 23 (2009) 5765–5772. https://doi.org/10.1021/ef900674b.

[62] N. Gao, A. Li, C. Quan, L. Du, Y. Duan, TG – FTIR and Py – GC / MS analysis on pyrolysis and combustion of pine sawdust, J. Anal. Appl. Pyrolysis. 100 (2013) 26–32. https://doi.org/10.1016/j.jaap.2012.11.009.

[63] H. Li, S. Niu, C. Lu, Y. Wang, Comprehensive Investigation of the Thermal Degradation Characteristics of Biodiesel and Its Feedstock Oil through TGA – FTIR, (2015). https://doi.org/10.1021/acs.energyfuels.5b01054.

[64] X. Wang, H. Chen, M. Zhang, H. Yang, Combustion characteristics of bio-oil and its kinetic analysis, Huazhong Keji Daxue Xuebao (Ziran Kexue Ban)/Journal Huazhong Univ. Sci. Technol. (Natural Sci. Ed. 36 (2008) 92–94. https://www.scopus.com/inward/record.uri?eid=2-s2.0-44249083488&partnerID=40&md5=dac466e96abf6321cd51f1e13ac5d6ce.

[65] B. Shrestha, Y. Le Brech, T. Ghislain, S. Leclerc, V. Carré, F. Aubriet, S. Hoppe, P. Marchal, S. Pontvianne, N. Brosse, A. Dufour, A Multitechnique Characterization

of Lignin Softening and Pyrolysis, ACS Sustain. Chem. Eng. 5 (2017) 6940–6949. https://doi.org/10.1021/acssuschemeng.7b01130.

[66] C.R. Shaddix, S.P. Huey, Combustion characteristics of fast pyrolysis oils derived from hybrid poplar, Dev. Thermochem. Biomass Convers. (1997) 1630.

[67] C. Wang, Y. Wu, Q. Liu, H. Yang, F. Wang, Analysis of the behaviour of pollutant gas emissions during wheat straw / coal co fi ring by TG – FTIR, Fuel Process. Technol. 92 (2011) 1037–1041. https://doi.org/10.1016/j.fuproc.2010.12.029.

[68] S. Wang, H. Lin, B. Ru, W. Sun, Y. Wang, Z. Luo, Comparison of the pyrolysis behavior of pyrolytic lignin and milled wood lignin by using TG–FTIR analysis, J. Anal. Appl. Pyrolysis. 108 (2014) 78–85. https://doi.org/10.1016/j.jaap.2014.05.014.

[69] Y. Ding, O.A. Ezekoye, S. Lu, C. Wang, Thermal degradation of beech wood with thermogravimetry / Fourier transform infrared analysis, Energy Convers. Manag. 120 (2016) 370–377. https://doi.org/10.1016/j.enconman.2016.05.007.

[70] K. Werner, L. Pommer, M. Broström, Thermal decomposition of hemicelluloses, J. Anal. Appl. Pyrolysis. (2014) 1–8. https://doi.org/10.1016/j.jaap.2014.08.013.

[71] W. Shurong, L.I.U. Qian, L.U.O. Zhongyang, W.E.N. Lihua, C.E.N. Kefa, Mechanism study on cellulose pyrolysis using thermogravimetric analysis coupled with infrared spectroscopy, 1 (2007) 413–419. https://doi.org/10.1007/s11708-007-0060-8.

[72] D.K. Shen, S. Gu, The mechanism for thermal decomposition of cellulose and its main products, Bioresour. Technol. 100 (2009) 6496–6504. https://doi.org/10.1016/j.biortech.2009.06.095.

4 An investigation into the break-up modes of bio-oil droplets from sugarcane bagasse in air and nitrogen atmosphere

The combustion of bio-oil derived from the pyrolysis of sugarcane bagasse is a relatively simple technology, the bio-oil is conducted by a line to a combustion chamber where it is atomized in a hot atmosphere The combustion of bio-oil derived from the pyrolysis of sugarcane bagasse is a relatively simple technology, the bio-oil is conducted by a line to a combustion chamber where it is atomized in a hot atmosphere [1], however, its control is very challenging, the phenomena associated with the production of pollutants, low stability in the process and excessive formation of unburned lead to a low efficiency [1–4]. These problems encountered are closely related to the dynamics of the drop during its heating.

The heating mechanism of a drop in a higher temperature environment occurs mainly by the combination of two phenomena, conduction, and convection with the hot gases around it. When the temperature is high enough to achieve the formation of a flame front, usually the two-layer model is used to describe the area outside the condensed phase, in this model in the layer between the condensed phase and the flame front. the heat is conducted by conduction to the surface of the liquid, if the liquid has the same boiling point then the evaporation will only be superficial

Usually, the temperature profile within the drop is assumed to be uniform, however, the presence of multi-components forms a surface layer on the surface of the drop that changes the conductivity and therefore the rate of heat transfer on the surface. causing the internal temperature changes to be considerable.

During the heating of the drop, several phenomena occur simultaneously, such as the evaporation of volatile compounds [5,6] and the formation of gases on the surface and inside the drop are of great importance since the vapors and gases form bubbles within the drop. droplets that grow, coalesce, and collapse to form microdroplets [7]. When the bubbles reach the surface of the drop, and the internal energy of the bubble exceeds the surface energy, the drop breaks, and the microdroplets are released, then the surface of the drop deforms to form an ejection [8].

Bio-oil is a complex mixture of chemical compounds in a wide range of chemical families and molecular weights [9–11], an important part of it is made up of high molecular weight compounds called pyrolytic lignin that increase the probability of forming unburned [12], Teixeira et al. [13] found that the presence of these high molecular weight compounds (Da <1000) increase the frequency of occurrence of micro-explosions.

Microbursts have the potential to improve atomization in the combustion chamber and this is a way to increase the efficiency of combustion in low calorific fuels [14]. just as it does. Lack of antecedents of drop evaporation experiments linked to the formation of carbonaceous structures [15] which in practical terms is one of the main limitations in the use of bio-oil as fuel.

In this work, an analysis of the microexplosions that occur when the bio-oil droplets are suspended in atmospheres of air and nitrogen is presented, from the images, the shape of the droplet was obtained and the evolution of the reduced diameter was reported. Allowing to classify, measure the intensity and frequency of occurrence of droplet breaking phenomena, and micro-explosions, the classification of these disruptive events sheds new light on the dynamics of the bio-oil droplets inside the combustion chambers and these data They can significantly help increase combustion efficiencies by reducing the degree of burnout, which will minimize the degree of contamination caused by the use of this technology.

4.1 Experimental

4.1.1 Droplet experiments

The suspended droplet experiments were carried out using an oven in which the droplet is exposed perpendicularly to a laminar stream of gas (Nitrogen or Air) that is heated by passing through a honeycomb, the 12 cm long ceramic honeycomb in alumina and with a pore size of 1 mm allows to increase the heat transfer area which allows the gas to heat up, it also allows curling the gas flow that passes through it, that is inside an oven, the laminar regime is necessary to avoid turbulent convective heat transfer and to bring the experiment to replicable conditions, as can be seen in Figure 4-1.

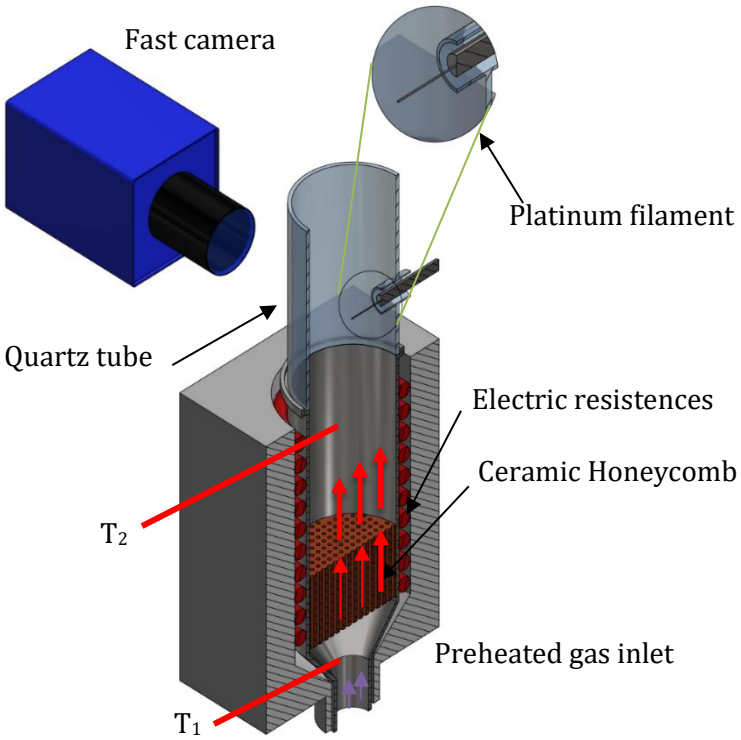

Figure 4-1 Experimental setup for the analysis of bio-oil micro explosions under pyrolysis and combustion conditions. T1 and T2 represent the thermocouples for controlling the resistors R1 and R2

The preheated gas enters the lower part of the oven which passes through a honeycomb to increase its temperature to the desired temperature (560°C), the thermocouple that

controls the electrical resistances of the oven is positioned two centimeters below the drop to guarantee a laminar flow, typically the gas flow is approximately 15 N ml/min of nitrogen or air depending on the type of experiment. In the upper part of the gas heating furnace, there is a quartz chamber with a lateral opening that allows the entry of platinum filament 75 μm in diameter with the suspended drop (2 mm) as can be seen in Figure 4-1. Perpendicular to the drop by the external part 15 cm from the quartz tube, a high-speed camera was located to follow the shape of the drop during heating, The images were acquired using a high-speed camera (LaVisión Imager Pro) coupled with a magnification lens Nikon AF-S micro Nikkor 105 mm the capture speed used was 500 fps, the photos obtained were taken in contrast, for this, a high-intensity white light source (Sumita LS-M352) with a diffuser was placed in the direction of the camera lens.

4.1.2 images post-processing

A recognition of the contours was carried out on each of the images, each frame obtained was treated to select the region where the identification of the contour will be carried out, eliminating the background and the filament, to only have the evolution of the drop. The script that allows contour measurement is written in Python that uses the Open-Cv ® library for contour detection, typically a suspended drop test contains a number 7500 frames, in each of them a suitable threshold is used to filter the bottom of the elements is binarized and erode operations are performed to detect the drop. The contour and area are measured in pixels and using a measurement pattern it is possible to obtain the physical magnitude of the diameter and the perimeter frame by frame.

4.2 Results

All the experiments were carried out with a bio-oil product of the pyrolysis of sugarcane bagasse at 560 °C, the chemical characteristics of the bio-oil were thoroughly reported in chapter 1 and the thermal decomposition characteristics were presented in chapter 2, the bio-oil was filtered using a 45 μm cellulose filter. the size of the drop varies in each test (2±0.3 mm), but the results are normalized concerning the initial size.

4.2.1 Contour identification

To achieve the identification of the contour, the section of interest of the photograph was cut preserving the same distribution of pixels. A thresholding operation was necessary to filter the image-making erode and Open CV library algorithm for the identification of contours. As can be seen in the image, in the original image it is possible to see the presence of a bubble inside the drop (this will be explained in detail, later on, the software recognizes the bubble inside the drop, but only the complete outline of the drop is Using this contour identification it is possible to analyze the evolutionary dynamics of the bio-oil droplets during their heating in atmospheres of air and nitrogen and classify the disruptive events that occur in the process.

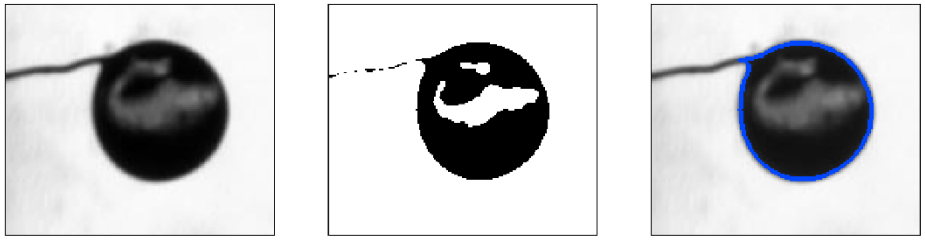

Figure 4-2 droplet postprocessing for contour identification

A contour identification sequence is presented in Figure 4-2, the first image on the left corresponds to the original image, the next one is the result of the transformation and troubleshooting operations and finally, the result of the contour identification can be seen superimposed on the original image.

4.2.2 suspended droplet dynamics in air atmosphere

The gas temperature was stabilized at 560 ° C before the drop entered the filming area, as mentioned in the methodology, the area of the drop was calculated using the photographs of the drop evolution until they no longer appear. apparent changes. The results for an experiment of a droplet suspended in an air atmosphere are shown in

¡Error! No se encuentra el origen de la referencia.. The dynamics of the droplet starts with a reduction in diameter, this occurs between 0 and 1.16 s (2.9% of the initial size) by the model described by C.K Law [16]in which the change in diameter is the result of surface evaporation rate. However, as bio-oil, it is a multi-component mixture with a molecular weight distribution ranging from 100Da to 1500Da [17–19]. Many of these low molecular weight compounds begin resounding evaporation forming bubbles inside the drop, this causes the drop to increase in size.

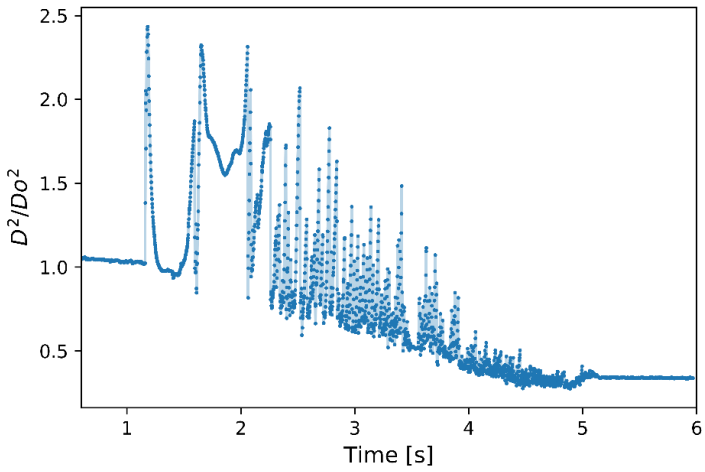

Figure 4-3 D^2/D_0^2 evolution for bio-oil droplets suspended in platinum bare in 560°C air atmosphere

The appearance of bubbles is the key step in the mechanism of formation of drop rupture events [3] and there are several mechanisms to release the gas within the formed bubble, the first mechanism is the transport of vapors through the film of liquid formed between the surface of the bubble and the surface of the drop where the mass transfer is dominated by a diffusive transport of vapors [20], however, it is also possible that the internal pressure in the bubble exceeds the maximum pressure that it can support the liquid layer [21,22] and a disruptive event occurs, breaking the continuity of the liquid and generating microdroplets as a result of this break [13,14].

Both events occur in the first peak that appears in the signal in Figure 4-3, to have a better understanding of this phenomenon an enlargement of the first peak is shown in Figure 4-4, in which an abrupt increase in the diameter between the point a and b, at

the point where the drop ejects a quantity of mass and the surface of the drop vibrates as a result of the ejection, as previously reported by Teixeira [13] and its size is reduced to point c, the reduction in size between point b and c is the result of an ejection event, it should also be remembered that this technique only allows us to see the two-dimensional projection of a three-dimensional shape, possibly in another plane the drop could have been significantly reduced. However, due to the scale of the effect, it is acceptable that the quantification of these phenomena is carried out in this way.

Followed by this event, the size increases again and the formation of bubbles leads the drop to a maximum located at point d, in which the vapor inside the drop is visible, however in this case the drop does not undergo a breaking event, as mentioned above the gas permeates the liquid layer through diffusive transport and the size drops exponentially from point d to f.

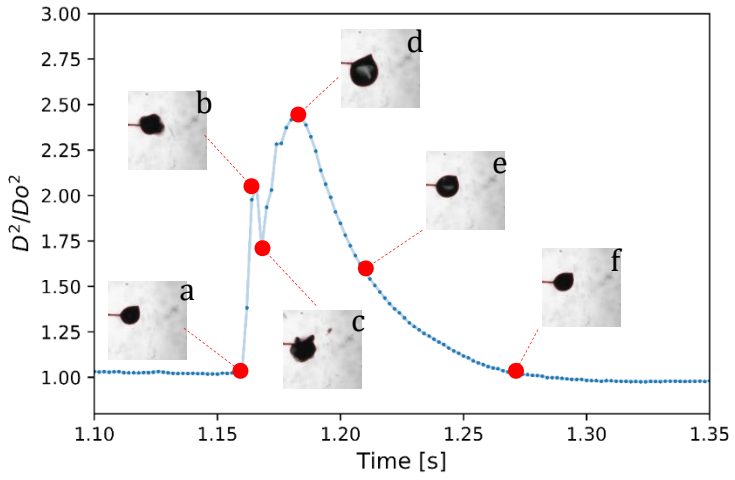

Figure 4-4 D^2/D_0^2 evolution for bio-oil droplets suspended in platinum bare in 560°C air atmosphere, description of evaporation releasing of vapors from bubble inside of a droplet of SCB Bio-oil

The conditions for this transport of gas through the liquid layer between the bubble and the droplet to occur largely depend on the rate of vapor formation and the average molecular weight. In the experiments carried out, this type of event was only visible

during the first moments of the experiment, this is attributable to the fact that the first compounds to evaporate are of low molecular weight, favoring diffusion through the liquid. On the other hand, the events that are after this stage are the result of a balance of phenomena that occur simultaneously.

The behavior of all the drop breaking events found are the product of the increase in pressure inside the drop by the vapors formed. The vapors come from vaporization and thermal decomposition of the bio-oil components. This vaporization occurs within the drop and not on its surface because there are nucleation points because in the bio-oil there are dissolved solids of high molecular weight [2,23] that contribute to nucleation. Figure 4-5 shows a segment of Figure 4-3 between 2.35 and 2.60 s.

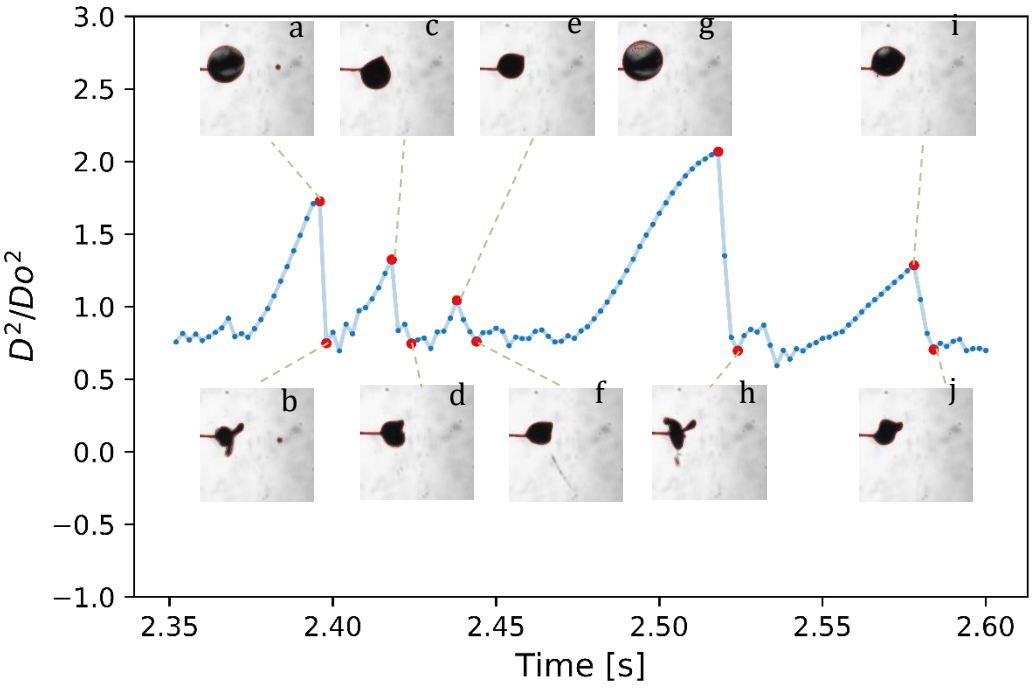

Figure 4-5 D^2/D_0^2 evolution for bio-oil droplets suspended in platinum bare in 560°C air atmosphere, description of break-up events

In **¡Error! No se encuentra el origen de la referencia.** you can see the occurrence of f ive consecutive events, each one begins with an increase in the size of the drop followed by a breakdown and deformation. The deformation of the drop is greater when the drop

has reached a larger diameter, the intensity of the event (I_e) can be measured as the difference between the values D^2/D_0^2 between the maximum and its minimum value for the peaks measured during the experiment (equation (4)**¡Error! No se encuentra el origen de la referencia.**).

$$I_e = \left[\left(\frac{D^2}{D_0^2} \right)_{max} - \left(\frac{D^2}{D_0^2} \right)_{min} \right] \quad (5)$$

Using the definition of event intensity, it was possible to measure each of these in the experiment, the intensity of each event is presented in **¡Error! No se encuentra el origen de la referencia.**, in this it is possible to observe that the intensity of the events decreases over time, this may occur because :

a.) The amount of gases by vaporization and thermal cracking is reduced as the size of the droplet decreases. However, gases from thermal cracking become important.

b.) Heating favors the formation of a solid product of depolymerization reactions of the lignin derivatives [24–26] present in the bio-oil, this increases internal nucleation and with this the number of bubbles within the drop.

c.) The heating forms an elastic skin [27] on the drop product of dehydration and polymerization reactions [28,29] that increases the surface tension allowing a greater expansion of the drop.

However, the frequency of occurrence of events increases until it reaches a maximum between 3 and 4 and then falls again as can be seen in the upper histogram of Figure 4-6. This behavior is closely related to the reduction in the formation of vapors inside the drop, at this time surface evaporation, facilitated by the formation of high molecular weight structures on the surface of the drop, shows that the intensity of the events is significantly reduced. In Figure 4-6 it can also be seen that the number of high-intensity events is reduced with the decrease in the size of the drop, this is linked with the reduction in the production of vapors

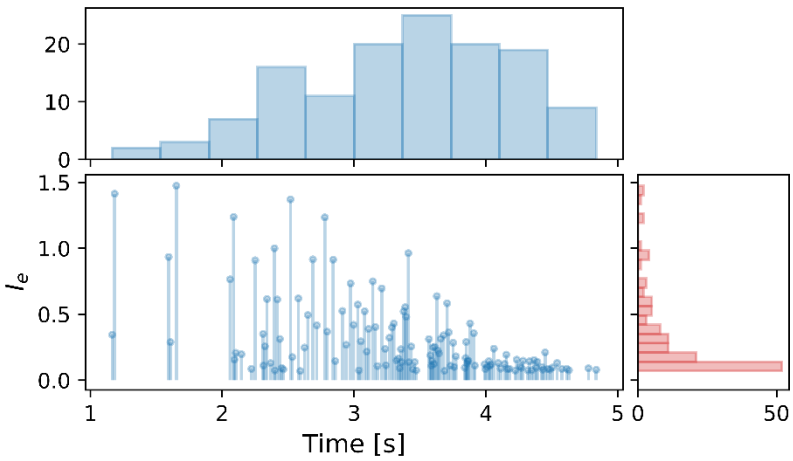

Figure 4-6 Events Intensity during bio-oil droplets suspended in platinum bare in 560°C air atmosphere, and distribution in time (upside) and Intensity distribution events (right side).

4.2.3 suspended droplet dynamics in a Nitrogen atmosphere

Suspended droplet experiments at 560 ° C were performed using SCB Bio-oil under a nitrogen atmosphere. The results of the contour detection are presented in Figure 7. The bio-oil drop shows a size reduction, reaching a minimum of 20% of the initial size. In the first stage, the bio-oil undergoes a process of liberation of volatile compounds such as low molecular weight such as alcohols, acids, aromatics, mono-phenols, and sugar derivatives such as 5-HMF [9], the high presence of these compounds Low molecular weight favors the formation of a drop breaking event.

The phase change temperatures of the compounds detectable by GC-Ms are between 60 and 300°C [30,31] so that nucleation boiling occurs within the droplets [32] and their size increases significantly. before breaking the surface and forming the ejecta. In the absence of air, the bio-oil begins to undergo thermal cracking which leads to the production of methane gas, carbon monoxide, hydrogen, and carbon dioxide, mainly macromolecular pyrolysis gases [33–36], with the very low molecular weight with high diffusivity in liquids, so the intensity of disruptive events decreases significantly.

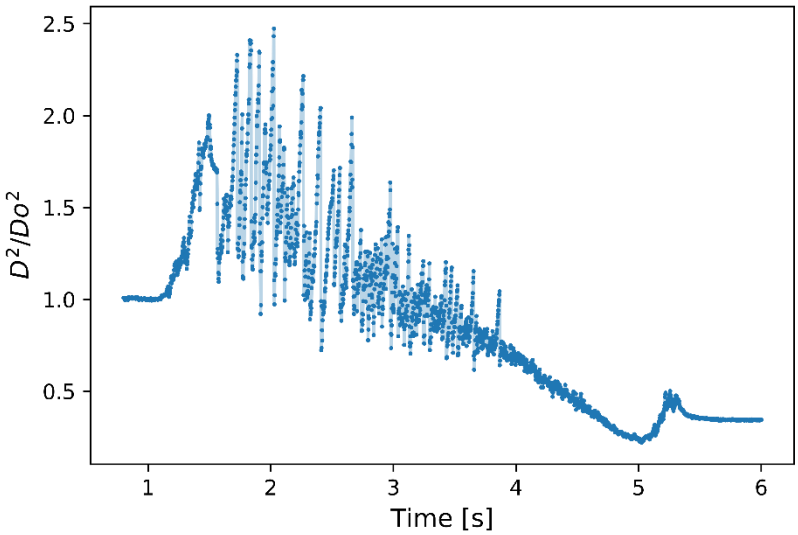

Figure 4-7 D^2/D_0^2 evolution for bio-oil droplets suspended in platinum bare in 560°C N_2 atmosphere

Regarding the occurrence of events, these occur more frequently during devolatilization that occurs in the first seconds. Then the intensity decreases considerably as the size of the droplet gets smaller. A series of events appears during the swelling solid formation stage. But these correspond to the collapse of the solid structure that is being formed (Figure 8).

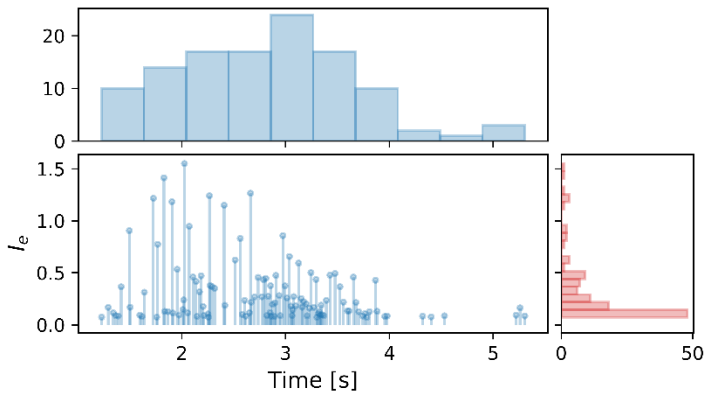

Figure 4-8 Events Intensity during bio-oil droplets suspended in platinum bare in 560°C air atmosphere, and distribution of intensity (right side).

High-magnitude events during oil pyrolysis are of low frequency and occur in the first seconds of the experiment, where the viscosity of the liquid is expected to be low, as seen in other works such as Solomon [37] by increasing the viscosity of liquids the magnitude of the choices is significantly reduced [11,38] this in large part because the crosslinking reactions increase the molecular weight and the surface tension the gas contained in the bubbles formed cannot be abruptly expelled from the drop and it is released mainly by diffusion.

It should also be noted that in the first seconds of heating there is the highest rate of release of volatiles so that the bubbles formed inside the drop reach a greater diameter and therefore greater pressure, when they reach the surface they explode with greater intensity

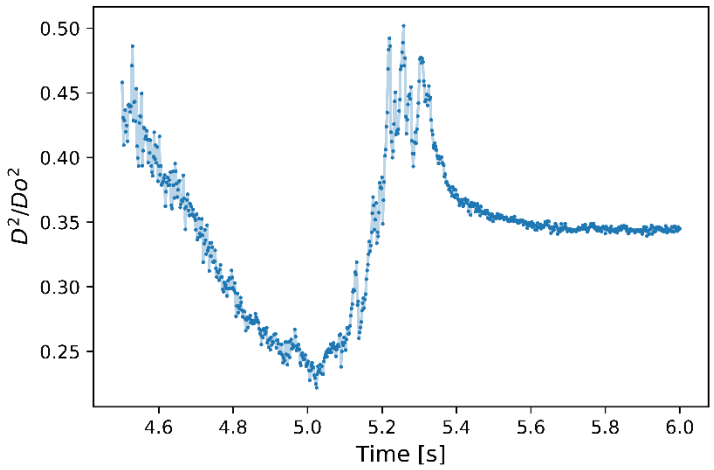

Figure 4-9 char formation, evidenced at the end of the experiment carried out in a nitrogen atmosphere

Under pyrolysis conditions, carbonization reactions by dehydration [27] and chain crosslinking [28] are of great importance, this is evident at the end of the test. High molecular weight compounds formed during thermal cracking have a high plasticity characteristic [39]. For this reason, in the end, they achieve an increase in their size. This swelling is characteristic of coking coals where the plasticity of the walls retain the

gases formed, expanding as a result of internal pressure [40]. Figure 4-9 shows an enlargement of **¡Error! No se encuentra el origen de la referencia.**

On the other hand, the droplet evaporation dynamics is not only influenced by the complex composition of the bio-oil, a predominant factor in the process obtain the transfer of heat from the outside to the center of the drop, the classic heating mechanism proposes that a hot environment transfers heat by conduction and if there is the movement of the gas around the drop also by convection, but this heat transfer from the outside to the inside of the drop is also limited by the formation of a layer of gases or vapors around the drop, As it is a multi-component mixture, this layer presents a mixture of gases with different enthalpies of vaporization, as well as relative densities and thermal conductivities, which seriously affect heat transfer and vaporization rate.

4.3 Conclusions

High magnitude events during pyrolysis and combustion have a low frequency of occurrence and are visible in the first seconds of the experiment where the viscosity of the liquid is still low, the magnitude of the events is also related to the speed of volatile formation and is strongly influenced by heat transfer. which is affected by the outer layer of the drop formed by the vapors and their differences in thermal properties

The formation of disruptive events always starts from the formation of bubbles inside the drop, the formation of bubbles is the key factor in the event of breaking of the drop if the time that the bubble remains inside the drop is very high pressure will increase sufficiently to break the barrier that covers the surface.

In the last stage of pyrolysis, the formation of Char could be measured, this char obtained after the pyrolysis process and the degradation and volatilization of many compounds products of pyrolysis is the result of the formation of porous carbonaceous structures formed by the swelling of a high molecular weight polymer that comes from

the crosslinking and dehydration reactions of the macro-polymers formed during pyrolysis

4.4 References

[1] A. Oasmaa, C. Peacocke, S. Gust, D. Meier, R. McLellan, Norms and standards for pyrolysis liquids. End-user requirements and specifications, Energy and Fuels. 19 (2005) 2155–2163. https://doi.org/10.1021/ef040094o.

[2] J. Lehto, A. Oasmaa, Y. Solantausta, M. Kytö, D. Chiaramonti, Fuel oil quality and combustion of fast pyrolysis bio-oils, VTT Publ. (2013) 79. https://doi.org/10.1016/j.apenergy.2013.11.040.

[3] C.R. Shaddix, S.P. Huey, Combustion characteristics of fast pyrolysis oils derived from hybrid poplar, Dev. Thermochem. Biomass Convers. (1997) 1630.

[4] R.H. C. R. Shaddix, D, Combustion Properties of Biomass Flash Pyrolysis Oils : Final Project Report, 1999. https://doi.org/10.2172/5983.

[5] P. Mellin, W. Yang, X. Yu, Comprehensive Secondary Pyrolysis in Fluidized-bed Fast Pyrolysis of Biomass, a Fluid Dynamics Based Modelling Effort, in: J.X. Joyce M. Xia D. (Ed.), Energy Procedia, Elsevier Ltd, 2015: pp. 281–284. https://doi.org/10.1016/j.egypro.2015.02.057.

[6] M. Pelucchi, K.P. Somers, U. Burke, C. Saggese, A. Frassoldati, E. Ranzi, H.J. Curran, T. Faravelli, Kinetic modelling of biofuels: Pyrolysis and auto-ignition of aldehydes, Chem. Eng. Trans. 37 (2014) 871–876. https://doi.org/10.3303/CET1437146.

[7] D.E. Spiel, The number and size of jet drops produced by air bubbles bursting on a fresh water surface, J. Geophys. Res. 99 (1994) 10289–10296. https://doi.org/10.1029/94JC00382.

[8] K.M. Butler, A Numerical Model for Combustion of Bubbling Thermoplastic Materials in Microgravity, 2002.

https://tsapps.nist.gov/publication/get_pdf.cfm?pub_id=861181.

[9] F. Stankovikj, M. Garcia-perez, TG-FTIR Method for the Characterization of Bio-oils in Chemical Families, Energy & Fuels. 30 (2017) 1689–1701. https://doi.org/10.1021/acs.energyfuels.6b03132.

[10] M. Garcia-Perez, A. Chaala, H. Pakdel, D. Kretschmer, C. Roy, Characterization of bio-oils in chemical families, Biomass and Bioenergy. 31 (2007) 222–242. https://doi.org/10.1016/j.biombioe.2006.02.006.

[11] J. D'alessio, M. Lazzaro, P. Massoli, V. Moccia, Thermo-optical investigation of burning biomass pyrolysis oil droplets, Symp. Combust. 27 (1998) 1915–1922. https://doi.org/10.1016/S0082-0784(98)80035-0.

[12] M. Garcia-Perez, P. Lappas, P. Hughes, L. Dell, A. Chaala, D. Kretschmer, C. Roy, Evaporation and combustion characteristics of biomass vacuum pyrolysis oils, IFRF Combust. J. 200601 (2006) 1–27.

[13] A.R. Teixeira, K.G. Mooney, J.S. Kruger, C.L. Williams, W.J. Suszynski, L.D. Schmidt, D.P. Schmidt, P.J. Dauenhauer, Aerosol generation by reactive boiling ejection of molten cellulose, Energy Environ. Sci. 4 (2011) 4306. https://doi.org/10.1039/c1ee01876k.

[14] D.C.K. Rao, S. Syam, S. Karmakar, R. Joarder, Experimental investigations on nucleation , bubble growth , and micro- explosion characteristics during the combustion of ethanol / Jet A-1 fuel droplets, Exp. Therm. Fluid Sci. 89 (2017) 284–294. https://doi.org/10.1016/j.expthermflusci.2017.08.025.

[15] T.R. Carlson, J. Jae, Y. Lin, G.A. Tompsett, G.W. Huber, Catalytic fast pyrolysis of glucose with HZSM-5 : The combined homogeneous and heterogeneous reactions, J. Catal. 270 (2010) 110–124. https://doi.org/10.1016/j.jcat.2009.12.013.

[16] C.H. Wang, X.Q. Liu, C.K. Law, Combustion and microexplosion of freely falling multicomponent droplets, Combust. Flame. 56 (1984) 175–197. https://doi.org/10.1016/0010-2180(84)90036-1.

[17] J. Montoya, B. Pecha, D. Roman, F. Chejne, M. Garcia-perez, Effect of temperature and heating rate on product distribution from the pyrolysis of sugarcane bagasse in a hot plate reactor, J. Anal. Appl. Pyrolysis. 123 (2017) 347–363. https://doi.org/10.1016/j.jaap.2016.11.008.

[18] C. Erlich, E. Bjornbom, D. Bolado, M. Giner, T. Fransom, E. Björnbom, D. Bolado, M. Giner, T.H. Fransson, Pyrolysis and gasification of pellets from sugar cane bagasse and wood, Fuel. 85 (2006) 1535–1540. https://doi.org/10.1016/j.fuel.2005.12.005.

[19] M. Carrier, T. Hugo, J. Gorgens, H. Knoetze, Comparison of slow and vacuum pyrolysis of sugar cane bagasse, J. Anal. Appl. Pyrolysis. 90 (2011) 18–26. https://doi.org/10.1016/j.jaap.2010.10.001.

[20] P.J. Dauenhauer, J.L. Colby, C.M. Balonek, J. Suszynski, L.D. Schmidt, Cutting-edge research for a greener sustainable future Reactive boiling of cellulose for integrated catalysis through an intermediate liquid †, Green Chem. 11 (2009) 1485–1704. https://doi.org/10.1039/b915068b.

[21] J. Wang, X. Qiao, D. Ju, C. Sun, T. Wang, Bubble nucleation , micro-explosion and residue formation in superheated jatropha oil droplet : The phenomena of vapor plume and vapor cloud, Fuel. 261 (2020) 116431. https://doi.org/10.1016/j.fuel.2019.116431.

[22] M.S. Oh, W.A. Peters, J.B. Howard, An experimental and modeling study of softening coal pyrolysis, AIChE J. 35 (1989) 775–792. https://doi.org/10.1002/aic.690350509.

[23] B. Scholze, C. Hanser, D. Meier, Characterization of the water-insoluble fraction from fast pyrolysis liquids (pyrolytic lignin) Part II . GPC , carbonyl goups , and 13 C-NMR, J. Anal. Appl. Pyrolysis. 59 (2001) 387–400.

[24] B. Shrestha, Y. Le Brech, T. Ghislain, S. Leclerc, V. Carré, F. Aubriet, S. Hoppe, P. Marchal, S. Pontvianne, N. Brosse, A. Dufour, A Multitechnique Characterization of Lignin Softening and Pyrolysis, ACS Sustain. Chem. Eng. 5 (2017) 6940–6949.

https://doi.org/10.1021/acssuschemeng.7b01130.

[25] Z. Xiong, S.S.A. Syed-hassan, X. Hu, J. Guo, J. Qiu, X. Zhao, Pyrolysis of the aromatic-poor and aromatic-rich fractions of bio-oil : Characterization of coke structure and elucidation of coke formation mechanism, Appl. Energy. 239 (2019) 981–990. https://doi.org/10.1016/j.apenergy.2019.01.253.

[26] Z. Xiong, S.S.A. Syed-hassan, J. Xu, Y. Wang, S. Hu, S. Su, Evolution of coke structures during the pyrolysis of bio-oil at various temperatures and heating rates, J. Anal. Appl. Pyrolysis. 134 (2018) 336–342. https://doi.org/10.1016/j.jaap.2018.06.023.

[27] Y. Chen, S. Lee, A. Tahmasebi, J. Bai, M. Mahoney, J. Yu, Review article A review of the state-of-the-art research on carbon structure evolution during the coking process : From plastic layer chemistry to 3D carbon structure establishment, Fuel. 271 (2020) 117657. https://doi.org/10.1016/j.fuel.2020.117657.

[28] W. Chaiwat, I. Hasegawa, T. Tani, K. Sunagawa, K. Mae, Analysis of cross-linking behavior during pyrolysis of cellulose for elucidating reaction pathway, Energy and Fuels. 23 (2009) 5765–5772. https://doi.org/10.1021/ef900674b.

[29] J.V. and G.M.B. Shoucheng Du, Characteristics and origin of char and coke from fast and slow, catalytic and thermal pyrolysis of biomass and relevant model compounds, Green Chem. Green. 15 (2013) 3214–3229. https://doi.org/10.1039/b000000x.

[30] F. Stankovikj, C.-C. Tran, S. Kaliaguine, M. V. Olarte, M. Garcia-Perez, Evolution of Functional Groups during Pyrolysis Oil Upgrading, Energy & Fuels. (2017) acs.energyfuels.7b01251. https://doi.org/10.1021/acs.energyfuels.7b01251.

[31] A.R. Teixeira, R.J. Hermann, J.S. Kruger, W.J. Suszynski, L.D. Schmidt, D.P. Schmidt, P.J. Dauenhauer, Microexplosions in the upgrading of biomass-derived pyrolysis oils and the effects of simple fuel processing, ACS Sustain. Chem. Eng. 1 (2013) 341–348. https://doi.org/10.1021/sc300148b.

[32] G. Lu, X. Wang, W. Yan, International Journal of Heat and Mass Transfer Nucleate

boiling inside small evaporating droplets : An experimental and numerical study, Int. J. Heat Mass Transf. 108 (2017) 2253–2261. https://doi.org/10.1016/j.ijheatmasstransfer.2017.01.081.

[33] D. Yepes, F. Chejne, Gasificación de biomasa residual en el sector floricultor , caso : Oriente Antioqueño Gasification of waste biomass in the flower industry , case : Eastern Antioquia, ION. 25 (2012) 49–55.

[34] G. Marrugo, C.F. Valdés, F. Chejne, Biochar Gasification: An Experimental Study on Colombian Agroindustrial Biomass Residues in a Fluidized Bed, Energy & Fuels. 31 (2017) 9408–9421. https://doi.org/10.1021/acs.energyfuels.7b00665.

[35] Z. Xiong, Y. Wang, S.S.A. Syed-Hassan, X. Hu, H. Han, S. Su, K. Xu, L. Jiang, J. Guo, E.E.S. Berthold, S. Hu, J. Xiang, Effects of heating rate on the evolution of bio-oil during its pyrolysis, Energy Convers. Manag. 163 (2018) 420–427. https://doi.org/10.1016/j.enconman.2018.02.078.

[36] S.I. Yang, M.S. Wu, T.C. Hsu, Spray combustion characteristics of kerosene/bio-oil part I: Experimental study, Energy. 119 (2017) 26–36. https://doi.org/10.1016/j.energy.2016.12.062.

[37] P.R. Solomon, M.A. Serio, E.M. Suuberg, Coal pyrolysis: Experiments, kinetic rates and mechanisms, Prog. Energy Combust. Sci. 18 (1992) 133–220. https://doi.org/10.1016/0360-1285(92)90021-R.

[38] A.R. Teixeira, K.G. Mooney, J.S. Kruger, C.L. Williams, W.J. Suszynski, L.D. Schmidt, D.P. Schmidt, P.J. Dauenhauer, Aerosol generation by reactive boiling ejection of molten cellulose, Energy Environ. Sci. 4 (2011) 4306–4321. https://doi.org/10.1039/c1ee01876k.

[39] J. Iván, M. Arbeláez, Kinetic Study and Phenomenological Modeling of a Biomass Particle during Fast Pyrolysis Process, Universidad Nacional de Colombia, 2016. http://bdigital.unal.edu.co/56371/1/1152202970.2016.pdf.

[40] J. Yu, V. Strezov, J. Lucas, G. Liu, T. Wall, A mechanistic study on char structure

evolution during coal devolatilization- experiments and model predictions, Proc. Combust. Inst. 29 (2002) 467–473.

5 On the modeling of the micro-explosions during the evaporation and pyrolysis of a bio-oil droplet.

The bio-oil from the fast pyrolysis of biomass exhibits a complex combustion and evaporation behavior, mainly due to the presence of chemical compounds with very marked volatility differences. Typically drop evaporation experiments show three stages: the first being a heating stage, followed by evaporation by bubbling and micro explosions [1–3], and finally, a remaining heavy fraction is pyrolyzed to form a carbonaceous structure[4,5].

In spray combustion of fuels with large differences in volatility in their components or artificial emulsions of oil/water such as diesel/water [6] or HFO/water[7], the occurrence of explosive evaporation of water or the most volatile components can be overserved. and this induces secondary atomization producing a large number of microparticles, Microexplosion improves the mixing of fuel and air during combustion, which results in an improvement in efficiency and a decrease in polluting emissions. [3,8,9].

In the case of microexplosions in bio-oils, experimental works can be found on the evaporation of pyrolytic oil droplets from lignocellulosic biomass [1,2,10,11] and

numerous studies on the kinetics under different atmospheres [12–14], which concluded that the size of the droplet, the rate of heating, as well as the composition play a fundamental role in the characteristics of the ejection process.

Currently, some models make it possible to relate the properties of the fuel such as surface tension and viscosity to quantify the intensity of the ejections generated by micro-explosions [15,16], by using the radius of the bubble before its burst and the properties of the liquid. However, generalizing an expression to predict the number of ejections is difficult to achieve due to the complex nature of the liquid, due to the change in physical properties that occurs as pyrolysis and thermal cracking occur.

It must be understood microexplosions as a set of closely linked phenomena that take place during the heating of liquids, where the formation and dynamics of the bubble are the key pieces. currently, there are very comprehensive studies showing isolated effects such as nucleation [17–19], coalescence [20–22], and bursting [23] of bubbles in liquid drops. However, few theoretical studies on bubble dynamics for bio-oil produced by biomass pyrolysis of biomass can be found in the literature.

While models for this phenomenon have already been proposed to explain the pyrolysis of plastics, such as the model presented by Butler [24], which takes into account the formation, coalescence, and explosion of the bubbles that cause micro-explosions, the formation of bubbles is overestimated due to its restriction that the radial differential elements cannot remain empty. In this work, experimental measurements of suspended droplet evaporations were carried out and the results were compared and explained using a novel numerical model. This is presented to describe the microexplosions of biooil droplets, this model includes the kinetics of the phenomenon itself, in addition to taking into account the speed of bubble formation and its dynamics

within the biooil droplets. Likewise, the effect of the nucleation speed on the behavior of the droplet dynamics was analyzed, as well as the bursting time of the bubbles that reach the surface.

5.1 Experimental

5.1.1 droplet experiments

The suspended droplet experiments were carried out using a cylindrical oven in which the droplet is exposed perpendicularly to a laminar stream of gas (Nitrogen or Air) that is heated by passing through a honeycomb heated with electric resistance, as can be seen in Figure 1.

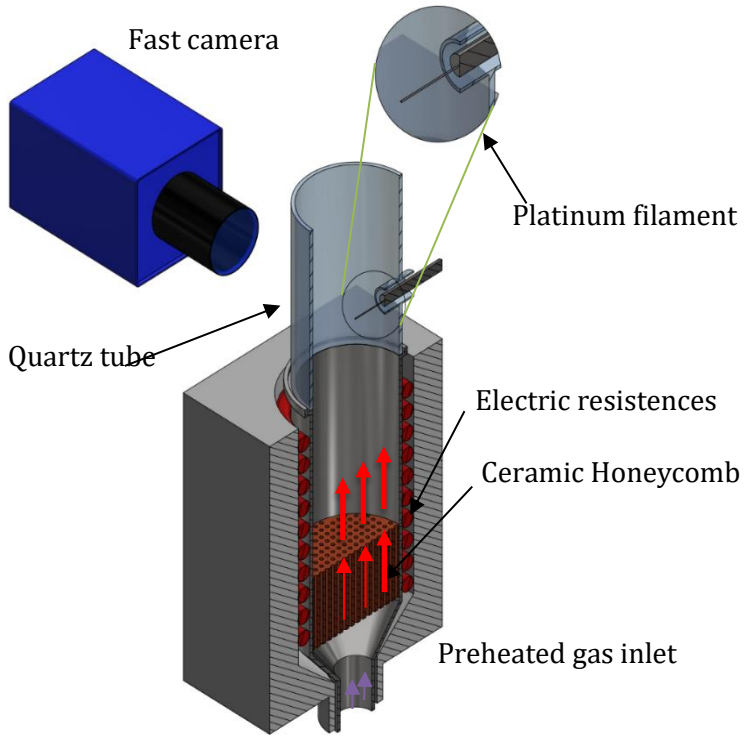

Figure 5-1 montaje experimental para el análisis de las micro explosiones de bio-aceite en condiciones de pirolisis y combustión. T1 y T2 representan las termocuplas para el control de las resistencias R1 y R2

The preheated gas enters the lower part of the oven which passes through a honeycomb to increase its temperature to the desired temperature, the thermocouple that controls the electrical resistances of the oven is positioned two centimeters below the drop to guarantee a laminar flow, typically the gas flow is approximately 15 ml per minute of nitrogen or air depending on the type of experiment. In the upper part of the gas heating furnace, there is a quartz chamber with a lateral opening that allows the entry of platinum filament 75 μm in diameter with the suspended drop as can be seen in figure 1. Perpendicular to the drop by the external part 15 cm from the quartz tube, a high-speed camera was located to follow the shape of the drop during heating, The images were acquired using a high-speed camera (LaVisión Imager Pro) coupled with a magnification lens Nikon AF-S micro Nikkor 105 mm the capture speed used was 500 fps, the photos obtained were taken in contrast, for this, a high-intensity white light source (Sumita LS-M352) with a diffuser was placed in the direction of the camera lens.

5.1.2 images post-processing

A recognition of the contours was carried out on each of the images, each frame obtained was treated to select the region where the identification of the contour will be carried out, eliminating the background and the filament, to only have the evolution of the drop. The script that allows contour measurement is written in Python that uses the Open-Cv ® library for contour detection, typically a suspended drop test contains a number 7500 frames, in each of them a suitable threshold is used to filter the bottom of the elements is binarized and erode operations are performed to detect the drop. The contour and area are measured in pixels and using a measurement pattern it is possible to obtain the physical magnitude of the diameter and the perimeter frame by frame.

To achieve the identification of the contour, the section of interest of the photograph was cut preserving the same distribution of pixels. A thresholding operation was necessary to filter the image-making erode operation for the identification of contours. Figure 2 shows a droplet of bio-oil suspended in platinum bare, in the original image

Figure 5-2a it is possible to see the presence of a bubble inside the drop (this will be explained in detail, later on, the software recognizes the bubble inside the drop, but only the complete outline of the drop is Using this contour identification it is possible to analyze the evolutionary dynamics of the bio-oil droplets during their heating in atmospheres of air and nitrogen and classify the disruptive events that occur in the process.

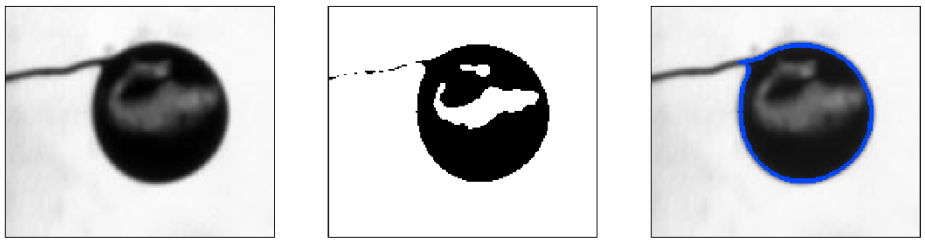

Figure 5-2 droplet postprocessing for contour identification

5.2 Mathematical model

5.2.1 Gas generation

The bio-oil droplet micro-explosion problem will be treated as a two-phase problem, the gas phase, and the liquid phase. The gas-phase fraction is called $\epsilon = V_g/V_d$ and the liquid phase fraction would be $(1-\epsilon) = V_l/V_d$ understanding that the Droplet volume $V_d$is the contribution of the volume of liquid V_l and gas V_g.

The gas formation depends on the rate of evaporation, which can be expressed as an Arrhenius-type equation, whereby the mass of liquid transformed into gas is defined as:

$$\frac{dm_l}{dt} = -(m_l - m_{l0}^*)Aexp\left(\frac{-E_a}{RT}\right) \quad (6)$$

Where m_l and m_{l0}^* represent the mass of liquid and the untransformed mass of liquid (in the case of pyrolysis is the char at the end of heating).

5.2.2 Bubble formation, growing, merging, and bursting

The formation of bubbles in droplets of multicomponent fuels because the phase change of light components during heating involves the appearance of bubbles by nucleation, growth, coalescence, and explosion.

Bubble seeds can appear by homogeneous nucleation, or heterogeneous nucleation when there are particles suspended within the liquid. The classical theory of homogeneous nucleation describes that the rate of appearance of bubbles can be expressed as a function of the concentration of liquid molecules per unit volume of liquid, their appearance frequency factor B, and the energy necessary to form a bubble with critical radius Ea_N [17,18,25] as shown below.

$$J_i = Bexp\left(-\frac{E_n}{RT}\right) \quad (7)$$

The growth of the bubbles generated by nucleation occurs by the evaporation and thermal decomposition of the bio-oil as expressed in equation (1). At any point within the drop, a quantity of gas is generated that is rapidly distributed to the nearest bubble. This assumption has experimental and theoretical validity when the characteristic mass diffusion time is less than the thermal time scale [19,26].

Differences in density between the bubbles formed to promote the movement of the bubbles within the liquid [27]. Stokes' law, which is the balance between the pushing force and the drag force, allows us to calculate the speed of movement of the bubbles within the drop, this is a function of the radius of the bubble r_b, and the viscosity of the liquid μ_l.

$$v_b = \frac{4(\rho_l - \rho_g)g\, r_b^2}{12\mu_l} \quad (8)$$

As the bubble moves through the liquid in the bubble, it increases in size until it reaches the surface of the drop, the time it remains on the surface is a key parameter to

determine the behavior of the micro-explosions. If the time it takes for a bubble on the surface is zero, it means that it explodes immediately reaches the surface, however, the intensity of the explosion increases with the time of exposure to the surface, there are expressions for the characteristic bursting time, such as in the one presented in Butler [24]as shown in equation (9).

$$t_c \approx 0.3467 \mu_l^{0.53} r_b^{1.78} v_b^{0.55} \quad (9)$$

5.2.3 Energy equation

For the heating of a drop of bio-oil where it has two phases, it is known that the relationship $(\rho_l C_{pl})/(\rho_l C_{pl})$ is large, therefore, it is valid to assume that these are in equilibrium thermal $T = T_g = T_l$ In this case, any heat transfer by internal radiation was neglected, energy dissipation by friction was also neglected, as was the effect of pressure on the energy balance, with the above the energy equation for a spherical drop in radial coordinates is expressed as follows:

$$\rho^* C_p^* \frac{dT}{dt} = \frac{1}{r^2}\frac{\partial}{\partial r}\left(r^2 k^* \frac{\partial T}{\partial r}\right) - \frac{H \partial m_l}{V_{l,0} \partial t} \quad (10)$$

The heat of vaporization H $(positive)$, k^* y C_p^* is the thermal conductivity and effective heat capacity. The differential equation must meet the appropriate conditions. Initially, all the drop is at the same temperature

$$T(r, 0) = T_0 \quad (11)$$

In the drop surface, convection and radiation are the dominant mechanisms, so the boundary condition can be written as

$$at\ r = r_d(t), -k^* \frac{\partial T}{\partial r} = \varepsilon \sigma_{SB}(T^4 - T_{env}^4) + h_c(T - T_{env}) \quad (12)$$

With ε as a surface emissivity, σ_{SB} is the Steffan-Boltzmann constant, and h_c is the convective coefficient, and the symmetry condition must be fulfilled in the center of the drop

$$at\ r = 0, \frac{\partial T}{\partial r} = 0 \qquad (13)$$

5.3 Numerical approach

In this section, we present a numerical solution to the problem of bubble formation within a drop of bio-oil during its pyrolysis. The model presented here is based on the generation of vapors within the drop, promoting the appearance of bubbles within the drop. This solution model considers bubbles as discrete elements that interact with the liquid medium. The dynamics of the bubbles are characterized by the speed of formation by nucleation, coalescence, movement, and bursting.

The geometry of the drop and the bubbles were assumed spherical as shown in Figure 5-3. To give a numerical solution, the domain of the drop was discretized at N radial nodes with (N-1) concentric spherical elements with volumes V_i, in at time t = 0 the drop has no bubbles or bubble seeds and the volume of each element is calculated with equation (14), and the temperature in all elements of the drop is equal to T_0 , When bubbles appear inside of the drop the volume of and the radius of each node is calculated proportionally to the radius of the drop at that instant $r_i = \lambda_i r_d$ where is a vector of N elements with values between zero and one.

$$V_i = \left(\frac{4\pi}{3}\right)(r_{i+1}^3 - r_i^3)\ i = 0 \ldots\ldots N \qquad (14)$$

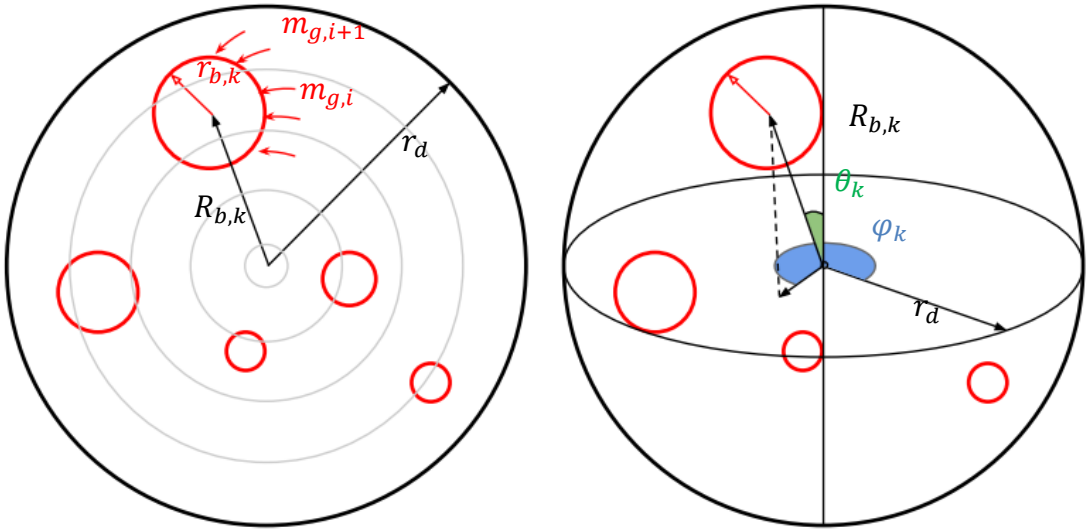

Figure 5-3 descripción geométrica de los nodos, y dimensiones generales usadas en el modelo, b) ubicación de una burbuja k dentro de la gota

In each differential element of the drop, the amount of gas generated is calculated, using equation (6), The mass of gas generated in the time differential in each element i $m_{g,i,t}$, is distributed to the bubbles N_{bi} that are completely or partially contained within element i according to equation (15),

$$m_{k,i,t} = \frac{\left(m_{g,i,t} - m_{g,i,t-\Delta t}\right)}{N_{b,i}} + m_{k,i,t-\Delta t} \qquad (15)$$

If there are no bubbles or seeds contained in element i, the mass of gas generated in that element is added to the mass of gas generated in the next element. Thus, if there are no bubbles in the drop, the mass of gas generated is released by surface evaporation:

$$N_{b,i} = 0 \ \therefore \ m_{g,i+1,t} = m_{g,i,t} \qquad (16)$$

Knowing the density of the gases and the new mass of each bubble, its radius is calculated, with this and equation (8) it is possible to calculate its speed and bubble displacement:

$$z_{k,t+\Delta t} = \frac{4(\rho_l - \rho_g)\, g\, r_{b,k,t+\Delta t}^2}{12\mu}\Delta t + z_{k,t} \quad (17)$$

$$z_{k,t} = R_{b,k}\cos(\theta_k) \quad (18)$$

The appearance of bubbles by homogeneous nucleation occurs by the accumulation of bubble fractions during a time differential in element i, when an integer value is achieved, a bubble is created in element $N_{b,i,t}$at time t.

$$N_{b,i,t} = N_{b,i,t-\Delta t} + Bexp\left(-\frac{E_n}{RT}\right)V_i\Delta t \quad (19)$$

For coalescence, if the difference between the centers of two bubbles is less than the sum of their radii, then these two bubbles are eliminated and a new one is created with the sum of their masses and located at the center of mass of the two bubbles.

The global mass balance during each time corresponds to the mass of the drop m_d which is the sum of the mass of all bubbles k and the mass of liquid in each element i

$$m_d = \sum_{k=1}^{K} m_{b,k} + \sum_{i=1}^{N} m_{l,i} \quad (20)$$

The space of the drop ϵ can be expressed as a function of the gas and liquid masses equation (21), and with this, it is possible to calculate the average properties ξ equation (22), for density, thermal conductivity, heat capacity, and viscosity.

$$\epsilon = \frac{V_g}{V_g + V_l} = \frac{m_g\rho_l}{m_g\rho_l + m_l\rho_g} \quad (21)$$

$$\xi_d = (1-\epsilon)\xi_l + \epsilon\xi_g \quad (22)$$

And the droplet radio is estimated as:

$$rd^3 = \frac{3}{4\pi}\left(\frac{m_d}{\rho_d}\right) \quad (23)$$

After recalculating the radius of the drop that includes the bubbles, it is necessary to determine the occupied volume and the mass of the liquid fraction in each element, to achieve this it is necessary to calculate the contribution of each bubble to the volume of

the shell, the volume of bubbles that is divided by a spherical shell, can be calculated based on its radial position, as can be seen in Figure 5-4,

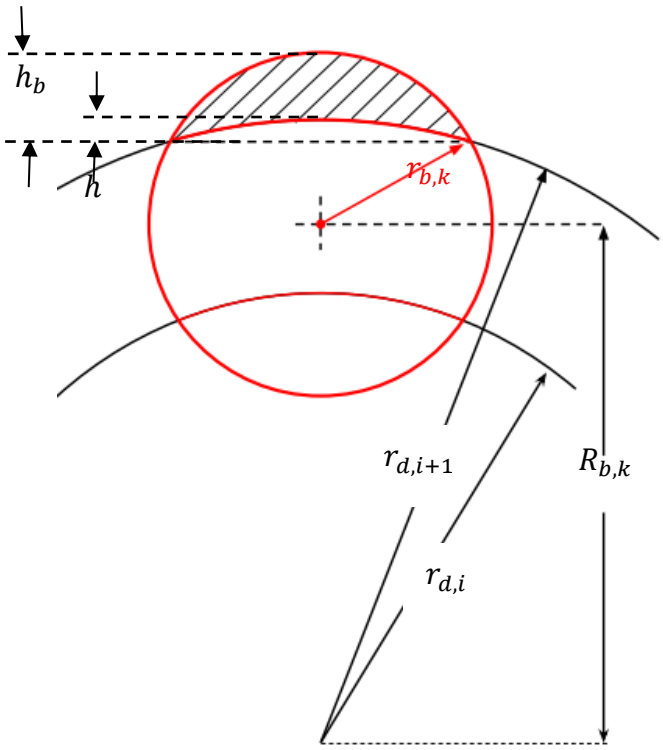

Figure 5-4 detail of a bubble passing through a drop differential element

the volume shaded in Figure 5-4 $\left(V_{bk|r_i}\right)$ corresponds to the upper volume of a bubble cut by a spherical plane and can with equation (24).

$$V_{bk|r_{i+1}} = \frac{\pi}{6}\left(h_b(3a^2 + h_b^2) - h(3a^2 + h^2)\right) \qquad (24)$$

where

$$a^2 = (r_b^2 - (r_b - h_b)^2)$$

$$h_b = \frac{(r_b + R_b)^2 - r_{d,n+1}}{2R_b}$$

$$h = \left(r_{d,n+1} - R_b\right) - (r_b - h_b)$$

so the volume of the bubble k contained in element i between the radii of the nodes $r_{d,i+1}$ and $r_{d,i}$ can be expressed as $V_{bk,i} = V_{bk|r_i} - V_{bk|r_{i+1}}$, with this, it is possible to calculate the contribution of each bubble to the volume of gas contained in the element and the mass of liquid in each element of the drop.

Once the mass of liquid in each element and the average properties are known, the energy equation is solved using finite differences along the radius of the drop, and the temperature in each element is calculated as the linear average of the adjacent nodes. As the diameter of the drop changes with time, it is necessary to establish a normalized radial coordinate with the radius of the drop at each time step λ that varies between zero and one for each radius of the drop.

$$\frac{\partial T}{\partial t} = \left(\frac{k_d}{\rho_d C_{pd}}\right)\frac{1}{r_d^2 \lambda^2}\frac{\partial}{\partial \lambda}\left(\lambda^2 \frac{\partial T}{\partial \lambda}\right) - \left(\frac{H}{\rho_d C_{pd}}\right)\frac{\partial m_l}{\partial t} \qquad (25)$$

With the new temperature field, the calculation procedure is repeated from the generated mass calculated with equation (6), as shown in the following calculation diagram

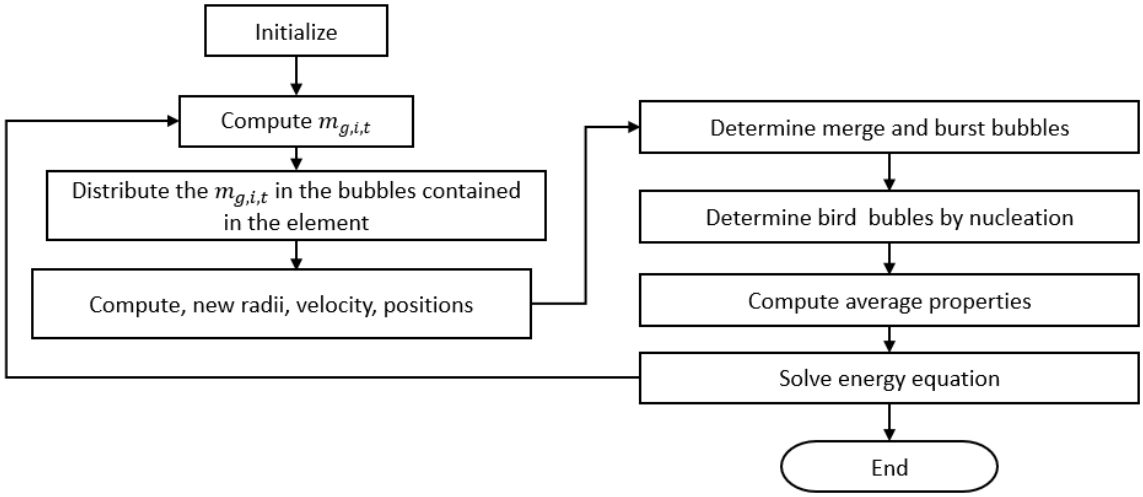

Figure 5-5 calculations flowchart for bubble dynamics

5.4 **Results**

Suspended droplet experiments at 560 °C were performed using SCB Bio-oil under a nitrogen atmosphere. The results of the contour detection are presented in Figure 7. The bio-oil drop shows a size reduction, reaching a minimum of 20% of the initial size. In the first stage, the bio-oil undergoes a process of liberation of volatile compounds such as low molecular weight such as alcohols, acids, aromatics, mono-phenols, and sugar derivatives such as 5-HMF [28], the high presence of these compounds Low molecular weight favors the formation of a drop breaking event.

The phase change temperatures of the compounds detectable by GC-Ms are between 60 and 300°C [29,30] so that nucleation boiling occurs within the droplets [31] and their size increases significantly. before breaking the surface and forming the ejecta. In the absence of air, the bio-oil begins to undergo thermal cracking which leads to the production of methane gas, carbon monoxide, hydrogen, and carbon dioxide, mainly macromolecular pyrolysis gases [32–35], with a very low molecular weight with high diffusivity in liquids, so the intensity of disruptive events decreases significantly.

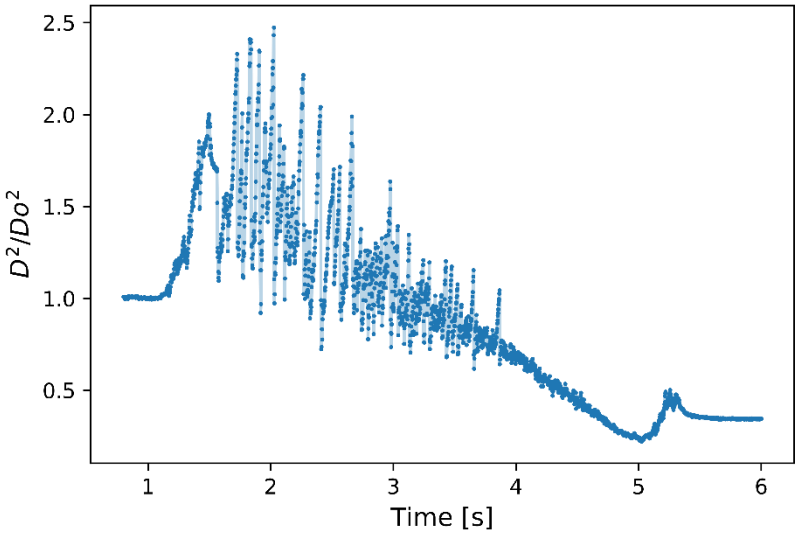

Figure 5-6 D^2/D_0^2 evolution for bio-oil droplets suspended in platinum bare in 560°C air atmosphere

This section presents the results of the proposed model and its solution strategy. The physical properties of the liquid and the vapors were assumed to be invariant in time, the values of the physical properties and activation energies were reported in Table 1.

Table 5-1 general properties and values used for calculations

Property	Units	Value	Method
Density (at 288K)	kg/m^3	1170	ASTM D4052-11
Kinematic viscosity (at 288K)	cSt	8.14 ±0.2	ASTM D445-12
Thermal conductivity	W/m.K	0.95 ± 0.2	[36]
Thermal conductivity of vapors	W/m.K	0.03 ± 0.1	[37]
Global Activation energy Ea	kJ/mol	200	[37]
Global Pre-exponential factor A	1/s	1.6e12	[37]

5.4.1 Effect of nucleation rate on droplet evaporation dynamics

Initially, the effect of bubble formation velocity on the proposed model was evaluated and as this modifies the dynamics of bubbles within the liquid drop, a total simulation time of 5 s with a fixed time step of 0.002 s, with 20 nodes and 19 elements was used to solve the problem numerically.

All the subplots in Figure 5-7show the evolution of D^2/D_0^2 over time, evaluating the effect of the nucleation velocity, in each of them the red line represents the case in which the nucleation velocity is equal to zero in which bubbles are not formed inside the drop and only surface evaporation occurs, Figure 5-7a and Figure 5-7b present the case in which the nucleation velocity is constant J=2 [1/s] and J= 10 [1/s], Figure 5-7c presents the case in which an Arrhenius bubble formation law was used described by equation (7) and finally Figure 5-7d presents the experimental results taken from chapter 3 of this thesis.

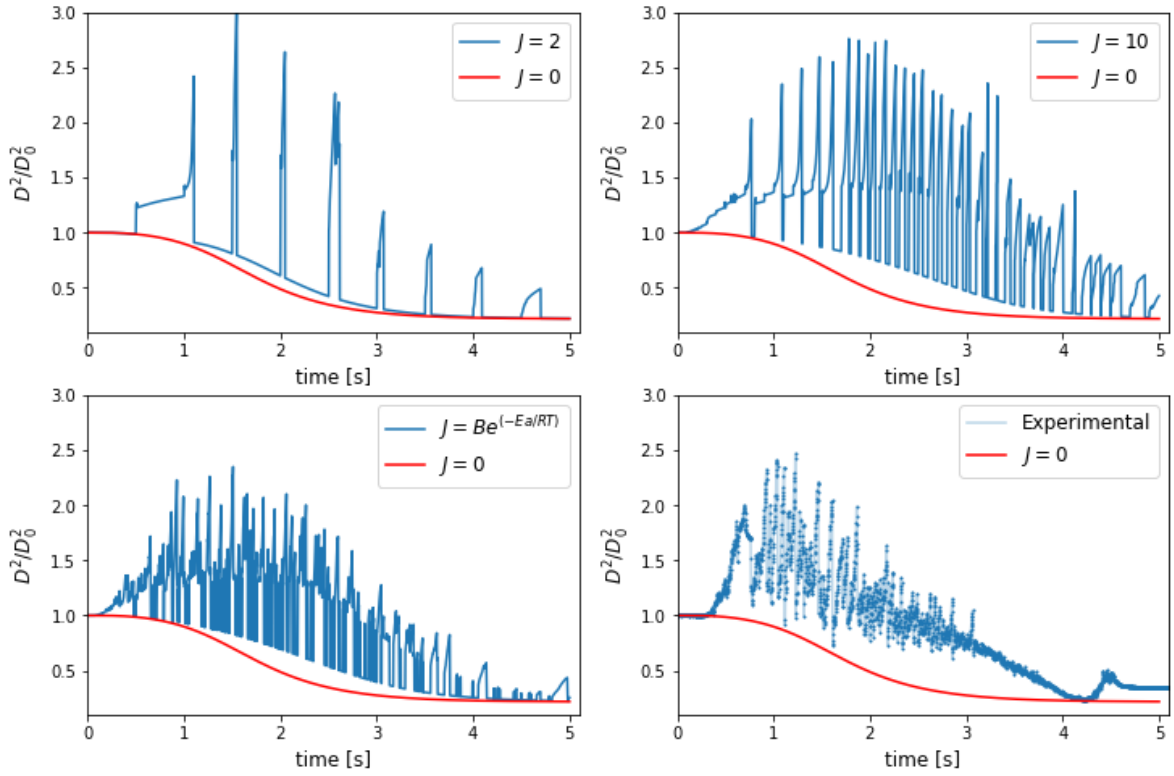

Figure 5-7 numerical results according to the variation of the nucleation rate J

A nucleation speed equal to 2 [1 / s], implies every second two bubbles with zero volume will be formed inside the drop, as the speed of growth of the bubble is greater than the speed of appearance than two peaks in a period of 1 s in Figure 5-7a are produced. These peaks correspond to the swelling of the drop due to the growth of the bubbles and movement to the surface where they explode. The intensity of the peaks decreases as time progresses because the amount of mass-generated at each time differential decreases, and this occurs regardless of whether the nucleation rate is constant or variable.

To evaluate the effect of the increase in nucleation speed, simulations were performed using a nucleation speed five times higher J = 10 [1/s], in this case, every second 10 bubbles were formed in each element which begins to grow, it can be observed that the frequency of occurrence of the explosion events does not correspond to 10 events in a period of 1s because the mass of gas generated is distributed in a greater number of bubbles reducing the growth speed and consequently the movement speed Inside the

drop before reaching the surface, we can also observe that disruptive events begin to increase their frequency of occurrence in the area where there is a higher speed of generation of gases and volatiles.

On the other hand, the homogeneous nucleation theory shows that the Arrhenius equation is adequate to describe the formation of bubble seeds, Figure 5-7c shows the results of the simulation in which an Arrhenius-type bubble formation law was used. described by the equation (7) and (19), for this simulation $E_n = 40$ [kj/mol] and a factor $B = 1.6e9[1/m^3 s]$. The behavior is very similar to the result obtained with J = 10. However, the frequency of occurrence of drop breaking events increases significantly, around 2 s of the simulation, this because the highest gas generation rate is achieved, and both the intensity and the frequency of swelling and explosions are reduced at the end of the simulation because very little gas is generated to distribute among the existing bubbles.

Figure 5-7d shows the experimental results of a bio-oil drop evaporation test in nitrogen, as described in chapter 3. It can be seen that the results of the simulations carried out, both with constant nucleation rates or using an Arrhenius-type expression, describe the expansion of the radius of the droplet as a result of the dynamics of bubble formation. Interestingly, it can be seen that in Figure 5-7d, about 0.5 to 1s, the formation of a peak product of the swelling of the first bubbles formed inside the drop is presented, this phenomenon was captured with the model proposed by this work, both at a constant nucleation rate as at Arrhenius-type nucleation rate.

It is evident in Figure 5-7d that the kinetics of a single step does not fully describe the phenomenon, since the line with J = 0 should approach the restitution minima, that is, after the formation of bubbles, they begin to increase their size, move, combine and travel to the surface where they meet the condition for them to explode, then, the drop is restored to its minimum radius value for the mass of liquid it has at that time. Which is equivalent to having the case with j = 0.

The temperature profiles are affected by changes in the radius of the droplet, a product of the frequency of the appearance of bubbles.

The formation of bubbles within the drop generates variations in the physical properties of the drop, as expressed in equation (17), especially the density, thermal conductivity, and calorific power significantly affect the temperature field of the drop. In Figure 5a the results of the solution of the energy equation are shown considering the local variation of the physical properties. As expected, a variation in the nucleation rate modified the heating profile and generates oscillations in the heating rates, as can be seen in Figure 5b

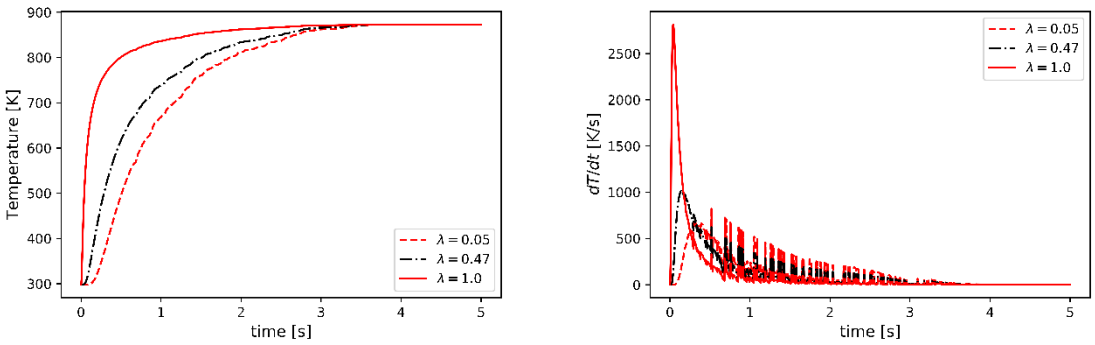

Figure 5-8 temperature field for J=B exp(-En/RT) and heating velocity

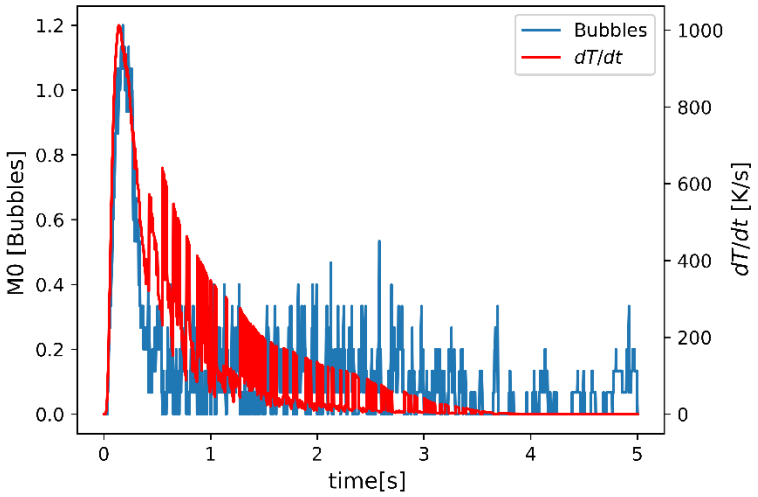

Figure 5-9 comparison between heating rate and bubble number in droplet

the appearance of bubbles inside the drop generates variations in the physical properties of the system. These variations are mainly reflected in oscillations in the rate of global warming of the drop. variations in the rate of heating appear to be strongly correlated with the generation of bubbles in the first stage of the evaporation process. As can be seen in figure 6, there is an overlap between the maximum heating rate reached and the number of bubbles generated. this explains that the bubble formation model is promoted by the effect of temperature. And the thermal oscillations within the droplet play a decisive role in the dynamics of micro-explosions.

However, according to the results of our simulations, the oscillations in the heating rate are important in the innermost nodes of the drop, that is to say, in the center of the drop a greater amount of thermal oscillations are generated than in the surface.

5.4.2 Effect of bursting on droplet evaporation dynamics

To understand the bursting of bubbles on the surface of the drop, it is necessary to consider several factors that influence the process. When the bubbles are formed within the drop, they move towards the surface, and their speed decreases due to the balance of forces [22,38]. When the drop reaches the surface the bubble growth phenomena continue to occur, and the drainage phenomenon begins, this phenomenon is characterized by the movement of the liquid layer on the surface of the bubble making the layer thinner and thinner until the bubble bursts.

The drainage time may increase during an evaporation and pyrolysis test because the viscosity of the bio-oil increases as a result of the formation of high molecular weight compounds, by polycondensation reactions [39,40], the bio-oil contains a large fraction of high molecular weight components derived from lignin [28,41] that are in equilibrium with the other components of the bio-oil, keeping them in the liquid phase [42], with the evaporation of the light components these heavy components form a liquid with a molecular weight above 1000Da that has a higher viscosity-increasing the time that the bubbles are on the surface.

To evaluate the drainage and explosion time in the drop's evaporation dynamics, a simulation was carried out setting a time for the bubbles that touch the surface, that is, when a bubble touches the surface of the drop, a timer starts until the time on the surface is greater than a defined drainage time, then the bubble bursts and its mass is no longer taken into account in the mass of the drop. In Figure 5-10 a, b, c the results of the simulations carried out using t_b = 0, 6 and 10 ms respectively are shown and finally, in Figure 5-10d the experimental results are presented for comparison purposes.

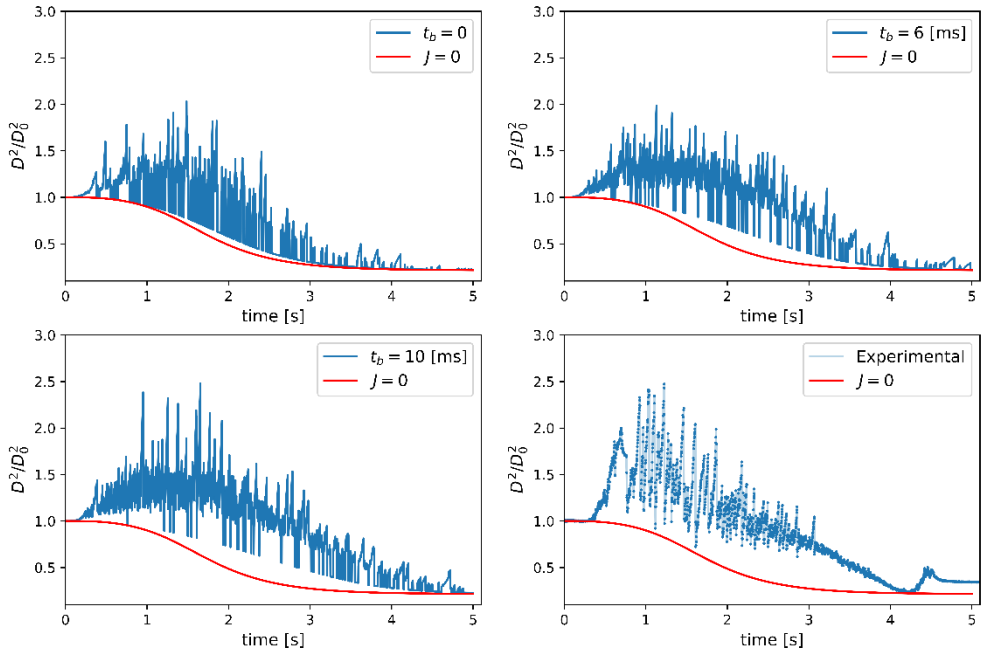

Figure 5-10 numerical results according to the variation of burstingtime with a nucleation rate J=B exp(-En/RT)

With a time t_b = 0 the bubbles that cross the border immediately explode, and the liquid drop is restored to its minimum radius. In figure 6 we can see that after the explosion of the bubbles that reach the surface, the drop reduces its size and this is slightly different from the behavior that would be obtained in the absence of bubbles, represented in the figure by the line J = 0 This is why the balance between the birth of the bubbles by nucleation and those that disappear by an explosion at each time step in

the whole drop is practically zero and this has the effect of reducing the swelling phenomenon of the drop.

The main difference found when increasing the drainage time to 6 or 10 ms is in the radius after the explosions do not fall to the minimum value that it can have because other bubbles may be on the surface, but they have not met the condition for burst and release the gases, keeping the bloat in the drop. Therefore, the increase in the drain time influences the dynamics of evaporation and pyrolysis of the bio-oil drop. On the other hand, the dynamics obtained using a drain time of 10 ms is very similar to the dynamics obtained experimentally.

As expected, the burst time affects the number of bubbles formed during the evaporation and pyrolysis of the bio-oil, even though the nucleation rate is the same for the three burst times evaluated, the longer the burst time there is a greater number of bubbles generated in a time differential as can be seen in figure 7a. This may be mainly because the longer the bubbles remain on the surface of the drop, the greater the swelling, and thus an increase in the number of bubbles generated by nucleation.

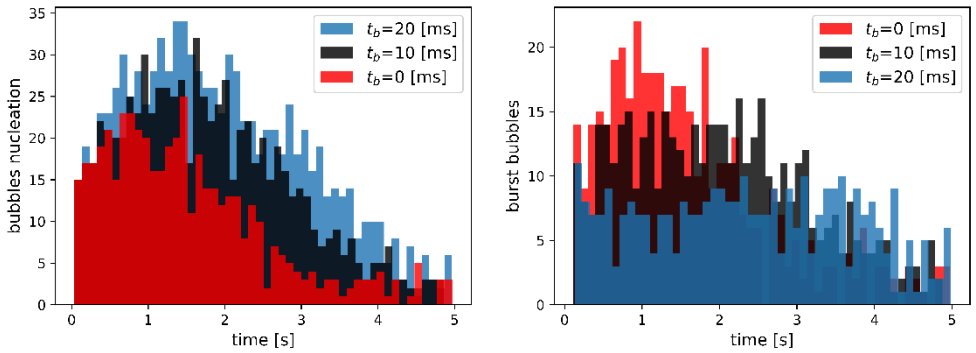

Figure 5-11 a) hist chart of bubbles born by nucleation at three different drainage time, b) hist chart of burst bubbles at three different drainage times.

On the other hand, increasing the retention time of bubbles on the surface (tb) reduces the number of bubbles that burst, as can be seen in Figure 7b, where it is shown that the number of bubbles that burst in the range of 1 to 2 s is greater than when an explosion time of 6 to 10 ms was used, this is physically explainable since the bubbles

remain longer on the surface, this reduction in the number of bubbles that burst, explains the fact that drop has a greater swelling.

5.5 Conclusions

In this work, a new model has been developed that allows predicting the dynamics of evaporation and pyrolysis of bio-oil droplets, taking into account the phenomena of nucleation, union, and an explosion of the bubbles that are responsible for micro-explosions, the Drain time modifies the dynamics of evaporation and pyrolysis of bio-oil. The intensity of the ejections is reduced in time due to the reduction in the nucleation rate, and also to the increase in the retention time on the surface due to the increase in the viscosity of the liquid phase.

the formation of bubbles within the drop generates variations in the thermal properties causing oscillations in the heating rate. falling peaks promote the appearance of new bubbles and this triggers the microexplosion mechanism microexplosion mechanism

5.6 References

[1] R. Calabria, F. Chiariello, P. Massoli, Combustion fundamentals of pyrolysis oil based fuels, Exp. Therm. Fluid Sci. 31 (2007) 413–420. https://doi.org/10.1016/j.expthermflusci.2006.04.010.

[2] M. Garcia-Perez, P. Lappas, P. Hughes, L. Dell, A. Chaala, D. Kretschmer, C. Roy, Evaporation and combustion characteristics of biomass vacuum pyrolysis oils, IFRF Combust. J. 200601 (2006) 1–27.

[3] Á. Muelas, M.S. Callén, R. Murillo, J. Ballester, Production and droplet combustion characteristics of waste tire pyrolysis oil, Fuel Process. Technol. 196 (2019). https://doi.org/10.1016/j.fuproc.2019.106149.

[4] C. Branca, C. Di Blasi, Combustion kinetics of secondary biomass chars in the kinetic regime, Energy and Fuels. 24 (2010) 5741–5750. https://doi.org/10.1021/ef100952x.

[5] Z. Xiong, S.S.A. Syed-hassan, X. Hu, J. Guo, J. Qiu, X. Zhao, Pyrolysis of the aromatic-poor and aromatic-rich fractions of bio-oil : Characterization of coke structure and elucidation of coke formation mechanism, Appl. Energy. 239 (2019) 981–990. https://doi.org/10.1016/j.apenergy.2019.01.253.

[6] P. Eng, D. Scarpete, Diesel-water emulsion, an alternative fuel to reduce diesel engine emissions. A review, Mach. Technol. Mater. (2013) 7–10.

[7] C.Y. Hsuan, S.S. Hou, Y.L. Wang, T.H. Lin, Water-In-Oil emulsion as boiler fuel for Reduced NOx emissions and improved energy saving, Energies. 12 (2019) 1–14. https://doi.org/10.3390/en12061002.

[8] M.L. Botero, Y. Huang, D.L. Zhu, A. Molina, C.K. Law, Synergistic combustion of droplets of ethanol, diesel and biodiesel mixtures, Fuel. 94 (2012) 342–347. https://doi.org/10.1016/j.fuel.2011.10.049.

[9] C.K. Law, C.H. Lee, N. Srinivasan, Combustion characteristics of water-in-oil emulsion droplets, Combust. Flame. 37 (1980) 125–143. https://doi.org/10.1016/0010-2180(80)90080-2.

[10] R.H. C. R. Shaddix, D, Combustion Properties of Biomass Flash Pyrolysis Oils : Final Project Report, 1999. https://doi.org/10.2172/5983.

[11] C.R. Shaddix, S.P. Huey, Combustion characteristics of fast pyrolysis oils derived from hybrid poplar, Dev. Thermochem. Biomass Convers. (1997) 1630.

[12] M.J. Wornat, B.G. Porter, N.Y.C. Yang, Single Droplet Combustion of Biomass Pyrolysis Oils, Energy & Fuels. 8 (1994) 1131–1142. https://doi.org/10.1021/Ef00047a018.

[13] C. Branca, C. Di Blasi, Multistep mechanism for the devolatilization of biomass fast

pyrolysis oils, Ind. Eng. Chem. Res. 45 (2006) 5891–5899. https://doi.org/10.1021/ie060161x.

[14] F. Stankovikj, A.G. McDonald, G.L. Helms, M. Garcia-Perez, Quantification of Bio-Oil Functional Groups and Evidences of the Presence of Pyrolytic Humins, Energy and Fuels. 30 (2016) 6505–6524. https://doi.org/10.1021/acs.energyfuels.6b01242.

[15] D.C.K. Rao, S. Syam, S. Karmakar, R. Joarder, Experimental investigations on nucleation , bubble growth , and micro- explosion characteristics during the combustion of ethanol / Jet A-1 fuel droplets, Exp. Therm. Fluid Sci. 89 (2017) 284–294. https://doi.org/10.1016/j.expthermflusci.2017.08.025.

[16] A.R. Teixeira, K.G. Mooney, J.S. Kruger, C.L. Williams, W.J. Suszynski, L.D. Schmidt, D.P. Schmidt, P.J. Dauenhauer, Aerosol generation by reactive boiling ejection of molten cellulose, Energy Environ. Sci. 4 (2011) 4306–4321. https://doi.org/10.1039/c1ee01876k.

[17] J.H. Han, C.D.A.E. Han, Bubble Nucleation in Polymeric Liquids . 11 . Theoretical Considerations, J. Polym. Sci. B Polym. Phys. 28 (1990) 743–761. https://doi.org/10.1002/polb.1990.090280510.

[18] J.L. Katz, Bubble Nucleation in Liquids, AIChE J. 21 (1975) 833–848. https://doi.org/10.1002/aic.690210502.

[19] D.C. Venerus, N. Yala, B. Bernstein, Analysis of diffusion-induced bubble growth in viscoelastic liquids, J. Non-Newtonian Fluid Mech. 75 (1998) 55–75. https://doi.org/10.1016/S0377-0257(97)00076-1.

[20] H. Schulz, Short history and present trends of Fischer – Tropsch synthesis, 186 (1999) 3–12.

[21] B.H. Davis, Overview of reactors for liquid phase Fischer – Tropsch synthesis, 71 (2002) 249–300.

[22] Y. Cheng, Y. Shen, D. Liu, J. Xu, Y. Sui, Numerical analysis of bubble bursting at the liquid surface by wave propagation, Int. J. Therm. Sci. 152 (2020) 106341. https://doi.org/10.1016/j.ijthermalsci.2020.106341.

[23] B.Y. Ni, A.M. Zhang, G.X. Wu, Simulation of a fully submerged bubble bursting through a free surface, Eur. J. Mech. B/Fluids. 55 (2016) 1–14. https://doi.org/10.1016/j.euromechflu.2015.08.001.

[24] K.M. Butler, A Numerical Model for Combustion of Bubbling Thermoplastic Materials in Microgravity, 2002. https://tsapps.nist.gov/publication/get_pdf.cfm?pub_id=861181.

[25] H.-Y. Kwak, Y.W. Kim, Homogeneous nucleation and macroscopic growth of gas bubble in organic solutions, Int. J. Heat Mass Transf. 41 (1998) 757–767. https://doi.org/10.1016/S0017-9310(97)00182-8.

[26] L. Hao, Analysis of bubble growth and motion dynamics in superheated liquid during flash evaporation, Int. J. Heat Mass Transf. 151 (2020) 119356. https://doi.org/10.1016/j.ijheatmasstransfer.2020.119356.

[27] S. Hoon, C. Park, J. Lee, B. Lee, A Simple Parameterization for the Rising Velocity of Bubbles in a Liquid Pool, Nucl. Eng. Technol. 49 (2017) 692–699. https://doi.org/10.1016/j.net.2016.12.006.

[28] F. Stankovikj, M. Garcia-perez, TG-FTIR Method for the Characterization of Bio-oils in Chemical Families, Energy & Fuels. 30 (2017) 1689–1701. https://doi.org/10.1021/acs.energyfuels.6b03132.

[29] F. Stankovikj, C.-C. Tran, S. Kaliaguine, M. V. Olarte, M. Garcia-Perez, Evolution of Functional Groups during Pyrolysis Oil Upgrading, Energy & Fuels. (2017) acs.energyfuels.7b01251. https://doi.org/10.1021/acs.energyfuels.7b01251.

[30] A.R. Teixeira, R.J. Hermann, J.S. Kruger, W.J. Suszynski, L.D. Schmidt, D.P. Schmidt, P.J. Dauenhauer, Microexplosions in the upgrading of biomass-derived pyrolysis

oils and the effects of simple fuel processing, ACS Sustain. Chem. Eng. 1 (2013) 341–348. https://doi.org/10.1021/sc300148b.

[31] G. Lu, X. Wang, W. Yan, International Journal of Heat and Mass Transfer Nucleate boiling inside small evaporating droplets : An experimental and numerical study, Int. J. Heat Mass Transf. 108 (2017) 2253–2261. https://doi.org/10.1016/j.ijheatmasstransfer.2017.01.081.

[32] D. Yepes, F. Chejne, Gasificación de biomasa residual en el sector floricultor , caso : Oriente Antioqueño Gasification of waste biomass in the flower industry , case : Eastern Antioquia, ION. 25 (2012) 49–55.

[33] G. Marrugo, C.F. Valdés, F. Chejne, Biochar Gasification: An Experimental Study on Colombian Agroindustrial Biomass Residues in a Fluidized Bed, Energy & Fuels. 31 (2017) 9408–9421. https://doi.org/10.1021/acs.energyfuels.7b00665.

[34] Z. Xiong, Y. Wang, S.S.A. Syed-Hassan, X. Hu, H. Han, S. Su, K. Xu, L. Jiang, J. Guo, E.E.S. Berthold, S. Hu, J. Xiang, Effects of heating rate on the evolution of bio-oil during its pyrolysis, Energy Convers. Manag. 163 (2018) 420–427. https://doi.org/10.1016/j.enconman.2018.02.078.

[35] S.I. Yang, M.S. Wu, T.C. Hsu, Spray combustion characteristics of kerosene/bio-oil part I: Experimental study, Energy. 119 (2017) 26–36. https://doi.org/10.1016/j.energy.2016.12.062.

[36] J. Lehto, A. Oasmaa, Y. Solantausta, M. Kytö, D. Chiaramonti, Fuel oil quality and combustion of fast pyrolysis bio-oils, VTT Publ. (2013) 79. https://doi.org/10.1016/j.apenergy.2013.11.040.

[37] W.L.H. Hallett, N.A. Clark, A model for the evaporation of biomass pyrolysis oil droplets, 85 (2006) 532–544. https://doi.org/10.1016/j.fuel.2005.08.006.

[38] D.E. Spiel, The number and size of jet drops produced by air bubbles bursting on

a fresh water surface, J. Geophys. Res. 99 (1994) 10289–10296. https://doi.org/10.1029/94JC00382.

[39] R.P.B. Ramachandran, G. Van Rossum, W.P.M. Van Swaaij, S.R.A. Kersten, Evaporation of biomass fast pyrolysis oil: Evaluation of char formation, Environ. Prog. Sustain. Energy. (2009). https://doi.org/10.1002/ep.10388.

[40] W. Chaiwat, I. Hasegawa, T. Tani, K. Sunagawa, K. Mae, Analysis of cross-linking behavior during pyrolysis of cellulose for elucidating reaction pathway, Energy and Fuels. 23 (2009) 5765–5772. https://doi.org/10.1021/ef900674b.

[41] M. Garcia-Perez, A. Chaala, H. Pakdel, D. Kretschmer, C. Roy, Characterization of bio-oils in chemical families, Biomass and Bioenergy. 31 (2007) 222–242. https://doi.org/10.1016/j.biombioe.2006.02.006.

[42] A.G.M.T. Siriwardhana, Aging and Stabilization of Pyrolitic Bio-Oils and Model Compounds, The University of Western Ontario, 2013. http://ir.lib.uwo.ca/cgi/viewcontent.cgi?article=3005&context=etd.